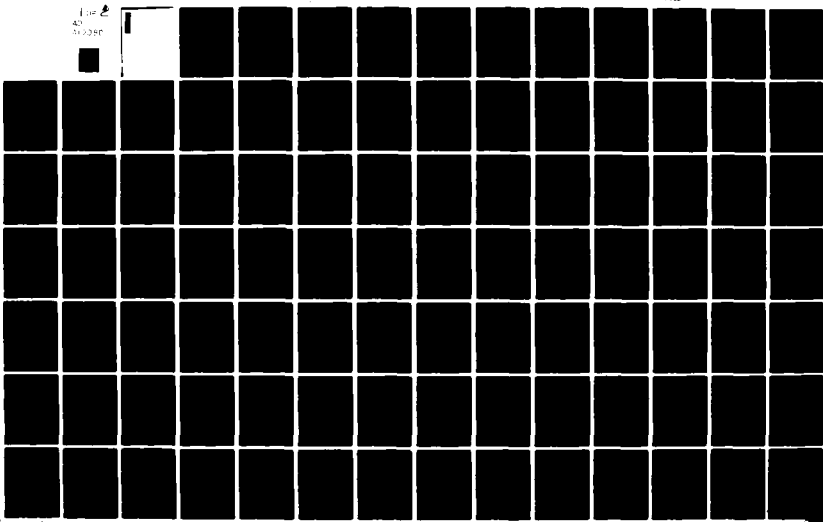


AD-A100 802 AIR FORCE INST OF TECH WRIGHT-PATTERSON AFB OH SCHO0--ETC F/6 20/9  
RESONANCE ABSORPTION OF LASER LIGHT BY WARM AND COLD PLASMAS, (U)  
MAR 81 J H RUBLE

UNCLASSIFIED AFIT/GENE/PH/81-9

NL

Line 2  
42  
362280

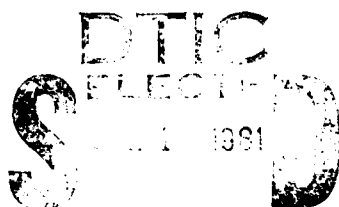


Accession For	
NTIS GRA&I	<input checked="" type="checkbox"/>
DTIC TAB	<input type="checkbox"/>
Unannounced	<input type="checkbox"/>
Justification	
By _____	
Distribution/	
Availability Copies	
Avail and/or	
Dist	Special
R	

RESONANCE ABSORPTION OF LASER LIGHT  
BY WARM AND COLD PLASMAS.

THESIS

AFIT/GNE/PH/81-9 John H. Ruble, Jr.  
2nd Lt USAF



Approved for public release; distribution unlimited

11-265

RESONANCE ABSORPTION OF LASER LIGHT  
BY WARM AND COLD PLASMAS

THESIS

Presented to the Faculty of the School of Engineering  
of the Air Force Institute of Technology  
Air University  
in Partial Fulfillment of the  
Requirements for the Degree of  
Master of Science

by  
John H. Ruble, Jr., B.S.N.E.  
2nd Lt USAF  
Graduate Nuclear Engineering  
January 1981

Approved for public release; distribution unlimited.

Acknowledgments

This work was undertaken to learn about laser-fusion in general and resonance absorption in particular. In written form, it is devoted to the latter. I would like to thank Major John Erkkila for his patience and guidance. Without his help I would not have accomplished what I did. He also deserves credit for developing the two-sweep method employed to solve the wave-equations in the plasma. I would also like to thank the Physics Department here at AFIT for giving me the chance to do this research. Last, but not least, my thanks goes to my family for tolerating the long hours required of me here.

John H. Ruble, Jr.

## Contents

	Page
Acknowledgments . . . . .	ii
List of Figures . . . . .	v
List of Symbols . . . . .	vii
Abstract . . . . .	ix
I. Introduction . . . . .	1
II. Linear Modeling . . . . .	5
Linearizing the Equations . . . . .	5
TE Mode Solution . . . . .	7
TM Mode Solution . . . . .	8
Consequences of the Density Profile . . . . .	9
Cold Plasma . . . . .	9
Second-Order Equations . . . . .	10
Landau Damping . . . . .	12
III. Numerical Methods . . . . .	17
Gridding . . . . .	17
Differencing the Equations . . . . .	19
Application of Boundary Conditions . . . . .	20
Zero Boundary Condition . . . . .	20
Radiation Boundary Condition . . . . .	21
IV. Results . . . . .	23
Parameters . . . . .	24
$E_x$ and $E_y$ . . . . .	24
$E_z$ (Longitudinal Electric Field) . . . . .	25
Cold Plasma . . . . .	25
Warm Plasma . . . . .	25
Spatial Dispersion . . . . .	27
The Plasma Wave . . . . .	29
Cold Plasma . . . . .	29
Warm Plasma . . . . .	30
Absorption . . . . .	32
Cold Plasma . . . . .	34
Warm Plasma . . . . .	34
Ponderomotive Force . . . . .	38
Hot Electron Energy . . . . .	40
Validity of Assumptions . . . . .	41
V. Conclusions . . . . .	44

Contents (Continued)

	Page
Bibliography . . . . .	47
Appendix A: Derivations . . . . .	49
Linearized Equations from Fundamental Equations TE Mode . . . . .	49
E" TE Mode . . . . .	51
Linearized Warm Plasma Equations from Fundamental Equations TM Mode . . . . .	52
Cold Plasma: E <sub>z</sub> " from Linearized Equations . . . . .	54
Warm Plasma: N <sub>1</sub> " and E <sub>z</sub> " from Linearized Equations . . . . .	55
Warm Plasma: B" and E <sub>z</sub> " from Linearized Equations . . . . .	56
Cold Plasma: Differenced Equations Solved for the Constants in the Plasma . . . . .	58
Warm Plasma: Difference Equations Solved for the Constants in the Plasma . . . . .	60
k <sub>z</sub> from E <sub>z</sub> " . . . . .	64
Ponderomotive Force (F <sub>NL</sub> ) . . . . .	65
Appendix B: Cold Plasma Data Curves . . . . .	68
Appendix C: Warm Plasma Data Curves . . . . .	90

List of Figures

<u>Figure</u>		<u>Page</u>
1	Density $n_0$ as a Function of $z$ in the Case of Linear Density Gradient . . . . .	1
2	Geometry for the Incident Electromagnetic Wave, TM Mode . . . . .	2
3	Geometry for the Incident Electromagnetic Wave, TE Mode . . . . .	3
4	Landau Damping ( $v_L/\omega = -im(\omega/\omega_p)$ as a Function of Location in the Plasma . . . . .	16
5	Power at Which Spatial Dispersion Becomes Important ( $2\pi V_{os}/\omega = \Delta z$ ) as a Function of Background Electron Temperature: Curve 1; Cold Plasma $T = (24.7\omega/v)^{2/3}$ , Curve 2; Warm Plasma $v_L/\omega = .1$ . . . . .	28
6	Regions of Validity (Indicated by Arrows) for the Warm and Cold Plasma Models . . . . .	31
7	Cold Plasma: Fraction of Laser Energy Resonantly Absorbed as a Function of Incident Angle . . . . .	35
8	Warm Plasma: Fraction of Laser Energy Resonantly Absorbed as a Function of Incident Angle ( $T = 637$ ev and $v_L/\omega = .1$ ) . . . . .	36
9	Ponderomotive Force for the Warm Plasma, $v_L/\omega = .1$ (Curve 1), and the Cold Plasma (Curve 2), for a Laser Flux of $10^{13}$ W/cm <sup>2</sup> and the Thermal Force $\nabla n_0 kT$ of the Plasma (Curve 3) . .	39
B-1 - B-7	Data for $v/\omega = .002$ . . . . .	69-75
B-8 - B-14	Data for $v/\omega = .008$ . . . . .	76-82
B-15 - B-21	Data for $v/\omega = .02$ . . . . .	83-89
C-1 - C-7	Data for $v_L/\omega = .1$ and $T/mc^2 = .0005$ .	92-98
C-8 - C-14	Data for $v_L/\omega = .09$ and $T/mc^2 = .00125$ . .	99-105

List of Figures (Continued)

<u>Figure</u>		<u>Page</u>
C-15 - C-21	Data for $v_L/\omega = .1$ and $T/mc^2 = .005$	. . 106-112
C-22 - C-28	Data for $v_L/\omega = .1$ and $T/mc^2 = .05$	. . 113-119
C-29 - C-35	Data for $v_L/\omega = .67$ and $T/mc^2 = .00125$	. 120-126
C-36 - C-42	Data for $v_L/\omega = .67$ and $T/mc^2 = .005$	. 127-133
C-43 - C-49	Data for $v_L/\omega = .67$ and $T/mc^2 = .01$	. . 134-140
C-50 - C-56	Data for $v_L/\omega = .67$ and $T/mc^2 = .1$	. . 141-147

### List of Symbols

B	Magnetic field
$B_{inc}$	Incident magnetic field
$B_{sc}$	Scattered or reflected magnetic field
$E_{inc}$	Incident electric field
$E_{sc}$	Scattered or reflected electric field
$E_x$	Electric field vector in x-direction
$E_z$	Electric field vector in z-direction
$F_{NL}$	Ponderomotive force
k	Free-space wave number
$k_z$	Wave-vector of longitudinal waves
L	Plasma critical length
m	mass of electron
$N_c, n_c$	Number density of electrons initially at the critical surface
$N_0, n_0$	Initial electron number density
$N_1, n_1$	Number density of hot electrons
s	Sine of incident angle
T	Electron temperature in ev
$T_H$	Temperature of hot electrons ( $\frac{1}{2} m v_{os}^2$ )
$v_{os}$	Velocity of hot electrons
$\gamma$	Ratio of specific heats (3 for this one-dimensional problem)
$\epsilon$	Dielectric constant in the plasma
$\theta$	Incident angle
$\lambda$	Free-space wavelength
$\lambda_D$	Debye length

$\lambda_z$	Wavelength of longitudinal waves
$\nu$	Electron-ion collision frequency (inverse bremsstrahlung)
$\nu_c$	Electron-ion collision frequency at the critical surface
$\nu_L$	Landau damping frequency (also L.D.C. $\times \omega$ )
$\phi$	Ratio of adjacent mesh space sizes
$\omega$	Frequency rad/sec of incident light
$\omega_p$	Electron plasma frequency

### Abstract

This is a study of the mechanisms and results of resonance absorption in warm and cold plasmas. Maxwell's equations and the plasma fluid equations (neglecting ion motion and assuming wavelike solutions in the x-direction) are linearized. The linearization is accomplished for a plasma with a positive number density gradient in the z-direction. Second-order equations are derived from the linearized set. These second-order equations are differenced and solved in the z-direction for the TM mode of propagation using a two-sweep algorithm with zero and radiation boundary conditions. The characteristics of the field quantities are investigated at various temperatures. Further,  $N_1$  (the plasma wave), the temperature of the hot electrons, and the nonlinear Ponderomotive force are calculated. Finally, resonance absorption by the plasma is calculated and peak absorptions of 50% are observed for both cold and low temperature warm plasmas. The validity of the assumptions is discussed referencing both power and temperature concerns. Possible nonlinear and time-dependent modifications to the theory are discussed. Landau damping is derived and its limitations considered. The two-sweep algorithm is found to give accurate results and its amenability to computer application makes it a desirable method.

## I Introduction

In this thesis the propagation and absorption of EM waves in cold and warm inhomogeneous plasmas are studied. It will be useful to start with a physical description of the fundamental concepts.

An electromagnetic wave can freely propagate in homogeneous plasma in which the natural frequency of the plasma,  $\omega_p = (4\pi n e^2/m)^{1/2}$ , is less than the frequency of the wave,  $\omega$ . Here  $n$  is the density of the electrons in the plasma,  $e$  their charge, and  $m$  their mass. When the frequency of the wave is less than the plasma frequency, the wave does not propagate but decays exponentially in the plasma. This exponentially decaying wave is called an evanescent wave.

An interesting problem occurs in an inhomogeneous plasma, then, when an electromagnetic wave is made to propagate from an underdense region ( $\omega > \omega_p$ ) to an overdense region ( $\omega < \omega_p$ ). It is the interaction of the EM wave with

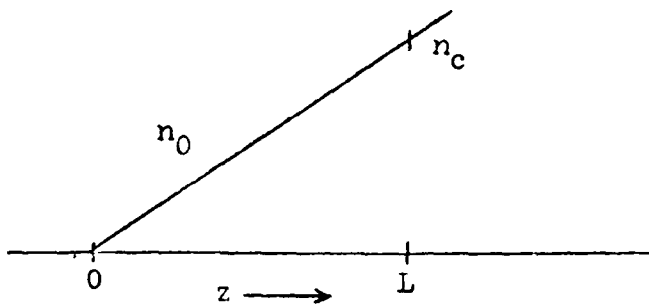


Fig 1. Density  $n_0$  as a Function of  $z$  in the Case of Linear Density Gradient

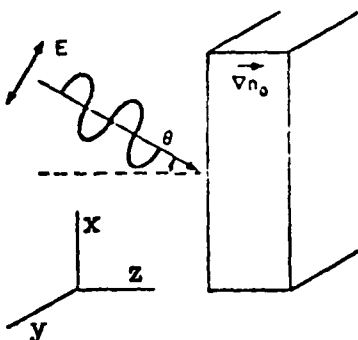


Fig 2. Geometry for the Incident Electromagnetic Wave, TM Mode

the plasma in this situation that is the subject of investigation in this thesis.

Consider an EM wave normally incident on a plasma in which  $n$  is increasing with  $z$  and independent of  $x$  and  $y$  as shown in Figure 1. For a wave propagating in the  $z$ -direction, reflection occurs at the plane in the plasma where  $\omega = \omega_p$ . This plane is called the critical surface. For the normally incident wave, the critical surface is analogous to the classical turning point (reflection point) where  $\cos^2 \theta = \omega_p^2/\omega^2$ . The mechanism by which energy is lost by the electromagnetic wave is collisional damping. This loss is insignificant when the plasma temperature is above 600 ev.

Significant losses can occur, however, when the EM wave is obliquely incident (at an angle  $\theta$  with respect to the normal). This situation is shown in Figure 2 for light propagating in the TM mode. In this mode of propagation, the EM wave has a component of its electric field pointed along the plasma density gradient. For this reason, the EM

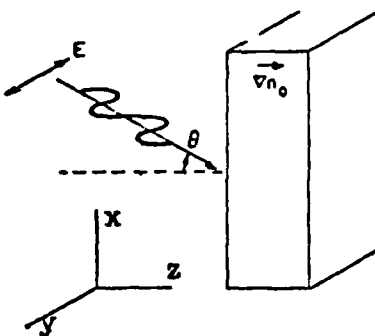


Fig 3. Geometry for the Incident Electromagnetic Wave, TE Mode

wave interacts strongly with the plasma at the critical surface. This interaction leads to an energy loss from the EM wave that is called resonance absorption. A model of this process is the specific objective of the following work.

Figure 3 depicts the alternative obliquely incident EM wave, which is propagating in the TE mode, and is not resonantly absorbed because no component of its electric field lies along the density gradient. As will be shown, this wave is reflected with no absorption at the classical turning point which is on the underdense side of the critical surface. The TM mode also undergoes reflection at this plane; however, the z-component of the electric field becomes an evanescent wave which "tunnels" into the critical surface. Here, the EM wave becomes very large and excites an electron plasma wave. The enhanced EM wave loses energy through collisions and the plasma wave is damped without collisions by interaction with electrons having a thermal velocity equal to its phase velocity. These losses are the

source of resonance absorption. The results of this study that demonstrate these ideas are included in Chapter IV along with additional process descriptions. The absorption of the EM energy by the electrons at the critical surface and the subsequent transfer of this energy into the random thermal motion (temperature) of other electrons will also be developed and discussed in Chapter IV.

The linear variation of density of a plasma models the plasma surrounding a laser fusion target which has been slightly heated to create a thin enclosing plasma. The electromagnetic wave considered is then the laser beam used to heat the plasma. Resonance absorption is expected to contribute significantly to the heating of the pellet because collisional losses are quite ineffective as the plasma (target) temperature increases.

The aim here is to develop a simple model of the absorption mechanisms and effects using a minimum of computer space and time. The effort will be described as follows. In Chapter II the equations to be solved which describe resonance absorption in a linear plasma are derived, as is the term that determines the damping of the plasma waves (Landau damping). In Chapter III the numerical methods for solving these equations are discussed, and the results are presented in Chapter IV. CGS (Gaussian) units will be used throughout this paper to enable comparison to related research.

## II Linear Modeling

Two types of plasmas were analyzed. First, a cold electron plasma with no electron pressure and then a plasma of warm electrons with a pressure gradient. In each case, the ions were assumed to be immobile and an electron-ion collision probability was included. The plasma density gradient necessary for resonance absorption was chosen as a linear ramp in the z-direction. The linear analysis was achieved by using Maxwell's equations and the plasma fluid equation for electron momentum. This chapter will outline the equations used and assumptions made in order to obtain the wave equations solved in the plasma. Complicated derivations of equations included in this work are contained in Appendix A.

### Linearizing the Equations

Maxwell's equations and the continuity and momentum equations for electrons are (in Gaussian units):

$$\begin{aligned}\frac{dn}{dt} + \nabla \cdot n\underline{v} &= 0 \\ mn\left(\frac{d\underline{v}}{dt} + \underline{v}\underline{v} + \underline{v} \cdot \nabla \underline{v}\right) + \nabla p &= e n \underline{E} \\ \nabla \times \underline{E} &= -\frac{1}{c} \frac{d\underline{B}}{dt} \\ \nabla \times \underline{B} &= \frac{4\pi}{c} \underline{j} + \frac{1}{c} \frac{d\underline{E}}{dt} \\ \nabla \cdot \underline{E} &= 4\pi e n \\ \nabla \cdot \underline{B} &= 0\end{aligned}\tag{2.1}$$

further

$$\begin{aligned} j &= n e \underline{v} \\ P &= \gamma T n \end{aligned} \tag{2.1}$$

where

$\underline{v}$  is the electron-ion (inverse bremsstrahlung) collision frequency

$n$  is the electron number density

$\underline{v}$  is the electron velocity

$m$  is the electron mass

$\gamma$  is the ratio of specific heats (3 in this one-dimensional problem)

$T$  is electron temperature in ev

$j$  is electron current

$\underline{B}$  is magnetic field intensity

$\underline{E}$  is electric field intensity

$e$  is electron charge

$P$  is electron pressure

Linearizing approximations were made assuming wavelike solutions as follows:

$$\begin{aligned} n &= n_0 + n_1 e^{-i\omega t} + iksx \\ \underline{v} &= \underline{v}_1 e^{-i\omega t} + iksx \\ \underline{E} &= \underline{E}_0 + \underline{E}_1 e^{-i\omega t} + iksx \\ \underline{B} &= \underline{B}_0 + \underline{B}_1 e^{-i\omega t} + iksx \end{aligned} \tag{2.2}$$

where

$s$  is the sine of the incident angle  $\theta$

Hence, steady-state solutions were the object of the investigation and oscillations around equilibrium values the result.

### TE Mode Solution

The transverse electric mode does not exhibit resonance absorption because its electric field is perpendicular to the plasma density gradient. This can be seen by examining the wave equation for  $E_y$ . To do this, the above quantities (Eqs 2.2) were substituted into Eqs (2.1) and resulted in the following set of equations for the TE mode.

$$E'_y = ikB_x$$

$$sE_y = B_z$$

$$iksE_y + E'_y = 4\pi n_1 e$$

$$-iksB_z + B'_x = -ik\epsilon E_y$$

$$an'_0 n_1 - an'_1 = 0$$

$$iks(n_0 - n_1) = 0$$

(2.3)

where

$$a = \frac{i4\pi e\gamma T}{cm(\omega + iv_L)},$$

' denotes differentiation with respect to  $z$

and

$$\epsilon = 1 - \omega_p^2/\omega^2(1 + iv/\omega) \quad (2.4)$$

Also,  $\omega_p$  is the local plasma frequency which is given by:

$$\omega_p^2 = \frac{4\pi n_0 e^2}{m}$$

From these equations was derived the fact that  $N_1 = 0$ , and that the second-order equation for  $E$  is:

$$E_y'' + k^2(\epsilon - s^2)E_y = 0 \quad (2.5)$$

Thus, there is no plasma wave generated and no resonance absorption occurs in the TE mode. This fact and Eq (2.5) are presented in Reference 1.

#### TM Mode Solution

A resonance is expected for the TM case where the electric field has a component parallel to the plasma density gradient. This, too, can be gleaned from an examination of the second-order equations derived from Eqs (2.1). First, the equations were solved for the TM mode with a plasma number density gradient again in the  $z$ -direction and an electron temperature. The resulting four equations model linear resonance absorption phenomena and formed the basis for this work.

$$\begin{aligned} ikB &= E'_x - iksE_z \\ -ik\epsilon E_x &= aiksn_1 - B' \\ -ik\epsilon E_z + a\beta n_1 - an'_1 &= iksB \\ iksE_x + E'_z &= 4\pi en_1 \end{aligned} \quad (2.6)$$

where  $\beta = \frac{1}{n_0} n'_0$  and all other variables have been previously defined.

Consequences of the Density Profile. As mentioned earlier, the plasma density variation was chosen as a linear ramp profile. The number density increased from virtually zero at the front face to  $1.12 \times 10^{19} \text{ cm}^{-3}$  two free-space wavelengths into the plasma. At that point, the plasma frequency ( $\omega_p$ ) equaled the frequency of the incident .001 cm (10  $\mu\text{m}$ ) light. This is the point at which resonance (formation of plasma waves) occurs and is called the critical surface. The linear variation in number density made it possible to write:

$$n_0 = n_c (z/L) \quad (2.7)$$

$$\beta = 1/z \quad (2.8)$$

$$\epsilon = 1 - z/(L + izv_c/\omega)$$

where

$n_c$  is the value of  $n$  at the critical surface

$v_c$  is the value of the electron-ion collision frequency at the critical surface

$L$  is the distance to the critical surface

$z$  is the position in the plasma (measured from the front face)

Cold Plasma. For the cold plasma case, the terms involving  $T$  in Eqs (2.6) are set to zero. This is the same as ignoring the term " $\nabla P$ " in the momentum equation and results in the following equations:

$$\begin{aligned}
 ikB &= E'_x - iksE_z \\
 ikeE_x &= B' \\
 -ikeE_z &= iksB \\
 iksE_x + E'_z &= 4\pi en_1
 \end{aligned} \tag{2.9}$$

where all the terms have been previously defined.

It is inconsistent to allow the electrons to have no temperature and assume a finite collision frequency since the two are related by (Ref 2:30, Eq 3.4):

$$v/\omega = 24.7 n_c/n_0 (T^{3/2}) ; T \text{ in ev} \tag{2.10}$$

However, the  $v/\omega$  damping must be included in the equations to avoid an infinite resonance condition at the critical surface. Later,  $v/\omega$  and Eq (2.10) will be used to obtain an effective temperature. Unless otherwise stated,  $v/\omega$  was chosen small enough so that only resonance absorption was observed.

### Second-Order Equations

The purpose of the preceding derivations was to obtain linearized equations which could be easily converted into wave equations for the quantities of interest. The algebraic manipulations resulting in these equations are included in Appendix A and here, only the second-order equations will be presented.

Only one second-order equation was necessary for the cold plasma. It was written in terms of  $E_z$  and took the form (Ref 1:572, Eq 3.1):

$$E_z'' + k^2(\epsilon - s^2)E_z + [E_z(\ln\epsilon)']' = 0 \quad (2.11)$$

For the warm plasma, it was necessary to write two coupled second-order equations. Two sets of these were derived from Eqs (2.6). The first set couples  $N_1$  and  $E_z$ :

$$E_z'' + (k^2\epsilon - k^2s^2)E_z = (4\pi e + aik)N_1' - aik\beta N_1 \quad (2.12)$$

and

$$aN_1'' + (a' - a\beta)N_1' + (4\pi\epsilon eik - a'\beta - ak^2s^2)N_1 = -ik\epsilon'E_z$$

while the next couples  $B$  and  $E_z$ .

$$\begin{aligned} E_z'' + (-\beta + \frac{ik\alpha ks^2}{(\epsilon + \alpha iks^2)})E_z' + (-k^2s^2 + \frac{ik\epsilon}{\alpha})E_z \\ = (-\frac{iks}{\alpha} + k^2s)B + \frac{s\beta B'}{(\epsilon + \alpha iks^2)} \end{aligned} \quad (2.13)$$

and

$$\begin{aligned} B'' - (\frac{\epsilon' + i\alpha'ks^2 + \alpha\beta iks^2}{(\epsilon + \alpha iks^2)})B' + (k^2\epsilon - k^2s^2)B \\ = E_z' iks \frac{(\epsilon\alpha' + \alpha\beta\epsilon - \alpha\epsilon')}{(\epsilon + \alpha iks^2)} \end{aligned}$$

where

$$\alpha = \frac{iT\gamma}{cm\omega(1 + iv_L/\omega)}$$

The warm plasma approximation is achieved by retaining the  $\nabla P$  term in the electron momentum equation. This resulted in the terms containing  $v_L/\omega$  in Eqs (2.6) which appears in  $\alpha$  of Eqs (2.13). This term  $(v_L/\omega)$ , which has thus far remained undefined, is an attempt to model Landau damping of the

plasma wave and will now be explained. Ginzburg's second-order equations (Ref 3:397, Eqs 20.35) for  $E_z$  and  $B$  are similar to Eqs (2.13) although they do not include Landau damping.

### Landau Damping

That there is Landau damping of plasma waves has been derived from the Vlasov equation:

$$\frac{df}{dt} + \mathbf{v} \cdot \nabla f + \frac{eE}{m} \cdot \frac{df}{dv} = 0 \quad (2.14)$$

There is linear and nonlinear Landau damping. The latter is associated with particle trapping when  $n_1 \approx n_0$  and is not within the limits of linear theory. The derivation of Landau damping from Vlasov's equation is discussed in detail by Chen (Ref 4:213-240) and Ginzburg (Ref 3:122-132), and I will follow Chen's method closely. The physical interpretation of linear Landau damping was hinted at earlier. Simply, the plasma wave is damped without collisions by exchanging its energy with particles satisfying the relation  $|\mathbf{v} - \mathbf{v}_z|t < \frac{\pi}{k} = \frac{\lambda}{2}$ . These are the particles in the distribution that have not yet traveled one-half wavelength with respect to the wave. Hence, initial conditions, such as the assumption of a Maxwellian velocity distribution, are important.

The form of Landau damping employed in this work was derived in the following way. First, wavelike solutions to the Vlasov equation are assumed with first-order perturbations on the equilibrium values. The solutions take the form:

$$f(r, v, t) = f_0(v) + f_1(r, v, t) \quad (2.15)$$

where

$$f_1 \propto e^{i(k_z - \omega t)}$$

Vlasov's equation then becomes:

$$-i\omega f_1 + ikV_z f_1 = \frac{e}{m} E_z \frac{df_0}{dv_z} \quad (2.16)$$

giving:

$$f_1 = \frac{ieE_z}{m} \frac{df_0/dv_z}{\omega - k_z V_z} \quad (2.17)$$

From Poisson's equation ignoring  $E_x$ :

$$ikE_z = -4\pi e n_1 = -4\pi e \iiint f_1 d^3 v \quad (2.18)$$

For a one-dimensional problem, the dispersion relationship becomes:

$$1 = \frac{\omega^2}{k_z^2} \int_{-\infty}^{\infty} \frac{df_0/dv_z}{(v_z - \omega/k)} dv_z \quad (2.19)$$

So, for large  $V_z$  and small damping, the dispersion relation results from an integration along the real axis plus a semicircle resulting from the integration around the pole in the complex  $V_z$  plane at  $V_z = \omega/k$ . Thus, the dispersion relation can be given by (Ref 4:216, Eq 7-56):

$$1 = \frac{\omega^2}{k_z^2} \left[ P \int_{-\infty}^{\infty} \frac{df_0/dv_z}{v_z - \omega/k} dv_z + \frac{i\pi df_0}{dv_z} \Big|_{V_z=\omega/k_z} \right] \quad (2.20)$$

where

P is the Cauchy principal value ( $\frac{k_z^2}{\omega}$  in this case).

The imaginary part of this dispersion relationship accounting for the wave damping is:

$$1 = i\pi\omega_p^2/k_z^2 \left. \frac{\hat{df}_0}{dv_z} \right|_{v_z=\omega/k_z} \quad (2.21)$$

for a Maxwellian:

$$\frac{\hat{df}_0}{dv_z} = \frac{-2v_z}{\sqrt{\pi} v + n^3} \exp\left(\frac{-v_z^2}{v_{th}^3}\right)$$

Therefore, since  $k_z^2 = v_L^2/v_c^2$  and we prefer not to make the substitution  $\omega = \omega_p$

$$-im(\omega/\omega_p) = 1.88 \left( \frac{v_\phi}{v_{th}} \right)^{3/2} \exp\left(\frac{-v_\phi}{v_{th}}\right) \approx v_L/\omega \quad (2.22)$$

where

$v_\phi$  has replaced  $v_z$  as the phase velocity of the wave

The wave equations for  $N_1$  and  $E_z$  were presented earlier.

The wave number in the  $z$ -direction ( $k_z$ ) for these waves was determined as:

$$k_z(z) = k \sqrt{\epsilon(z)} / \sqrt{\gamma T/mc^2} \quad (2.23)$$

where

$$k = \omega/c$$

The complete derivation of Eq (2.23), including assumptions, is included in Appendix A. The wavelength and phase velocity of the longitudinal waves were determined directly from

$k_z$ . The desired result,  $v_L/\omega$  was then obtained from Eq (2.22) as a function of  $z$  throughout the plasma and is shown in Figure 4. Note that  $v_L/\omega$  is temperature independent, since in the ratio  $v_\phi/v_{th}$  each quantity has a  $T^{1/2}$  dependence. Past the critical surface, the wave is exponentially attenuated by  $\epsilon$  so Landau damping is not tediously modeled there.

Still, the expression for Landau damping Eq (2.22) fails when  $v_\phi \approx v_{th}$ , and  $v_\phi = 2v_{th}$  when  $\epsilon = .4$  or about halfway into the plasma. In that region,  $v_L/\omega$  is large which makes for a bad approximation, since the pole in the complex integration (Eq 2.20) lies far from the real axis. This, coupled with the fact that the plasma wave is generated closer to the front boundary for increasing temperatures, causes a breakdown of the warm plasma model at high temperatures. This will be discussed in Chapter IV. Simply, for the bulk of the results presented in this work,  $v_L/\omega$  was taken as a constant in the plasma. Still, as will be shown later, the correct form of  $v_L/\omega$  is important. Having presented here the equations, assumptions, and some background, the next chapter will deal with the numerical methods used to solve the problem.

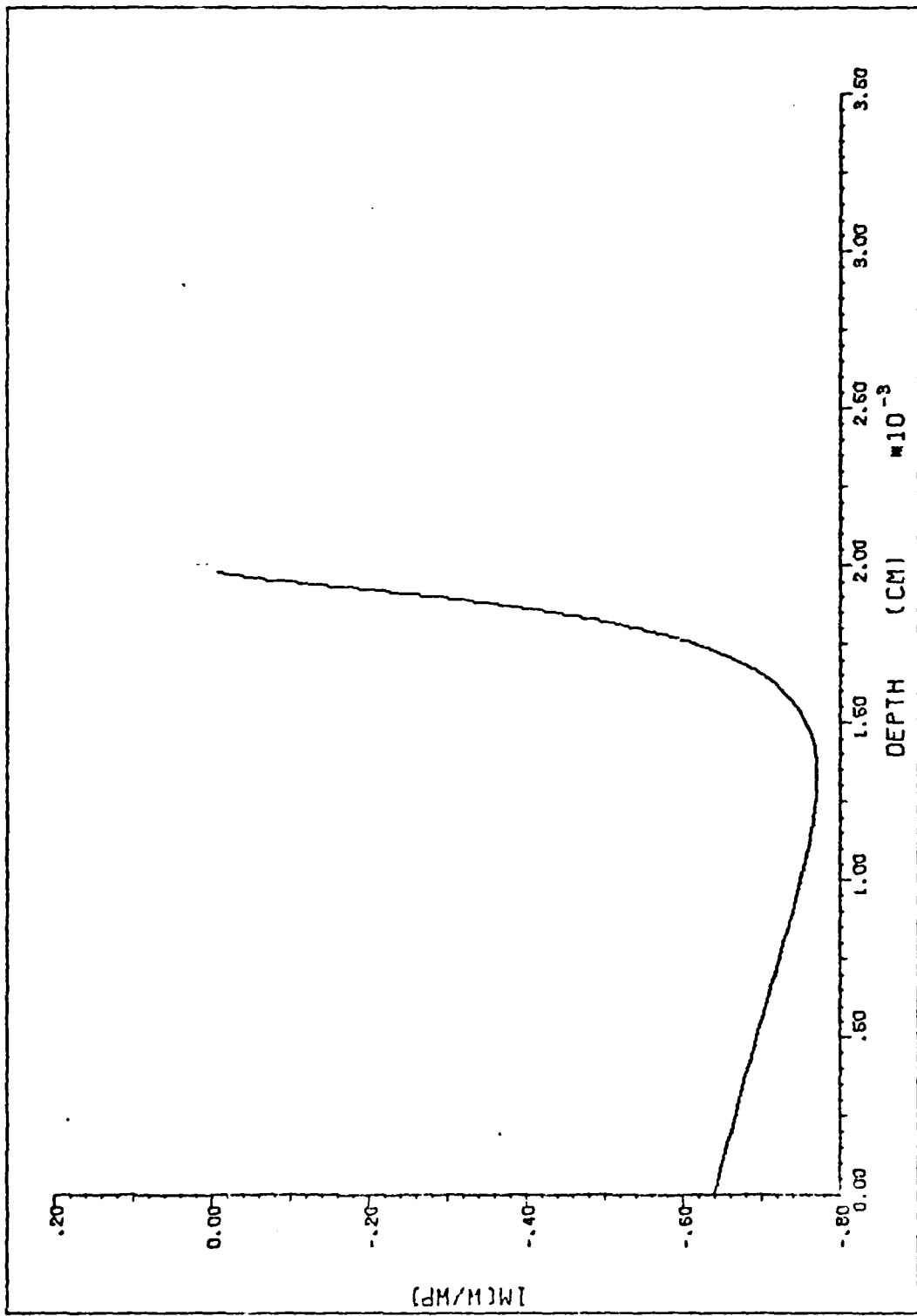


Fig 4. Landau Damping ( $v_L/\omega = -\text{im}(\omega/\omega_p)$ ) as a Function of Location in the Plasma

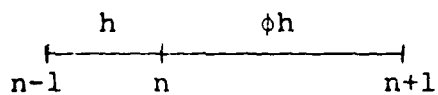
### III Numerical Methods

Starting with the appropriate set of Eqs (2.6) or (2.9), second-order equations were derived that described the fields inside the plasma. For the cold case, it was found that one equation for  $E_z$  could be written. But, for the warm plasma, a set of two coupled equations was required. The equations, (2.11) and (2.13), were solved numerically inside the plasma subject to appropriate boundary conditions. The values thus generated were used to solve for the other field quantities,  $N_1$ ,  $v_{os}$  and the Ponderomotive force. This entire procedure will be described in detail.

#### Gridding

The numerical solution began with a choice of a gridding scheme. Due to the resonance expected at the critical surface, very fine numerical resolution was needed in that region. However, the same resolution was not necessary in other parts of the plasma so a differential gridding scheme was adopted. This affected the form of the central difference approximations to the first and second derivatives in Eqs. (2.11) and (2.13).

The problem of derivatives across these nonuniform spaces was handled by adopting a technique used by Smith (Ref 5:139). Beginning with adjacent nonequal mesh spaces:



The Taylor series expansion of a function  $A(z)$  about a point "n" can be written in two ways.

$$A_{n+1} = A_n + \phi h A' + \frac{1}{2} h^2 \phi^2 A'' + (\text{terms of order } h^3) \quad (3.1)$$

$$A_{n-1} = A_n - h A' + \frac{1}{2} h^2 \phi^2 A'' - (\text{terms of order } h^2)$$

eliminating  $A''$  gives:

$$A' = \frac{A_{n+1} - \phi^2 A_{n-1} - (1 - \phi^2) A_n}{\phi h (1 + \phi)} \quad (3.2)$$

and eliminating  $A'$  results in:

$$A'' = \frac{A_{n+1} + \phi A_{n-1} - A_n - \phi A_n}{\phi^2 h^2 / 2 + \phi h^2 / 2} \quad (3.3)$$

The error in the second-derivative approximation is of order  $h$  and is the driving source of numerical error.

The majority of the plasma was gridded with equal mesh spaces in which case, Eqs (3.2) and (3.3) reduce to standard centered differences. Two mesh sizes were specified: a very fine mesh spacing (on the order of  $\frac{v_L}{\omega} \times 10^{-2}$ ) near the critical surface to resolve the resonance peak and a coarser gridding (on the order of  $\frac{\lambda}{10} \rightarrow \frac{\lambda}{100}$ ) in the rest of the plasma. The size of the mesh spaces (coarse and fine) was determined somewhat by trial and error. Each was reduced until the field values and absorption did not change. The coarser gridding was required to be smaller for the warm plasma case due to the plasma waves present before the

critical surface. In the region between the two extremes, each mesh space was doubled until the spacing was slightly less than or equal to the predetermined coarse grid maximum. The remainder of the grid was then completed with equal mesh spaces of that size.

#### Differencing the Equations

To implement the sweep method employed, the value of each variable at mesh point "n" was assumed to be representable by:

$$E_{z(n+1)} = PE_{zn} + Q \quad (3.4)$$

in the cold case, and for the coupled case

$$\begin{aligned} E_{z(n+1)} &= KE_{z(n)} + LB_{(n)} + M \\ B_{(n+1)} &= NE_{z(n)} + OB_{(n)} + R \end{aligned} \quad (3.5)$$

where

K, P, Q, L, M, N, O, and R are constants

These equations were used in conjunction with Eqs (3.2) and (3.3) to difference Eqs (2.11) and (2.13). The objective was to solve the differenced equations for the values of the constants at each mesh point in the plasma subject to the correct boundary conditions. Details of the derivation are included in Appendix A.

### Application of Boundary Conditions

The equations were solved by employing boundary conditions at the front face and past the critical surface in the plasma. The two-sweep method began by setting the fields equal to zero past the critical surface in the plasma. Two wavelengths past the critical surface was chosen as the point where the fields vanished. This distance proved to be adequate to assure sufficient decay since the wave was decaying exponentially in this region. After applying this boundary condition, the constants in Eqs (3.4) and (3.5) were evaluated at each mesh point. The sweep began at the point where the fields vanished and progressed point by point to the front face, where the radiation boundary condition was applied. The radiation boundary condition forced conservation of the fields at that point and determined their values. Then it was a simple matter to solve for the field quantities point by point using the previously determined constants.

Zero Boundary Condition. The zero boundary condition took the form:

$$E_z(4\lambda) = B(4\lambda) = 0 \quad (3.6)$$

which was interpreted as:  $P = Q = L = M = N = O = R = K = 0$   
Due to this boundary condition, the constants not multiplying a variable (M and R from Eqs 3.4 and 3.5) were found to be identically zero throughout the plasma. Therefore, they were not necessary and the equations became:

$$E_z(n+1) = PE_z(n) \quad (3.7)$$

for the cold plasma, and

$$E_z(n+1) = KE_z(n) + LB(n) \quad (3.8)$$

$$B_z(n+1) = NE_z(n) + OB(n)$$

for the warm plasma. In other words, the fields were assumed to vanish two free space wavelengths past the critical surface. This was accomplished by setting the constants equal to zero at that point. This made some of the constants unnecessary. The remainder of the constants were then determined at each mesh point marching toward the front face of the plasma.

Radiation Boundary Condition. At the front face, the radiation boundary condition was applied. From the fact that:

$$\begin{aligned} E_{inc} &= E_{0_{inc}} e^{ik(sx + \cos\theta z)} \\ B_{inc} &= B_{0_{inc}} e^{ik(sx + \cos\theta z)} \\ E_{sc} &= E_{0_{sc}} e^{ik(sx - \cos\theta z)} \\ B_{sc} &= B_{0_{sc}} e^{ik(sx - \cos\theta z)} \end{aligned} \quad (3.9)$$

it can be shown that

$$E'_{sc} + ik\cos\theta E_{sc} = 0 \quad (3.10)$$

and

$$B'_{sc} + ik\cos\theta B_{sc} = 0$$

and since  $E = E_{inc} + E_{sc}$  and  $B = B_{inc} + B_{sc}$ :

$$E'_z + ik\cos\theta E = 2ik\cos\theta E_{inc} \quad (3.11)$$

$$B' + ik\cos\theta B = 2ik\cos\theta B_{inc}$$

These (Eqs 3.11) are the radiation boundary conditions appropriate at the front face. They were applied to the electric field in the cold plasma case and to the electric and magnetic fields when they were coupled in the warm plasma case.

The radiation boundary condition was applied by solving the Taylor series expansion of the field at the front face simultaneously with the wave equation Eqs (2.11) or (2.13). The equations are each solved for the first derivative of the desired quantity ( $E_z$  or  $B$ ). Since each is treated similarly, only  $E_z$  will be developed in this discussion. The solution is then substituted into the radiation boundary condition and that equation is solved for  $E_z$ . When  $E_z$  has been found, the forward sweep begins using Eqs (3.7) and (3.8). The complete derivation of the application of the radiation boundary condition is contained in Appendix A.

The forward sweep completes the calculation of the differenced variable(s). Other quantities of interest were then calculated using Eqs (2.3) or (2.6). Plots of these quantities are contained in Appendices B and C for both cases and a discussion of the results follows here.

#### IV Results

A wide variety of conditions were investigated and a large body of results obtained from the two computer codes written to implement the two-sweep algorithm just described. In this chapter the major results will be presented. The data from which these results were derived is contained in Appendices B and C. The figures in these Appendices indicate the spatial variation of important quantities in the plasma. The quantities investigated were the x and z components of the electric field, the magnetic field, the oscillation velocity of the hot ( $n_1$ ) electrons, and the Ponderomotive force (time-averaged Lorentz force or radiation pressure). The collisional and collisionless (Landau damping) absorption of the electromagnetic waves energy was also determined as a function of the angle of incidence.

Some of the results, such as the percentage of the laser energy absorbed by the plasma are independent of power, barring instabilities, while others scale as the electric field ( $n_1$  and  $V_{os}$ ). Ponderomotive force is directly proportional to power as is the energy of the hot electrons ( $T_H$  ev). The results will be discussed independent of power scaling and then the effect of power will be considered. Temperature effects, such as Landau damping, will be dealt with as they apply. Finally, the validity of these methods will be discussed referencing both power and temperature concerns.

### Parameters

Some parameters were not varied throughout the analysis. They are now identified for reference and comparison with other works.

$$E_z^{\text{inc}} = \sin\theta$$

$$E_x^{\text{inc}} = \cos\theta$$

$$B_{\text{inc}} = -1$$

$$\lambda = .001 \text{ cm (} 10 \mu\text{m free space wavelength)}$$

$$\omega = 1.88 \times 10^{14} \text{ sec}^{-1}$$

$$n_c = 1.12 \times 10^{19} / \text{cm}^3 \text{ (critical number density)}$$

$$k = 2\pi/\lambda = 6283 \text{ cm}^{-1}$$

$$L = .002 \text{ cm (critical length)}$$

It is readily determined that  $P_0$ , the incident power in this analysis, was  $120 \text{ W/cm}^2$ . As mentioned, linear power scaling was employed to determine values of variables of interest at current laser powers.

### $E_x$ and $B_y$

The field quantities  $E_x$  and  $B_y$  were calculated for both cold and warm plasmas and are included in the Appendices for reference. Although  $E_x$  does exhibit a peak at the critical surface, its value there varies from only 2-4 esu over all the cases investigated. The transverse magnetic

field was virtually unaffected by the resonance at the critical surface, and its peak in the plasma remained approximately 1.5 esu throughout the study. Since  $E_x$  does not contribute to resonance absorption other than through collisions, and drifts involving the magnetic field were not considered, these two quantities were not of significant interest and will not be further discussed.

#### $E_z$ (Longitudinal Electric Field)

The magnitude and characteristics of  $E_z$  are of interest because it is the component of the electric field that excites the plasma wave and is responsible for resonant absorption.

Cold Plasma. The longitudinal field in the cold plasma exhibits a marked resonance at precisely the critical surface. The magnitude of the field is inversely proportional to the value of  $v/\omega$ . The fact that  $|E_z|_{\max} \propto v/\omega$  was derived by Ginzburg (Ref 3:388). Some comparisons were made with the maximum electric fields predicted by other authors. For various angles of incidence, results comparable to those of Denisov (Ref 1:574) were observed. For example, for  $\sin\theta = .3$ ;  $v/\omega = .002$ ,  $|E_z|_{\max} = 52$  and for  $v/\omega = .02$ ,  $|E_z|_{\max} = 5.1$  at the same angle of incidence. The magnitude of  $E_z$  and its dependencies are much different for the warm plasma.

Warm Plasma. Linear Landau damping, as well as collisional inverse-bremsstrahlung, affect the longitudinal

electric field in the warm plasma regime. As noted earlier, temperature effects moved the resonance peak of  $E_z$  toward the front of the plasma. The magnitude of the field at resonance was also much less than that observed in the cold plasma. The damping was more severe and the resonance moved further to the left as temperature increased. The fact that the field maximum decreased is not surprising since the turning point of the wave varies with temperature. The wave turns (is reflected) when:

$$\epsilon = \gamma T / c m \omega (1 + i v_L / \omega) \quad (4.1)$$

Hence, for higher temperatures the wave is reflected closer to the front of the plasma (at a larger  $\epsilon$ ) and the evanescent region becomes larger. This allows less of the evanescent wave to reach the critical surface and initiate resonant absorption. The wavelength of this electrostatic wave ( $E_z$ ) is, not surprisingly, the same as that for  $n_1$ :

$$\lambda_z(z) = \lambda \sqrt{\gamma T / m c^2} / \sqrt{\epsilon(z)} \quad (4.2)$$

This wavelength ( $\lambda_z$ ) derived from  $k_z$  (see Appendix A) was observed in the study. It follows from Eq (4.2) that for higher temperatures, in regions where  $\epsilon$  is small, the wavelength is greater than that of the incident light and  $\lambda_z$  clearly approaches infinity at the critical surface. For low temperature cases, the wavelength can be much shorter than the incident wavelength very near the critical surface. Examples of this can be seen in Appendix C. For

instance, one may compare the wavelengths of  $E_z$  near the critical surface in Figures C-8 and C-15.

Spatial Dispersion. To conclude this discussion of the longitudinal electric field, the effect of spatial dispersion will be addressed. Ginzburg (Ref 3:389) suggests that the use of a local value of  $\epsilon$  will not be valid if the electron encounters vastly different electric fields during its travel in the characteristic time under consideration. Ginzburg's equation for the distance over which  $E_z$  decreases to half its maximum value in a cold plasma is (Ref 3:389, Eq 20.24):

$$\Delta z = L v_c / \omega \quad (4.3)$$

The results obtained here for the cold plasma obey this relationship. This accounts for gridding difficulties encountered as  $v/\omega$  was reduced because in addition to the increase of  $|E_z|_{\max}$ , the scale length given by Eq (4.3) decreased. The scale length is on the order of a Debye length for the cold plasma when  $v/\omega = .002$ . The gradient lengths observed in the warm plasma are clearly longer. Figure 5 shows for each temperature at what power the hot electrons ( $n_1$ ) will travel one scale length in one period  $(\frac{2\pi}{\omega})$ . At powers higher than this, spatial dispersion should not be ignored. The scale length referred to is the same as that above, i.e. the distance over which  $E_z$  decreases to one-half its maximum value. The figure shows both the cold plasma case and the warm plasma results for  $v_L/\omega = .1$ . The

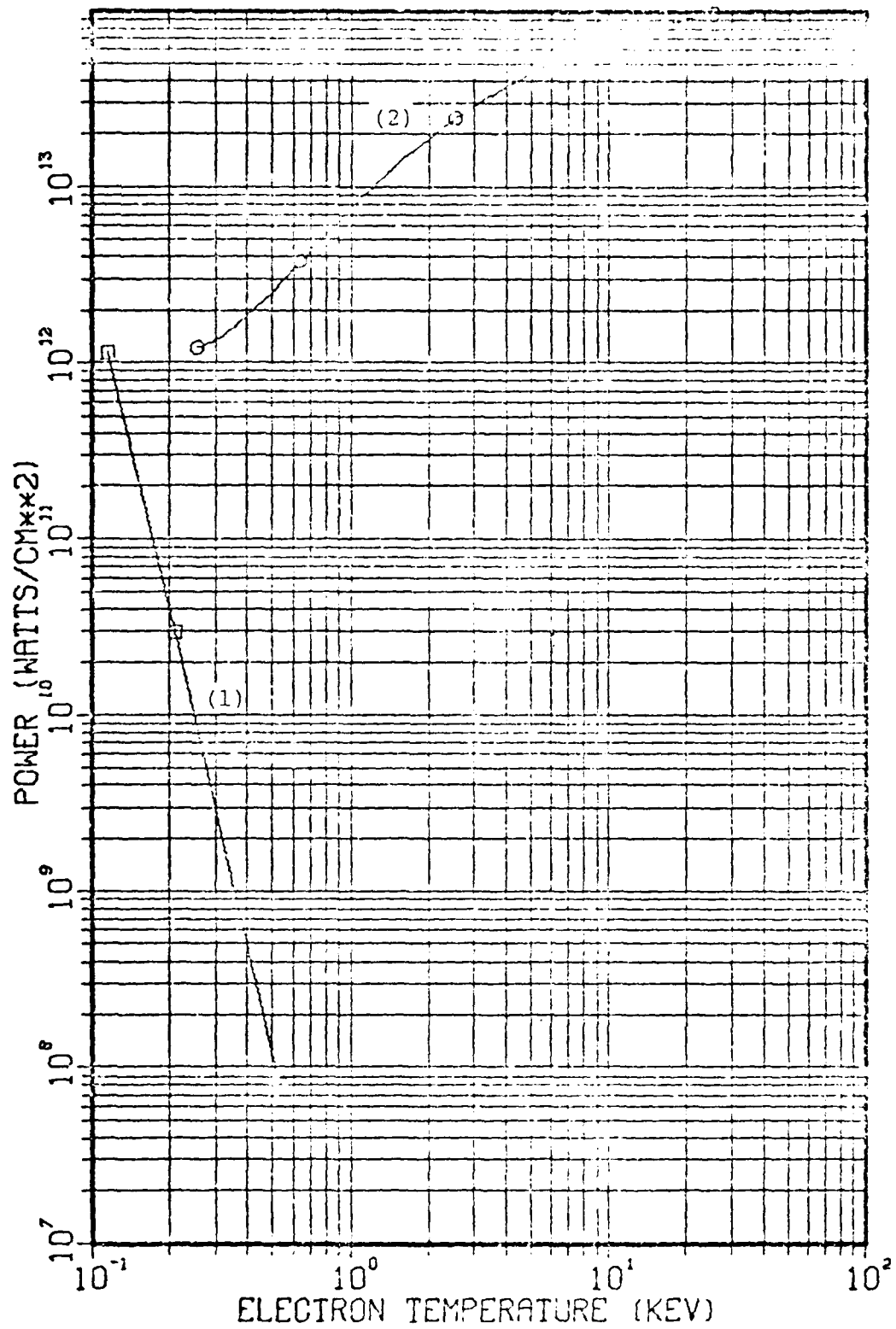


Fig 5. Power at Which Spatial Dispersion Becomes Important ( $2\pi V_{OS}/\omega = \Delta z$ ) as a Function of Background Electron Temperature: Curve 1; Cold Plasma  $T = (24.7\omega/v)^{2/3}$ , Curve 2; Warm Plasma  $v_L/\omega = .1$

results for the warm plasma when  $v_L/\omega = .67$  are not significantly different. Spatial dispersion will not be considered as a limiting factor in the models application. Still, it warrants more study, and the above is offered as both a motivation and a starting point.

#### The Plasma Wave ( $n_1$ )

A plasma wave exists because the electric field has a component ( $E_z$ ) along the density gradient in the plasma causing charge imbalance and, hence, a restoring force. The electrons oscillate at the phase velocity  $\omega/k_z$ , where  $k_z$  here is the same as the  $k_z$  derived earlier for  $E_z$ . In the cold plasma, the enhancement of  $n_1$  at the critical surface is so large as to cause concern over the linearizing approximation  $n_0 \gg n_1$ . In the warm plasma, the wave generally has a smaller amplitude and is itself allowed to damp noncollisionally by exchanging its energy with colder electrons in the body of the Maxwellian distribution. Thus, the wave is a key performer in both the warm and cold scenarios.

Cold Plasma. The cold plasma wave is very much like  $E_z$ . In fact, no second-order equation was solved for  $n_1$ , and it was obtained by using the calculated values of  $E_z$  in an equation derived from the four basic relationships Eqs (2.9).

$$n_1 = -\epsilon'E_z/\epsilon 4\pi e \quad (4.4)$$

Clearly,  $n_1$  behaves much like  $E_z$  and, like  $E_z$ , it is prevented from becoming infinite at the critical surface by collisions. The plasma waves relationship to  $E_z$  leads to the cold model predicting increasing  $n_1$  for increasing temperatures (decreasing  $v/\omega$ ). Figure 6 shows the variation of  $n_1$  with temperature for the cold plasma, and the warm plasma with  $v_L/\omega = .1$ . The figure demonstrates this by detailing for what power and temperature the peak plasma wave amplitude (near the critical surface) equals  $1.12 \times 10^{19} \text{ cm}^{-3}$  (the value of  $n_0$  at the critical surface). This further serves to show when the linearizing approximation  $n_0 \gg n_1$  is valid. The region of validity is shown on the figure for both the cold and warm plasma models. The additional restriction on the validity of the warm model will be explained later. The characteristics of the warm plasma electron wave will now be explored.

Warm Plasma. When temperature effects are introduced,  $n_1$  is reduced greatly in magnitude and spread over a larger portion of the plasma. For high temperatures large waves exist far from the critical surface and may even impinge on the front boundary. This translation of the wave from the critical surface to the boundary occurs because as the electron temperature increases, the hot electrons created at the critical surface are allowed to transfer their energy more readily to the other electrons in the distribution. This suggests that a temperature dependent as well as spatially dependent Landau damping is appropriate.

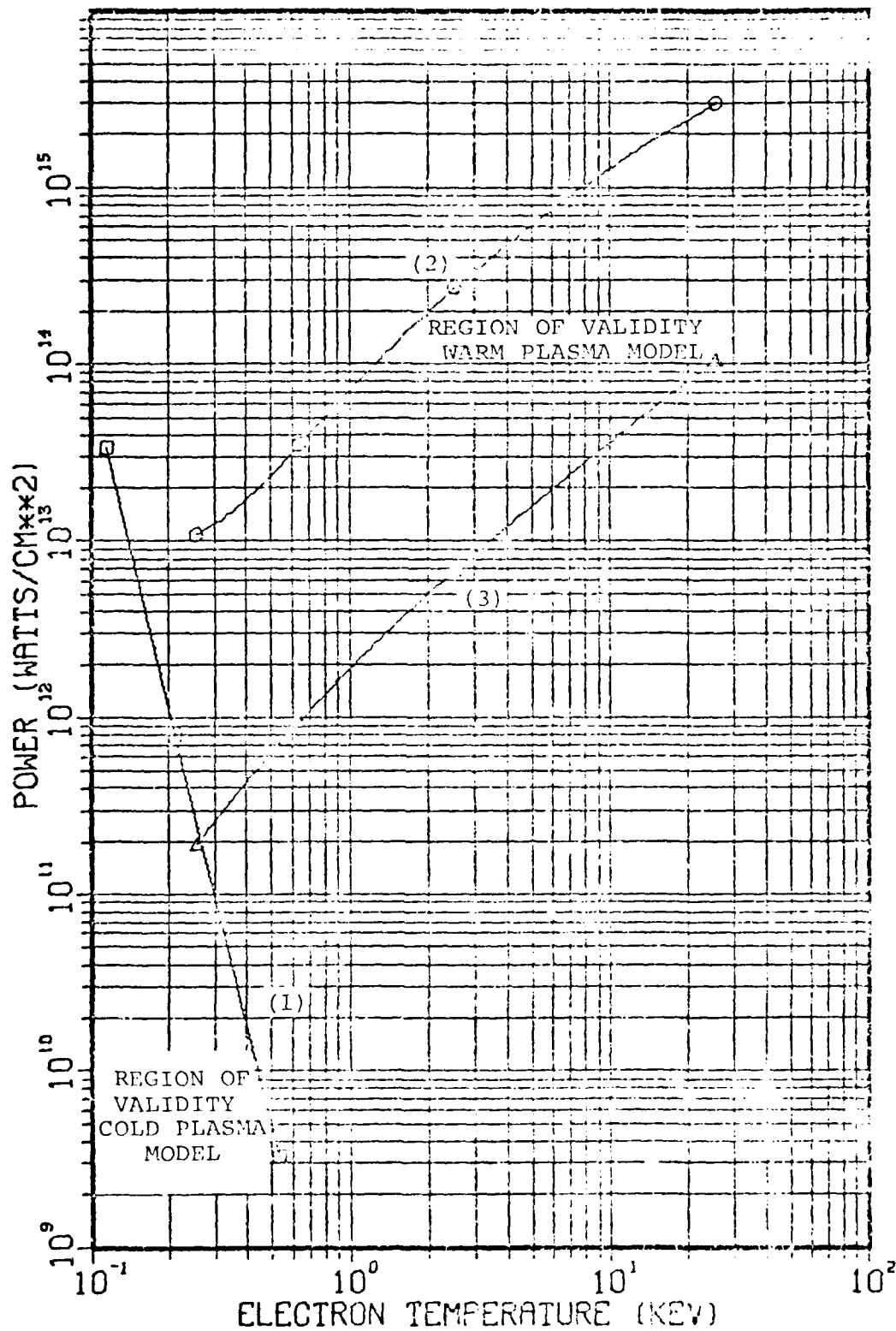


Fig 6. Regions of Validity (Indicated by Arrows) for the Warm and Cold Plasma Models. Regions are bounded by the following curves representing limiting assumptions: Curve 1; cold plasma  $n_1=n_0$ ; Curve 2; warm plasma  $(v_L/\omega=.1) n_1=n_0$ , Curve 3; warm plasma  $(v_L/\omega=.1) v_H=v_c$ .

Nevertheless, as mentioned earlier, the electron plasma wave should be greatly attenuated in the vicinity of the front face because  $v_H \approx v_C$  there. The reason for this (discussed in Chapter II) is that when  $v_H \approx v_C$ , the pole in the integration of Eq (2.19) lies far from the real axis and contributes a large imaginary part (damping) to  $v_L$ . This effect is ignored in the derivation of Eq (2.22) and thus Figure 4 does not show this large damping and it was not incorporated into the model.

In the warm plasma, as in the cold,  $n_1$  was derived from the field quantities. In this case  $E_z'$ ,  $B$  and Eqs (2.6) were used. The equation derived was:

$$n_1 = (E_z' + sB'/\epsilon) / \left( \frac{aik\epsilon^2}{\epsilon} + 4\pi e \right) \quad (4.5)$$

and centered differences were used for the derivatives. In addition to describing the variation of the peak of  $n_1$  with temperature for  $v_L/\omega = .1$ , Figure 6 shows where the velocity of the hot electrons equals that of the cold. The significance of this has been discussed, and the plot establishes a lower bound on the region of validity of the warm plasma model. The plasma's absorption of the electromagnetic energy will now be considered.

### Absorption

Two methods of absorption of electromagnetic energy by the plasma were analyzed. They were collisional (electron-ion inverse bremsstrahlung) and collisionless (Landau

damping of the plasma wave). Other absorption mechanisms, including instabilities, were ignored.

The power absorbed was calculated by comparing the reflected electric field at the boundary of the plasma with the incident field. The reflected fraction "R" was derived in the following way. Since:

$$E_z^{sc} = E_z^{tot} - E_z^{inc} \quad (4.6)$$

where

$E_z^{sc}$  is the scattered electric field at the front face

$E_z^{inc}$  is the incident field ( $\sin\theta$ )

and  $E_z^{tot}$  is the value of the field at the front face

The value of  $E_z^{sc}$  is determined because the values of the total and incident field are known. From geometry:

$$E_x^{sc} = E_z^{sc}/\tan\theta \quad (4.7)$$

and thus

$$R = \frac{\langle S_z \rangle_{sc}}{\langle S_z \rangle_{inc}} \quad \text{or} \quad \frac{E_x^{sc} E_x^{sc*}}{\cos^2\theta} \quad (4.8)$$

where

$\langle S_z \rangle$  is the average value of the Poynting vector in the z-direction

This determines R, the percent of the incident field reflected.

The absorption of the laser power varies with the angle of incidence. As the angle of incidence increases, the classical turning point moves toward the front of the plasma, and the longitudinal electric field travels further through the evanescence region before reaching the critical surface. For small angles,  $E_x$  is the dominant field and electron motion is nearly parallel to the density gradient. Hence, the electrostatic charge separation is small (Ref 1: 574). Therefore, an angle of maximum absorption is achieved between these two extremes. It is accepted theoretically (Ref 3) and has been proven experimentally (Ref 6) that this angle lies between  $20^\circ$  and  $25^\circ$  for the critical length under consideration. Although the absorption of the field in cold and warm plasmas has somewhat the same magnitude, the methods of absorption are different. This will now be explained.

Cold Plasma. The energy absorption in the cold plasma is due solely to the collisional damping of  $E_z$ . This resonance absorption is shown in Figure 7 to have a maximum of about 50% at  $18^\circ$ . This is in agreement with cold plasma work in general and for a low temperature warm plasma investigated by Forslund (Ref 7) using methods similar to those employed in this work.

Warm Plasma. The warm plasma absorbs energy from the electrostatic wave through electron-ion collisions and also as the plasma wave is Landau damped. As can be seen

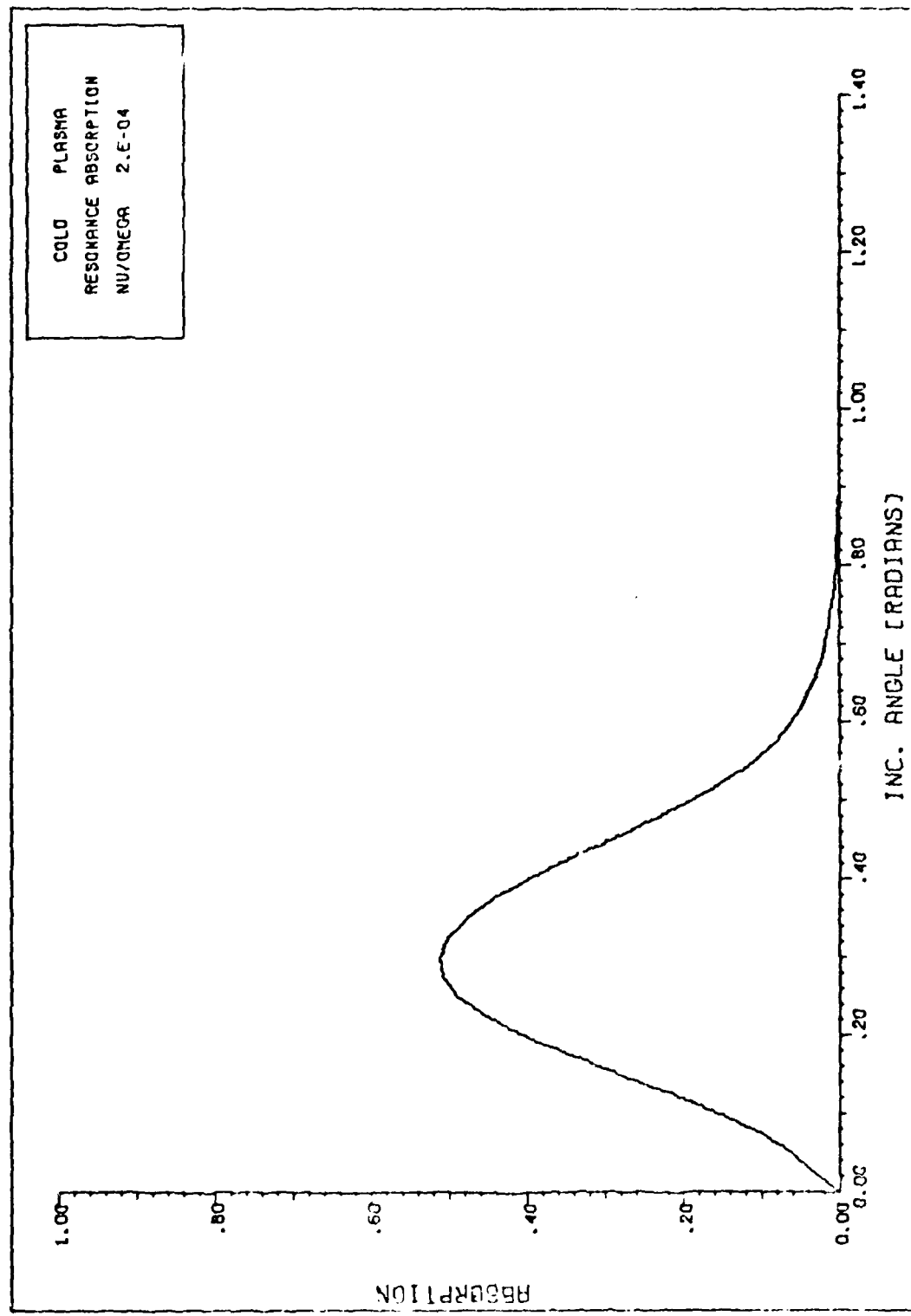


Fig 7. Cold Plasma: Fraction of Laser Energy Resonantly Absorbed as a Function of Incident Angle

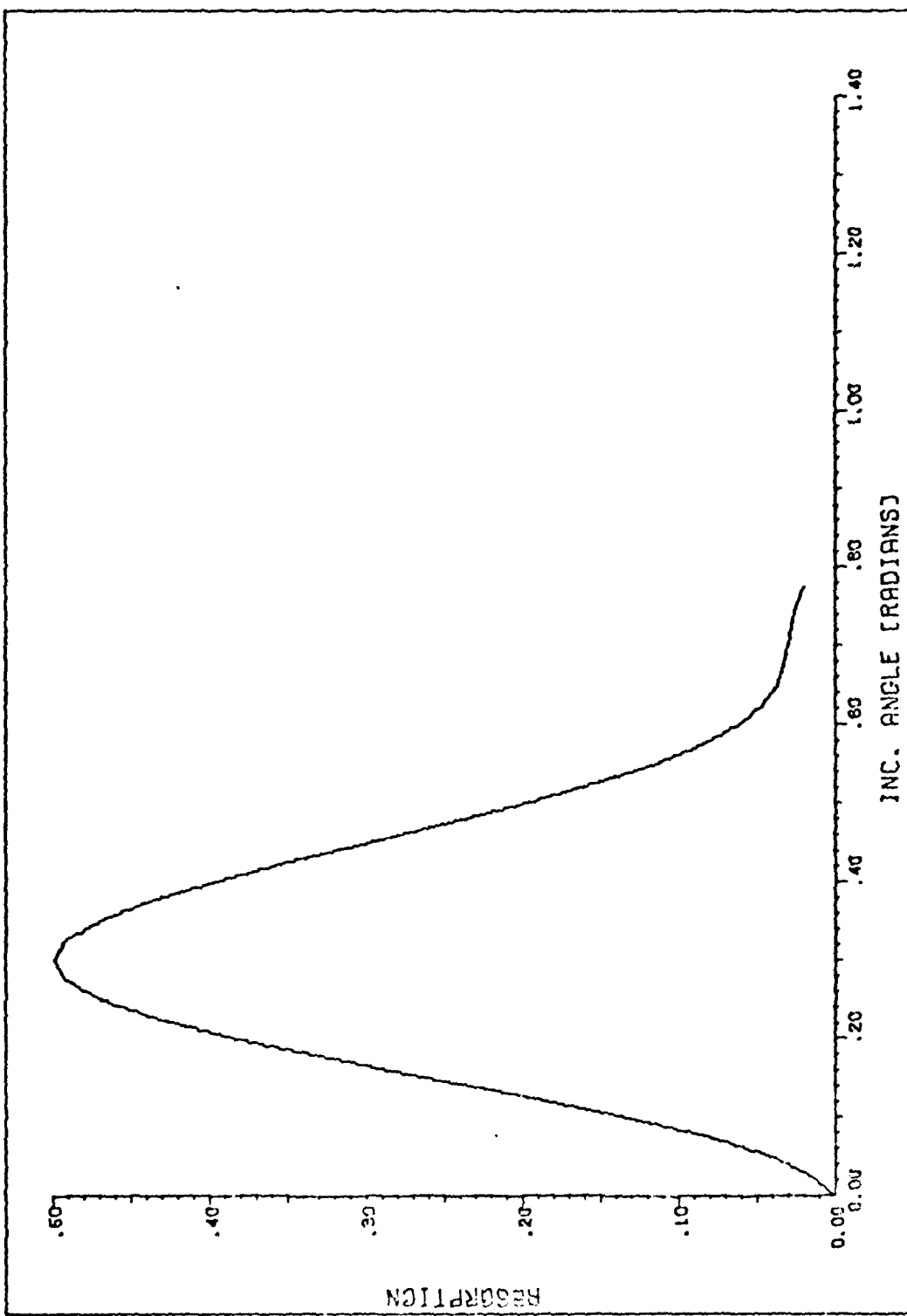


Fig 8. Warm Plasma: Fraction of Laser Energy Resonantly Absorbed as a Function of Incident Angle ( $T = 637$  ev and  $v_L/v_T = 1$ )

from Figure 8, the absorption due to Landau damping appears to compensate for the reduction in magnitude of  $E_z$  and the consequential reduction in electron-ion collisional absorption. Absorptions of nearly 50% were seen for this low temperature case ( $T = 637$  ev) which is similar to the cold plasma results and those of Forslund (Ref 7). However, absorption results for the warm plasma are highly sensitive to the form of Landau damping used, especially at high temperatures.

Modeling Landau damping as a linearly increasing function of  $z$  with a maximum, as it appears in Figure 4, proved unsuccessful. This attempt was curtailed when widely differing absorptions were attained for only small variations in the slope of the linear section. This can be explained by looking at the different number of electrons ( $N_1$ ) that are heavily damped between two cases (two different slopes). Then, absorption would be a trade-off between this energy exchange with electrons and the propagation of the wave away from the critical surface. For example, at large angles of incidence and high temperatures, anomalous absorption occurred due to the closeness of the plasma wave to the boundary and the field structure there. In one case ( $T = 5100$  ev and  $\theta = 1.1$  radians) greater than 30% absorption was observed.

For the above reasons, it is doubtful that anything concrete can be said about absorption due to Landau damping at high temperatures until some of the assumptions made in

deriving it are relaxed. However, these results lead one to believe that Landau damping should be temperature dependent.

#### Ponderomotive Force

The Ponderomotive force is a nonlinear force caused by the gradient of the electric field. As one can see from Figure 9, it is large at very low power densities and, including its effects, might be the first thing one would suggest as an improvement to this steady-state model. The force is derived from the electron momentum equation by Chen in Refs 4 and 8. His derivation is also included in Appendix A of this report. Ponderomotive force is included here as a result derived from the previously calculated field quantities  $E_x$  and  $E_z$ . The equation solved was:

$$F_{NL} = - \frac{\omega_p^2}{\omega^2} \frac{\nabla E_s^2}{16\pi} \quad (4.9)$$

where

$F_{NL}$  is the Ponderomotive force  
and  $E_s^2 = E_x^2 + E_z^2$  is  $2\langle E^2 \rangle$

Thus, it acts on both ions and electrons, but is more effective by the factor  $\frac{m_i}{m_e}$  on the electrons.

The behavior of  $F_{NL}$  is similar in both the cold and warm plasma. In both, it exists primarily at the critical surface. The negative force in front of the critical

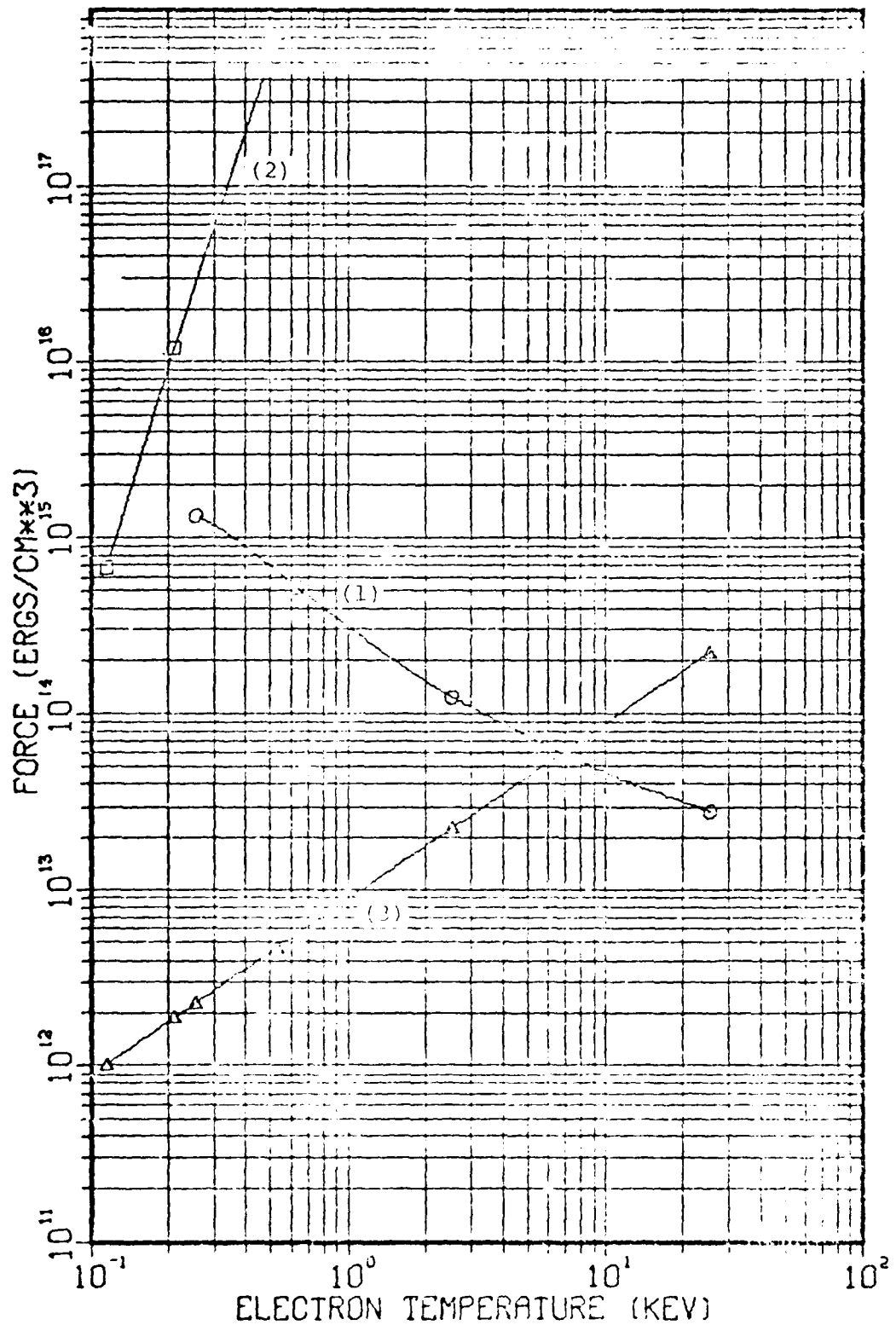


Fig 9. Ponderomotive Force for the Warm Plasma,  $v_L/\omega = .1$  (Curve 1), and the Cold Plasma (Curve 2), for a Laser Flux of  $10^{13} \text{ W/cm}^2$ ) and the Thermal Force  $\nabla n_0 kT$  of the Plasma (Curve 3)

surface serves to pull electrons from the higher density region to the lower. This results in the density profiles observed in experiments (Ref 9) and modeled by theoreticians (Refs 10 and 11). Evidently, the force causes a depression in the density profile in front of the critical surface. This new profile, when allowed to smooth, becomes a step profile causing the plasma to go from underdense ( $\omega_p/\omega < 1$ ) to overdense ( $\omega_p/\omega > 1$ ) in a very short distance. This effect is modeled successfully in Ref 11 for an electron temperature of 2 Kev. They observed a maximum Ponderomotive force of  $1.25 \times 10^3$  ergs/cm<sup>4</sup> at 120 W/cm<sup>2</sup> while for 2.55 Kev and  $v_L/\omega = .67$ , a value of  $1.5 \times 10^3$  ergs/cm<sup>4</sup> was obtained in this work with a linear profile. The Ponderomotive force is very large in the cold plasma due to the steep gradient in  $E_z$ . Figure 9 shows the Ponderomotive force as a function of temperature for a power of  $10^{13}$  W/cm<sup>2</sup>. The plot also includes the thermal pressure force of the plasma  $kT\nabla(n_0)$ .

#### Hot Electron Energy ( $T_H$ )

The velocity of the hot electrons is a concern because they may escape the plasma without depositing their energy if they get too hot. This would reduce energy absorption. In fact, these suprathermal electrons have been observed and have been given a great deal of attention (Refs 12 and 13).

In this work the temperature of the electrons was determined by their oscillation velocity ( $v_{os}$ ). The  $v_{os}$  in the cold plasma is the familiar  $eE/m(v - i\omega)$ , while in the warm plasma, additional terms appear due to the pressure gradient. For the warm plasma:

$$v_{os} = \frac{eE}{m(v - i\omega)} - \frac{ik\gamma T n_1}{n_0^m(v_L - i\omega)} + \frac{\gamma T n_1 n_0'}{n_0^2 m(v_L - i\omega)} - \frac{\gamma n_1' T}{(v_L - i\omega) m n_0} \quad (4.10)$$

where all the terms have been previously defined.

The pressure related terms in Eq (4.10) are small corrections to the electric field term and it was discovered that they could be ignored. However, the velocities plotted in Appendices B and C include the effects of these terms, as do Figures 5 and 6.

Note that Figure 6 shows at what powers and temperatures the energy of the hot electrons is equal to that of the background (cold) electrons. Since Landau damping requires  $v_\phi \gg v_{th}$ , this curve provides an important check on the warm plasma model.

#### Validity of Assumptions

This is a discussion of the major assumptions made in this report. An important assumption is that the ions are immobile. Other concerns are the validity of the linearizing approximations and the effect of spatial dispersion.

Both Ponderomotive and Coulomb forces act on the ions. The Coulomb forces are small and can be ignored. The result of the Ponderomotive force is the modification of the plasma number density profile mentioned earlier. It has been shown interferometrically that the Ponderomotive force can modify the plasma density profile in about a picosecond (Ref 10:184). This result was obtained by illuminating glass microballoons with a Nd-YAG laser. Hence, the plasma was penetrated to a critical density of  $10^{21} \text{ cm}^{-3}$ . The experiment was conducted at a power of  $10^{14} \text{ W/cm}^2$ , and the profile modification was observed when  $F_{NL} \approx F_{NP}$ . The time scale of interest in the steady-state problem developed here is on the order of  $10^{-15}$  seconds, somewhat shorter than that above. The Ponderomotive force, although large, will not cause the ions to move appreciably in  $10^{-15}$  seconds.

The Ponderomotive force is shown in Figure 9 for a power of  $10^{13} \text{ W/cm}^2$ . Since  $\Delta t \approx \sqrt{\frac{\Delta x_{mn}}{P}} \gg \frac{2\pi}{\omega}$  at this power and at still higher powers, one can reasonably say that ion motion is insignificant in one time period.

The effect of spatial dispersion was discussed earlier and will be summarized here. It seems that the cold plasma model will definitely be affected by spatial dispersion, and the warm plasma model should also incorporate it for application of the theory at powers higher than those indicated in Figure 5. Still certain density profiles could be found for both the cold and warm cases where the effect of spatial dispersion would be minimized (longer critical

lengths and larger collision frequencies immediately come to mind).

For the purpose of this work, two concrete limits were chosen on the validity of the models. For each temperature, these factors limit the powers at which the models can be applied. The first factor is the validity of the linearizing approximation  $n_1 \ll n_0$ . For powers greater than that at which  $n_1 = n_0$  this approximation is invalid. There is no lower limit placed on the powers for which the cold plasma model is applicable. The warm plasma is limited by Landau damping to powers where the velocity of the hot electrons is greater than the velocity of the cold. This is also shown on Figure 6. Spatial dispersion remains as an additional concern.

## V Conclusions

The linear models of cold and warm plasma resonance absorption developed here give results comparable to those obtained by other theoretical means and experiments. The paper serves as a collection of many facts, theories, and ideas about resonance absorption. The results indicate that the numerical methods are sound and the method was found to be conservative of computer time and space. When ion motion is ignored, the steady-state method is applicable to powers of interest in today's fusion program. Their respective areas of applicability are indicated in Figure 6. Correct modeling of Landau damping and spatial dispersion could strengthen or weaken the preceding statements. Because resonance absorption is a more efficient way to absorb laser energy than simple collisional absorption, lasers of fusion devices should be positioned such that maximum resonance absorption is achieved. Of course, it is not that simple, since targets are spherical and uniform energy deposition is desired for the implosion. Also, the ideal angle will change with the density profile. Still, resonance absorption will play an important part in a laser fusion device, and this work is only a starting point in the process of applying the technique to the machine. If these models are to contribute further in this process, they might be improved in the following ways.

Current work in the field should give one some idea as to what direction a follow-on study might take. In recent works, there is little mention of Landau damping while ion motion and subsequent profile-strengthening have been investigated. This suggests that a nonlinear analysis can be used to more exactly model the warm plasma, and that time dependence is also important. The large effect that Landau damping had on the absorption of electromagnetic energy in this study is additionally troubling. These suggest possible areas where an improvement on the current models can be made.

An important improvement to the warm model would be the ability to correctly model the expected final distribution function. This could be incorporated by using the Vlasov equation instead of the momentum equation. If this were done, the assumption of a Maxwellian distribution could be relaxed and a bump-on-the-tail distribution function could be used. Then, Landau damping could be tackled in a straightforward manner and some of the problems experienced here could be overcome. This would also allow for an assessment of the interaction between the two temperatures (relaxation time) that has not been addressed here.

More simple, perhaps, would be to relax the assumption of immobile ions in a step-by-step manner. After one case has been studied, the initial profile can be adjusted by applying the corrective force calculated in that

steady-state case and moving the particles. The new profile could then be illuminated and the procedure repeated.

A similar approach could be used to investigate nonlinear effects. First, the problem could be solved by the methods herein. Then, the values obtained could be used to solve Eqs (2.1) to the next order. This nonlinear analysis might prove fruitful if more accurate results were desired or instabilities were a concern.

It would be useful to investigate the stability of the two-sweep algorithm employed in this analysis and to determine its applicability to related sets of equations.

In conclusion, the linear modeling of warm and cold plasma behavior gave results, including absorption, comparable to experiments and other work on resonance absorption. The behavior of the important quantities was detailed and physically explained. Important consequences of resonant absorption were shown and the regions of theory validity were established. Various ways to improve the models were suggested.

## Bibliography

1. Chen, F. F. and R. B. White. "Amplification and Absorption of Electromagnetic Waves in Overdense Plasmas," Plasma Physics, 16: 565-587. Pergamon Press, 1974.
2. Erkkila, J. H. Laser Light Scattering and Absorption in Dense, Spherically Symmetric Plasmas. UCRL 51914, Lawrence Livermore Laboratories (December 1975).
3. Ginzburg, V. L. Propagation of Electromagnetic Waves in Plasmas. New York: Gordon and Breach, 1961.
4. Chen, F. F. Introduction to Plasma Physics. New York: Plenum Press, 1977.
5. Smith, G. D. Numerical Solutions of Partial Differential Equations. 139. London: Oxford Press, 1965.
6. Manes, K. R. et al. "Polarization and Angular Dependence of  $1.06 \mu\text{m}$  Laser-Light Absorption by I-minar Plasmas," Physical Review Letters, 39:(5) 281-284 (August 1977).
7. Forslund, D. W. et al. "Theory and Simulation of Resonant Absorption in a Hot Plasma," Physical Review A, 11:(2) 679-683 (February 1975).
8. Chen, F. F. "Physical Mechanisms for Laser-Plasma Parametric Instabilities," University of California Los Angeles (August 1973).
9. Attwood, D. T. et al. "Interferometric Confirmation of Radiation-Pressure Effects in Laser-Plasma Interactions," Physical Review Letters, 40:(3) 184-187 (16 January 1978).
10. Forslund, D. W. et al. "Absorption of Laser Light on Self-Consistent Plasma Density Profiles," Physical Review Letters, 36:(1) 35-38 (5 January 1976).
11. Mayer, F. J. et al. "Electromagnetic Structure Resonances in Inhomogeneous Plasma Layers," Physical Review Letters, 40:(1) 30-34 (2 January 1978).
12. Forslund, D. W. et al. "Theory of Hot-Electron Spectra at High Laser Intensity," Physical Review Letters, 39:(5) 284-288 (1 August 1977).

13. Estabrook, K. and W. L. Kruer. "Properties of Resonantly Heated Electron Distributions," Physical Review Letters, 40:(1) 42-45 (2 January 1978).

## Appendix A: Derivations

### Linearized Equations from Fundamental Equations TE Mode

Equations:

$$mn\left(\frac{dv}{dt} + vV + V \cdot \nabla V\right) + \nabla p = enE$$

$$\nabla \times E = -\frac{1}{c} \frac{dB}{dt}$$

$$\nabla \times B = \frac{4\pi}{c} j + \frac{1}{c} \frac{dE}{dt}$$

(A.1)

$$\nabla \cdot E = 4\pi ne$$

$$\nabla \cdot B = 0$$

$$j = neV$$

For TE mode (see Figure 3) assuming wavelike solutions

$$E = E_{0y} + E_{1y} e^{iksx - i\omega t}$$

$$B = B_{0x} + B_{1x} e^{iksx - i\omega t} + B_{0z} + B_{1z} e^{iksx - i\omega t}$$

where quantities with subscript (1) are perturbations about equilibrium so:

$$\nabla \times E = -\frac{d}{dz} \hat{E}_y^i + \frac{d}{dx} \hat{E}_y^k ; \text{ where } E_y = E_{y0} + E_{y1} e^{-i\omega t}$$

and

$$\begin{aligned} -\frac{1}{c} \frac{dB}{dt} &= -\frac{1}{c} \frac{dB_{0x}}{dt} + \frac{i\omega}{c} B_{1x} e^{-i\omega t} + -\frac{1}{c} \frac{dB_{0z}}{dt} \\ &+ \frac{\omega}{c} B_{1z} e^{-i\omega t} \end{aligned}$$

therefore, since  $\nabla \times E = - \frac{1}{c} \frac{dB}{dt}$ ,

$$-\frac{d}{dz} E_{1y} e^{-i\omega t} - \frac{d}{dz} E_{0y} = -\frac{1}{c} \frac{dB_{0x}}{dt} + ik B_{1x} e^{-i\omega t}$$

$$\frac{d}{dx} E_y e^{-i\omega t} + \frac{d}{dx} E_{0y} = -\frac{1}{c} \frac{dB_{0z}}{dt} + ik B_z e^{-i\omega t}$$

and:

$$-\frac{d}{dz} E_y = ik B_x \quad (A.2)$$

$$sE_y = B_z \quad (A.3)$$

Now we must use

$$\nabla \times B = \frac{4\pi}{c} j + \frac{1}{c} \frac{dE}{dt}$$

First, we will find  $j$  from the momentum equation:

$$\begin{aligned} & -i\omega n_0 v_1 e^{-i\omega t} - i\omega n_1 v_1 e^{-2i\omega t} + v n_0 v_1 e^{-i\omega t} + v n_1 v_1 e^{-2i\omega t} \\ & = [en_0 E_0 + en_1 E_y e^{-2i\omega t} + en_1 E_0 e^{-i\omega t} + en_0 E_1 e^{-i\omega t} \\ & \quad - \frac{d\gamma T n_0}{dz} - \frac{d\gamma}{dz} T n_1 e^{-i\omega t}] / m \end{aligned}$$

this gives upon neglecting products of second-order perturbations

$$\begin{aligned} & en_0 E_0 - \frac{d\gamma T n_0}{dz} = 0 \\ & mn_0 v_1 e^{-i\omega t} (v - i\omega) + mn_1 v_1 e^{-2i\omega t} (v - i\omega) \\ & = en_1 E_{1y} e^{-2i\omega t} + en_1 E_0 e^{-i\omega t} + en_0 E_{1y} e^{-i\omega t} \\ & \quad - \frac{d}{dz} \gamma T n_1 e^{-i\omega t} \end{aligned}$$

neglecting second-order terms and dropping subscripts gives

$$n_0 v_1 = [en_1 E_0 e^{-i\omega t} + en_0 E_1 e^{-i\omega t} - \frac{d}{dz} \gamma T n_1 e^{-i\omega t}] / m(v - i\omega) - ik \epsilon_y e^{-i\omega t}$$

therefore, since  $j = n_0 e v_1$

$$iksB_z + \frac{d}{dz} B_x = \left( \frac{-ik + i4\pi e^2 n_0}{cm(\omega + iv)} \right) E_y + \frac{i4\pi e \gamma T d n_0 n_1}{cm(\omega + iv) dz n_0} - \frac{\gamma T i 4\pi e}{cm(\omega + iv)} \frac{dn_1}{dz}$$

This yields, when accounting for direction,

$$\left[ -iksB_z + \frac{dB_x}{dz} \right] \hat{j} = ike \epsilon_y \hat{j} + \left[ a \frac{dn_0}{dz} \frac{n_1}{n_0} - a \frac{dn_1}{dz} \right] \hat{k} - iks(n_1) \hat{i}$$

this gives

$$-iksB_z + \frac{dB_x}{dz} = -ike \epsilon_y \quad (A.4)$$

and for equilibrium values

$$a \frac{dn_0}{dz} \frac{n_1}{n_0} - a \frac{dn_1}{dz} = 0 \quad \text{and} \quad -iks(n_1) = 0$$

#### E" TE Mode

To find the wave equation for  $E_y''$ , substituting Eqs (A.2) and (A.3) into (A.4)

$$\begin{aligned}
 -i\kappa s(sE_y) + \frac{1}{ik} \frac{d}{dz} \left( -\frac{d}{dz} E_y \right) &= -ik E_y \\
 ks^2 E_y - \frac{1}{k} E_y'' - \kappa \epsilon E_y &= 0 \\
 E_y'' + k^2 (\epsilon - s^2) E_y &= 0
 \end{aligned} \tag{A.5}$$

Linearized Warm Plasma Equations from Fundamental Equations  
TM Mode

To find the four basic TM mode equations and eventually second-order equations, we again begin with Eqs (A.1)

$$mn \left( \frac{dV}{dt} + vV + \underline{V} \cdot \nabla \underline{V} \right) + \nabla P = enE$$

↓  
second order

neglecting products of other second-order terms and linearizing for wavelike perturbations

$$\begin{aligned}
 -n_0 i\omega V_1 + v n_0 V_1 + \frac{1}{m} \frac{dP_0}{dz} + \frac{1}{m} \frac{dP_1}{dz} + \frac{i\kappa s}{m} P_1 \\
 = \frac{e(n_0 + n_1)}{m} (E_0 + E_1)
 \end{aligned}$$

so

$$\frac{e}{m} n_0 E_0 = \frac{1}{m} \frac{dP_0}{dz}$$

and

$$j_1 = en_0 V_1 = \frac{e^2}{m} \frac{(n_1 E_0 + n_0 E_1)}{(v - i\omega)} - \frac{e}{m} \frac{dP_1}{dz} - \frac{e}{m} i\kappa s P_1$$

$$\text{from } \nabla \times \underline{B} = \frac{4\pi}{c} \underline{j} + \frac{1}{c} \frac{d\underline{E}}{dt} \tag{A.6}$$

$$\frac{4\pi}{c} j = \frac{4\pi}{c} \frac{e^2}{m} \frac{(n_1 E_0 + n_0 E_1 - \frac{dP_1}{edz} - \frac{iks}{e} P_1)}{(v - i\omega)} \quad (A.7)$$

since,

$$\underline{E} = E_0 + E_1 e^{i(ksx - \omega t)}$$

and  $E$  has  $x$  and  $z$  components,

$$\frac{1}{c} \frac{dE}{dt} = - \frac{i\omega}{c} E_x - \frac{i\omega}{c} E_z \quad (A.8)$$

where  $E_x$  and  $E_z$  are the perturbed quantities ( $E_{x1}$  and  $E_{z1}$ )

Since we know that

$$en_0 E_0 = \frac{dP_0}{dz}$$

giving

$$n_1 E_0 = \frac{n_1 \gamma T}{en_0} \frac{dn_0}{dz} \hat{k} \quad (A.9)$$

from (A.6), (A.7), (A.8) and (A.9)

$$\begin{aligned} iks(B_0 + B_1) \hat{k} - \frac{d(B_0 + B_1)}{dz} \hat{i} &= \frac{4\pi e^2}{(v - i\omega)cm} \left( \frac{n_1 \gamma T}{en_0} \frac{dn_0}{dz} \hat{k} \right. \\ &\quad \left. - \frac{\gamma n_1 iks T}{e} \hat{i} - \frac{\gamma T}{e} \frac{dn_1}{dz} \hat{k} + n_0 E_x \hat{i} + n_0 E_z \hat{k} \right) \\ &\quad - ikE_x \hat{i} - ikE_z \hat{k} \end{aligned}$$

so, for the perturbed quantities

$$-\frac{dB}{dz} = -ik\epsilon E_x - aiksn_1 \quad (a)$$

(A.10)

$$-ik\epsilon E_z + a\beta n_1 - a \frac{dn_1}{dz} = iksB \quad (b)$$

$$\text{now } \nabla \times E = -\frac{1}{c} \frac{dB}{dt}$$

or, for the perturbed quantities

$$-ik\epsilon E_z + \frac{dE_x}{dz} = ikB \quad (A.11)$$

and  $\nabla \cdot E = 4\pi e(n_0 + n_1)$  yields

$$ik\epsilon E_x + \frac{dE_z}{dz} = 4\pi e n_1 \quad (A.12)$$

#### Cold Plasma: $E_z''$ from Linearized Equations

Now we will derive the second-order equation for  $E_z''$  in a cold collisional plasma beginning with Eqs (A.10)

$$\frac{dB}{dz} = ik\epsilon E_x \text{ and } -ik\epsilon E_z = iksB$$

Employing Eq (A.11) gives

$$-ik\epsilon E_z + \frac{d}{dz} \left[ \frac{dB}{dz} / ik\epsilon \right] = ikB$$

differentiating

$$-ik\epsilon E_z = iksB$$

yields

$$\frac{dB}{dz} = -\frac{1}{s} \left( \frac{d\epsilon}{dz} + \frac{dE_z}{dz} \right)$$

therefore

$$ik\epsilon s^2 E_z - \frac{d}{dz} \left[ \frac{d\epsilon}{dz} + \frac{dE_z}{dz} / ik\epsilon \right] = - ik\epsilon E_z$$

multiply through by  $ik$

$$k^2 (s^2 - \epsilon) E_z - \frac{d}{dz} \frac{E_z}{\epsilon} \frac{d\epsilon}{dz} + E_z'' = 0$$

clearly,

$$\frac{E_z}{\epsilon} \frac{d\epsilon}{dz} = E_z (\ln \epsilon)'$$

$$\frac{d}{dz} [E_z (\ln \epsilon)'] = [E_z (\ln \epsilon)']'$$

and thus

$$k^2 (\epsilon - s^2) E_z + [E_z (\ln \epsilon)']' + E_z'' = 0 \quad (A.13)$$

Warm Plasma:  $N_1''$  and  $E_z''$  from Linearized Equations

Equations for the plasma wave in terms of the electrostatic component will now be derived using Eqs (A.10), (A.11) and (A.12). Eq (A.11) gives

$$E_x' = \frac{siKB + iksE_z}{s} \quad (A.14)$$

Eq (A.12) gives

$$iksE_x' + E_z'' = 4\pi\epsilon n_1' \quad (A.15)$$

Eliminating  $E_x'$  between Eqs (A.14) and (A.15) and using Eq (A.10.b) for  $iksB$  gives:

$$(-ik\epsilon E_z + a\beta n_1 - a \frac{dn_1}{dz} + iks^2 E_z)ik + E_z'' = 4\pi en_1' \quad (A.16)$$

or

$$E_z'' + (k^2\epsilon - k^2s^2)E_z = (4\pi e + aik)N_1' - aik\beta n_1 \quad (A.16)$$

Now for  $N_1''$ :

differentiating (A.10.b) w.r.t.z

$$-ik\epsilon E_z' - ik\epsilon'E_z + a'\beta n + a\beta n' - a'n' - an'' = iksB' \quad (A.16)$$

from (A.10.a) and (A.12)

$$B' = aiksn + \epsilon \left[ \frac{4\pi en - E_z'}{s} \right] \quad (A.17)$$

substituting  $B'$  from (A.17) into (A.16)

$$-ik\epsilon E_z' - ik\epsilon'E_z + a'\beta n + a\beta n' - a'n' - an''$$

$$= iks aiksn + \epsilon \left[ \frac{4\pi en - E_z'}{s} \right]$$

and

$$aN_1'' + (a' - a\beta)N_1' + (4\pi\epsilon eik - a'\beta - ak^2s^2)N_1$$

$$= -ik\epsilon'E_z \quad (A.18)$$

Warm Plasma:  $B''$  and  $E_z''$  from Linearized Equations

Now we shall derive second-order equations coupling  $B_y$  and  $E_z$  in the warm plasma. Beginning with (A.10.a)

$$n = \frac{-ik\epsilon E_x + \frac{dB}{dz}}{aik\epsilon} \quad (A.19)$$

using (A.12) and (A.19) one arrives at;

$$- \alpha k^2 s^2 E_x + \alpha iks E_z' = - ik\epsilon E_x + dB/dz \quad (A.20)$$

where

$$\alpha = \frac{a}{4\pi\epsilon}$$

differentiating (A.20) w.r.t.z. and using (A.11) for  $E_x'$

$$(ik\epsilon' - \alpha' k^2 s^2) E_x + (ik\epsilon - \alpha k^2 s^2) (ikB + iksE_z) \\ + \alpha' iksE_z' + \alpha iksE_z'' = B'' \quad (A.21)$$

using (A.20) to eliminate  $E_x$  in (A.21)

$$(ik\epsilon' - \alpha' k^2 s^2) \left[ \frac{-\alpha iksE_z' + B'}{(ik\epsilon - \alpha k^2 s^2)} \right] + (ik\epsilon - \alpha k^2 s^2) \\ (ikB + iksE_z) + \alpha' iksE_z' + \alpha iksE_z'' = B'' \quad (A.22)$$

Using (A.12) to eliminate  $n$  and  $n_1$  from (A.10.b) and using (A.20) to eliminate  $E_x$  while employing (A.11) to eliminate  $E_x'$  from the result, one obtains:

$$- ik\epsilon E_z + \frac{\alpha \beta iks (-\alpha iks E_z')}{(ik\epsilon - \alpha k^2 s^2)} + \frac{\alpha iks B'}{(ik\epsilon - \alpha k^2 s^2)} \\ + \alpha E_z' + \alpha k^2 s B + \alpha k^2 s^2 E_z - \alpha E_z'' = iks B$$

or

$$\begin{aligned} -\alpha E_z'' + & \left( \frac{-i\beta\alpha^2 k s^2}{(\epsilon + \alpha i k s^2)} + \alpha \beta \right) E_z' + (\alpha k^2 s^2 - i k \epsilon) E_z \\ = & (i k s - \alpha k^2 s) B - \frac{\alpha \beta s B'}{(\epsilon + \alpha i k s^2)} \end{aligned} \quad (A.23)$$

Substituting (A.23) into (A.22) for  $E_z''$  yields for  $B''$  after algebra.

$$\begin{aligned} B'' - & \left( \frac{\epsilon' + i \alpha' k s^2 + \alpha \beta i k s^2}{(\epsilon + \alpha i k s^2)} \right) B' + (k^2 \epsilon - k^2 s^2) B \\ = & E_z' i k s (\epsilon \alpha' + \alpha \beta \epsilon - \alpha \epsilon') / (\epsilon + \alpha i k s^2) \end{aligned} \quad (A.24)$$

#### Cold Plasma: Differenced Equations Solved for the Constants in the Plasma

Now we will difference Eq (A.13) for  $E_z$  in the cold plasma employing techniques described in the paper. Eq (A.13) can be written as;

$$a_z E_z + \frac{d}{dz} [E_z b_z] + E_z'' = 0$$

where

$$a_z = k^2 (\epsilon - s^2)$$

$$b_z = (\ln \epsilon)'$$

thus

$$a_z E_z + E_z c_z + b_z E_z' + E_z'' = 0$$

where

$$c_z = \frac{db_z}{dz}$$

Accounting for differential mesh spacing and substituting

$E_{n+1} = pE_n + q$  and  $E_n = p_{n-1}E_{n-1} + q_{n-1}$  gives:

$$\begin{aligned} & \left( a_n + c_n + \frac{b_n p_n}{\alpha_n} - \frac{b_n (1 - \phi^2)}{\alpha_n} + \frac{p_n}{\beta_n} - \frac{1}{\beta_n} - \frac{\phi}{\beta_n} \right) E_n \\ &= \left[ -\frac{b_n q_n}{\alpha_n} - \frac{q_n}{\beta_n} \right] + \left[ \frac{b_n \phi^2}{\alpha_n} - \frac{\phi}{\beta_n} \right] E_{n-1} \end{aligned} \quad (A.25)$$

where

$$\alpha_n = \phi h (1 + \phi) \quad \text{and} \quad \beta_n = \frac{\phi^2 h^2}{2} + \frac{\phi h^2}{2}$$

therefore,

$$p_{n-1} = \frac{\frac{b_n \phi^2}{\alpha_n} - \phi / \beta_n}{c_1} \quad (A.26)$$

$$q_{n-1} = \frac{-\left( \frac{b_n q_n}{\alpha_n} + \frac{q_n}{\beta_n} \right)}{c_1} \quad (A.27)$$

where

$$c_1 = \left( a_n + c_n + \frac{b_n p_n}{\alpha_n} - \frac{b_n (1 - \phi^2)}{\alpha_n} + \frac{p_n}{\beta_n} - \frac{1}{\beta_n} - \frac{\phi}{\beta_n} \right)$$

When the zero boundary condition is applied  $q(N)$  is set to zero, and the remainder of the  $q_n$ 's become  $\phi$  by Eq (A.27). All the  $p_n$ 's are specified by Eq (A.26) and at the front

face, the radiation boundary condition is applied. How that boundary condition is applied follows.

Eliminating  $E_z''$  between the Taylor series expansion of  $E_z$  at the first mesh point, and the wave-equation (A.13) one obtains:

$$0 = \frac{2(E_2 - E_1)}{h^2} - \frac{2}{h} E' \Big|_1 + a_z E_1 + c_z E_1 + b_z E' \Big|_1$$

where  $a_z$ ,  $b_z$ , and  $c_z$  have been previously defined and  $\Big|_1$  means evaluated at the first mesh point. Using the radiation boundary condition for  $E'$  and the fact that  $E_2 = p_1 E_1 + q_1$  the above equation becomes

$$\frac{2(p_1 E_1 + q_1 - E_1)}{h^2} - \frac{2}{h}(2ik\cos\theta E_{inc} - ik\cos\theta E_1) \\ + a_z E_1 + c_z E_1 + b(2ik\cos\theta E_{inc} - ik\cos\theta E_1)$$

Solving for  $E_1$

$$E_1 = - \frac{\left[ \frac{2q_1}{h^2} - \frac{2}{h}(2ik\cos\theta E_{inc}) + b_z 2ik\cos\theta E_{inc} \right]}{\frac{2p_1}{h^2} - \frac{2}{h^2} + \frac{2ik\cos\theta}{h} + a_z + c_z - b_z ik\cos\theta}$$

(A.28)

#### Warm Plasma: Difference Equations Solved for the Constants in the Plasma

The first step in the solution process is to solve for the constants relating adjacent field quantities. Eqs (A.23) and (A.24) were solved in general as follows:

$$a_1 B'' + b_1 B' + c_1 B = d_1 z' + e_1 z \quad (A.29)$$

$$a_2 z'' + b_2 z' + c_2 z = d_2 B' + e_2 B ; \quad z = E_z \quad (A.30)$$

taking

$$z_{n+1} = f_n B_n + g_n z_n + h_n$$

$$B_{n+1} = k_n B_n + \ell_n z_n + p_n$$

When differential mesh spacing is applied to the derivatives (A.29) becomes;

$$\begin{aligned} & \left( \frac{a_1}{D} k_n - \frac{a_1}{D} - \frac{a_1 \phi}{D} + \frac{b_1 k_n}{A} - \frac{b_1 (1 - \phi^2)}{A} + c_1 - \frac{d_1 f_n}{A} \right) B_n \\ & + \left( \frac{a_1}{D} \ell_n + \frac{b_1 \ell_n}{A} - \frac{d_1 g_n}{A} + \frac{d_1 (1 - \phi^2)}{A} - e_1 \right) z_n \\ & = \left( - \frac{a_1}{D} \phi + \frac{b_1}{A} \phi^2 \right) B_{n-1} + \left( - \frac{d_1}{A} \phi^2 z_{n-1} \right) \\ & + \left( - \frac{a_1}{D} p_n - \frac{b_1}{A} p_n + \frac{d_1}{A} h_n \right) \end{aligned} \quad (A.31)$$

where

$$A = \phi h (l + \phi) \quad \text{and} \quad D = \frac{\phi^2 h^2}{2} + \frac{\phi h^2}{2}$$

Similarly, from (A.30);

$$\begin{aligned}
 & \left( \frac{d_2}{A} (1 - \phi^2) - \frac{d_2}{A} k_n + \frac{a_2}{D} f_n + \frac{b_2}{A} f_n - e_2 \right) B_n \\
 & + \left( \frac{a_2}{D} g_n - \frac{a_2}{D} - \frac{\theta a_2}{D} + \frac{b_2}{A} g_n - \frac{b_2}{A} (1 - \theta^2) + c_2 - \frac{d_2}{A} \ell_n \right) z_n \\
 & = \left( - \frac{a_2 \phi}{D} + \frac{b_2}{A} \phi^2 \right) z_{n-1} + \left( - \frac{d_2}{A} \phi^2 \right) B_{n-1} \\
 & + \left( - \frac{a_2 h_n}{D} - \frac{b_2}{A} h_n + \frac{d_2}{A} p_n \right) \quad (A.32)
 \end{aligned}$$

Eqs (A.31) and (A.32) can be written as

$$\begin{aligned}
 Q B_n + R z_n &= s_1 B_{n-1} + s_2 z_{n-1} + s_3 \\
 \text{and} \quad (A.33)
 \end{aligned}$$

$$T B_n + u z_n = v_1 B_{n-1} + v_2 z_{n-1} + v_3 \text{ respectively.}$$

Since we know

$$B_n = k_{n-1} B_{n-1} + \ell_{n-1} z_{n-1} + p_{n-1} \text{ and}$$

$$z_n = f_{n-1} B_{n-1} + g_{n-1} z_{n-1} + h_{n-1}$$

Eqs (A.33) can be solved simultaneously for the constants

$k, \ell, p, f, g$  and  $h$ .

$$B_n = \frac{us - Rv}{Qu - RT} \quad \text{and} \quad z_n = \frac{Qv - Ts}{Qu - TR}$$

where  $s$  and  $v$  are the right-hand sides of Eqs (A.33).

Clearly

$$\begin{aligned}
 f_{n-1} &= \frac{QV_1 - Ts_1}{Qu - TR} \\
 g_{n-1} &= \frac{QV_2 - Ts_2}{Qu - TR} \\
 h_{n-1} &= \frac{QV_3 - Ts_3}{Qu - TR}
 \end{aligned} \tag{A.34}$$

and

$$\begin{aligned}
 k_{n-1} &= \frac{us_1 - RV_1}{Qu - TR} \\
 l_{n-1} &= \frac{us_2 - RV_2}{Qu - TR} \\
 p_{n-1} &= \frac{us_3 - RV_3}{Qu - TR}
 \end{aligned} \tag{A.35}$$

Two equations are solved for the radiation boundary condition. They are derived as was Eq (A.28) but they involve both  $z_1$  and  $B_1$ .

$$\begin{aligned}
 & \left( \frac{k_1}{h_1} - \frac{1}{h_1} - \frac{h_1}{2} b_1 ik \cos \theta + \frac{h_1}{2} c_1 + ik \cos \theta \right) B_1 \\
 & + \left( \frac{l_1}{h_1} + \frac{h_1}{2} d_1 ik \cos \theta - \frac{h_1 e_1}{2} \right) z_1 \\
 & = \left( - \frac{p_1}{h_1} + \frac{h_1}{2} d_1 2 ik \cos \theta z_1^{\text{inc}} - \frac{h_1}{2} b_1 2 ik \cos \theta B_y^{\text{inc}} \right. \\
 & \quad \left. + 2 ik \cos \theta B_y^{\text{inc}} \right) \tag{A.36}
 \end{aligned}$$

and

$$\begin{aligned} & \left( \frac{f_1}{h_1} + \frac{h_1}{2} d_2 ik \cos \theta - \frac{h_1}{2} e_2 \right) B_1 \\ & + \left( \frac{g_1}{h_1} - \frac{1}{h_1} - \frac{h_1}{2} b_2 ik \cos \theta + \frac{h_1}{2} c_2 + ik \cos \theta \right) z_1 \\ & = \left( - \frac{h_1}{h_1} + \frac{h_1}{2} d_2 2 ik \cos \theta B_y^{inc} - \frac{h_1}{2} b_2 2 ik \cos \theta z_z^{inc} \right. \\ & \quad \left. + 2 ik \cos \theta z_z^{inc} \right) \quad (A.37) \end{aligned}$$

where

$h_1$  is the first mesh interval

$H_1$  is part of  $z_2$  (i.e.  $z_2 = f_1 B_1 + g_1 z_1 + H_1$ )

Eqs (A.36) and (A.37) can be written as

$$W_1 B_1 + x_1 z_1 = Y_1$$

$$W_2 B_1 + x_2 z_1 = Y_2$$

Since all the constants are known  $z_1$  and  $B_1$  are obtained simultaneously.

$k_z$  from  $E_z''$

It is possible to derive the wave number and wavelength in the plasma from the second-order equation. The equation for  $E_z''$  in the warm plasma is;

$$\begin{aligned}
 E_z'' + \left( -\beta + \frac{i\beta\alpha ks^2}{(\epsilon + \alpha iks^2)} \right) E_z' + \left( \frac{ik\epsilon}{\alpha} - k^2 s^2 \right) E_z \\
 = \frac{s\beta B'}{(\epsilon + \alpha iks^2)} + \left( k^2 s - \frac{iks}{\alpha} \right) B
 \end{aligned} \tag{A.23}$$

for small  $\alpha$  ignoring all terms except for  $E_z$  Eq (A.23) becomes a simple differential equation with an oscillating part determined by the coefficient of  $E_z$ , which is:

$$k^2 \left( \frac{(1 + iv_L/\omega)}{\gamma T/mc^2} - s^2 \right) \tag{A.38}$$

for  $v_L/\omega$  small and neglecting  $s^2$  in Eq (A.38) the wave number of the oscillating function is the square root of the right-hand side.

$$k_z^{(z)} = k \sqrt{\epsilon(z)} / \sqrt{\gamma T/mc^2} \tag{A.39}$$

The wavelength  $\frac{2\pi}{k}$  is clearly determined also.

#### Ponderomotive Force ( $F_{NL}$ ) (Ref 4:257-58)

Beginning with the electron equation of motion:

$$m \frac{dV}{dt} = -e[E(r) + VxB(r)] \tag{A.40}$$

assuming an electric field of the form

$$E = E_s(r) \cos \omega t$$

neglecting  $V \times B$  of Eq (A.40)

$$m dV_1/dt = -e E(r_0)$$

$$V_1 = - (e/m\omega) E_s \sin \omega t = dr_1/dt \quad (A.41)$$

and integrating over time:

$$\delta r_1 = (e/m\omega^2) E_s \cos \omega t \quad (A.42)$$

Since  $r_0$  is the initial position of the particle.

Expanding  $E(r)$  about  $r_0$  one obtains;

$$E(r) = E(r_0) + (\delta r_1 \cdot \nabla) E \bigg|_{r=r_0} + \dots$$

from Maxwell's equation,  $B_1$  can be found as

$$\nabla \times E = - dB/dt$$

$$B_1 = - \frac{1}{\omega} \nabla \times E_s \bigg|_{r=r_0} \sin \omega t \quad (A.43)$$

now the second-order part of Eq (A.40) is

$$m dV_2/dt = -e [(\delta r_1 \cdot \nabla) E + V_1 \times B_1] \quad (A.44)$$

Substituting (A.41), (A.42), and (A.43) into (A.44) gives  
after time averaging

$$m \left\langle \frac{dV_2}{dt} \right\rangle = - \frac{e^2}{m\omega^2} \frac{1}{2} [ (E_s \cdot \nabla) E_s + E_s \times (\nabla \times E_s) ] = F_{NL} \quad (A.45)$$

reducing by expanding the double cross product gives:

$$F_{NL} = -\frac{1}{4} \frac{e^2}{m\omega^2} \nabla E_s^2 \quad (A.46)$$

which is the force on a single electron. The force density is found by multiplying (A.46) by  $n_0$ . In terms of  $\omega_p$  this becomes:

$$F_{NL} = -\frac{\omega_p^2}{\omega^2} \frac{\nabla E_s^2}{16\pi} \quad (A.47)$$

since  $\omega_p^2/\omega^2 = z/L$  in our plasma:

$$F_{NL} = -\frac{1}{16\pi} \frac{z}{L} \nabla E_s^2 \quad (A.48)$$

## Appendix B: Cold Plasma Data Curves

This appendix contains quantities of interest as a function of position in a cold plasma for a power of 120 watts/cm<sup>2</sup>. Power scaling relationships are given in the body of the paper. The curves are grouped according to the collision frequency used. Each group contains:

$E_z$  (E longitudinal) in e.s.u.

$E_x$  (E transverse) in e.s.u.

$N_1$  the hot electron number density (cm<sup>-3</sup>)

$F_{NL}$  the Ponderomotive force per cubic centimeter

$v_{transverse}$  the velocity of the hot electrons due to

$E_x$  in cm/sec

$v_{longitudinal}$  the velocity of the hot electrons due to

$E_z$  in cm/sec

$B$  the magnetic field in Gauss

Note that  $v_{os}$  used in the paper is the square root of the sum of the squares of  $v_{transverse}$  and  $v_{longitudinal}$ . Since each group of figures is the same save the value of  $v/\omega$ , collective figure titles will be given and the figures simply numbered. The following are the titles:

Figures B-1 - B-7; Data for  $v/\omega = .002$

Figures B-8 - B-14; Data for  $v/\omega = .008$

Figures B-15 - B-21; Data for  $v/\omega = .02$

Please note that the legend of each figure contains additional information.

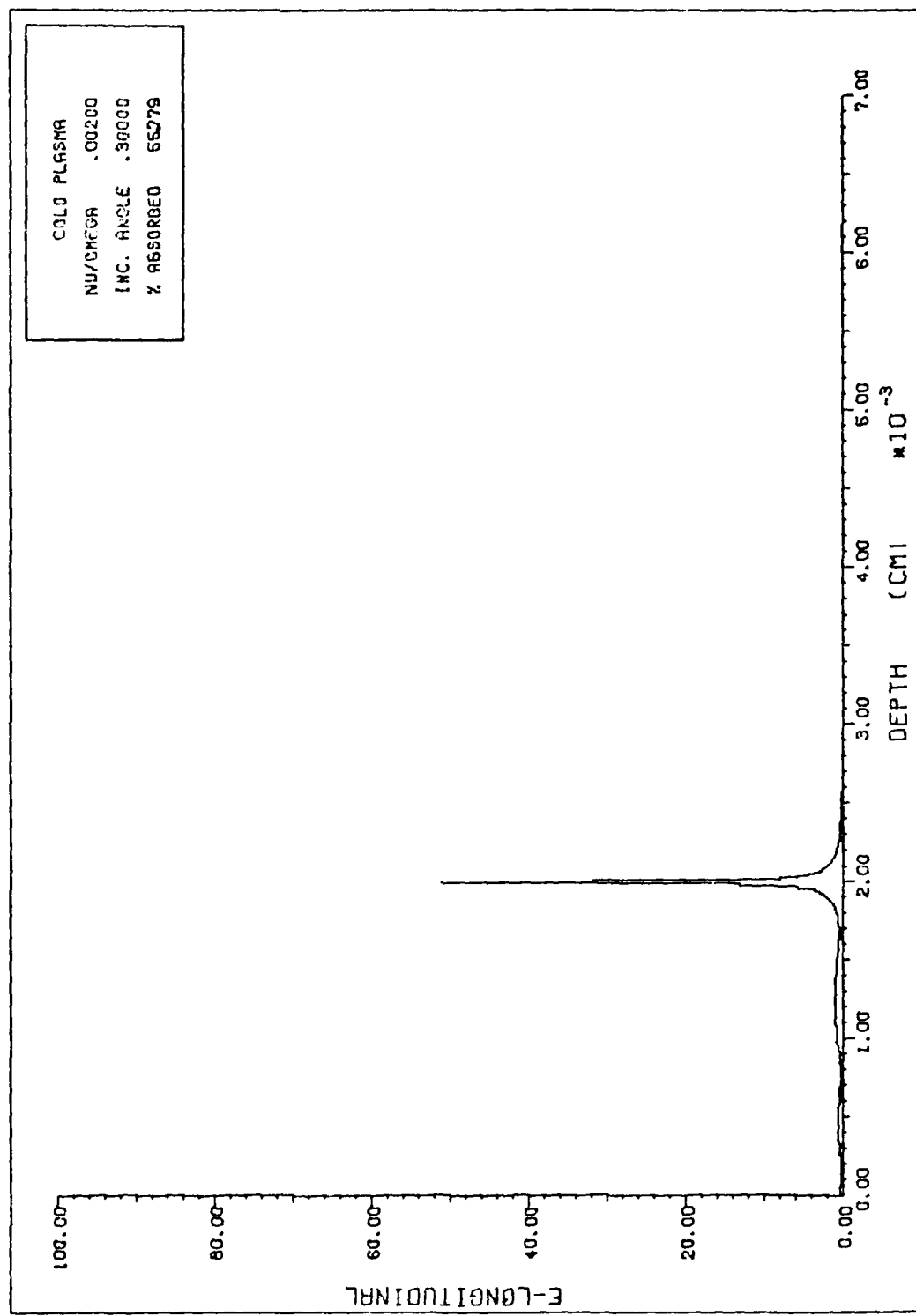


Figure B-1.

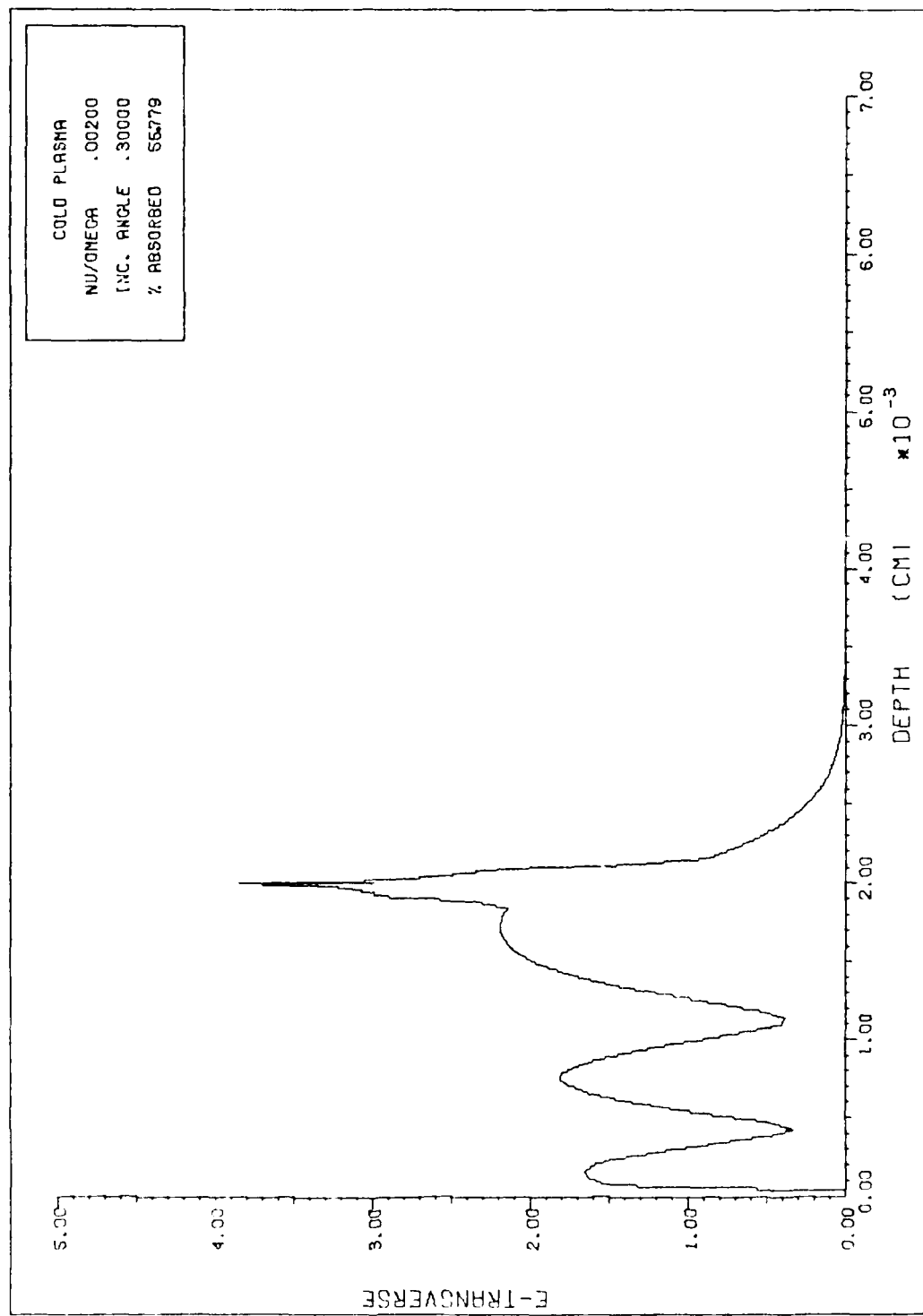


Figure 2-2.

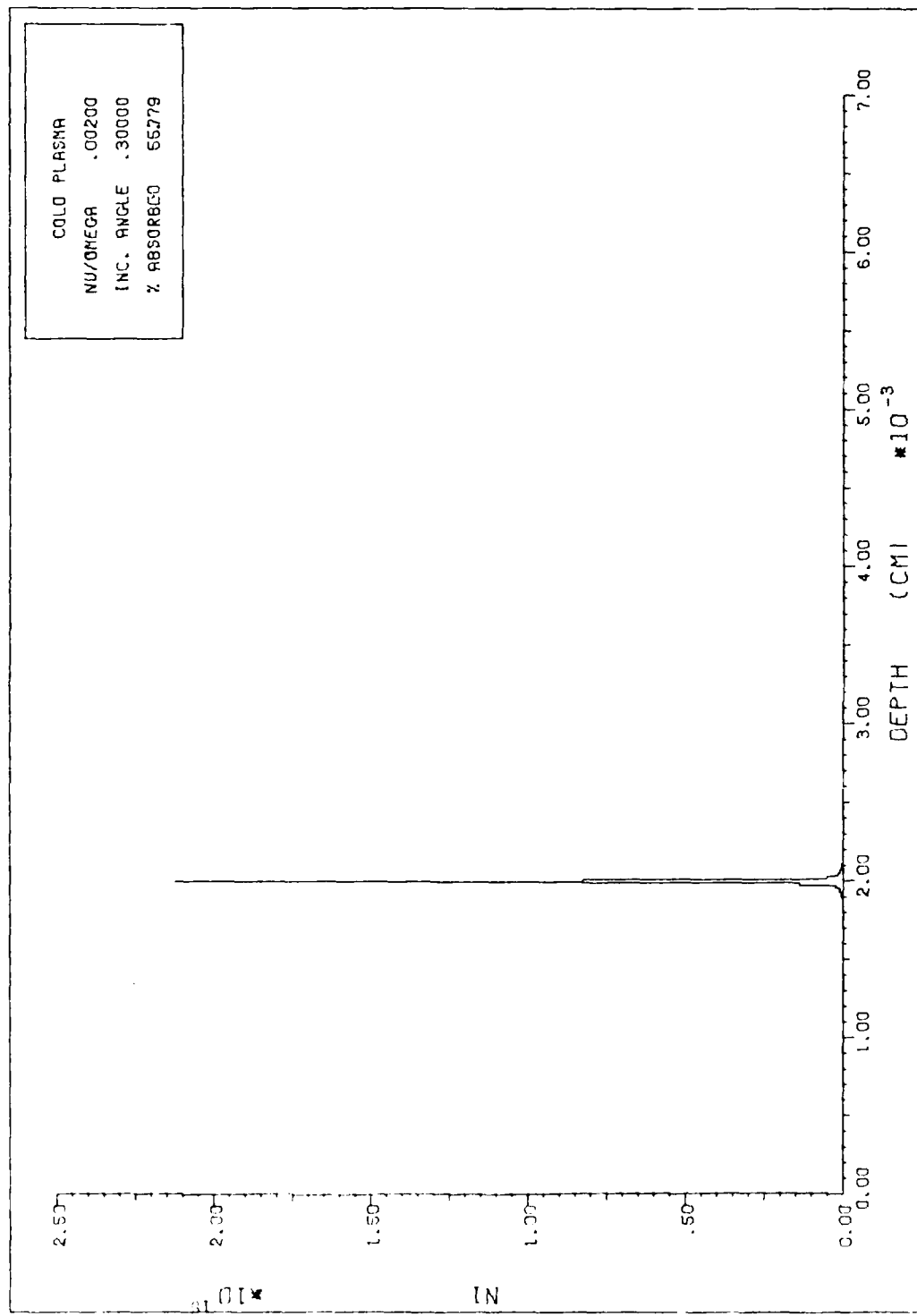
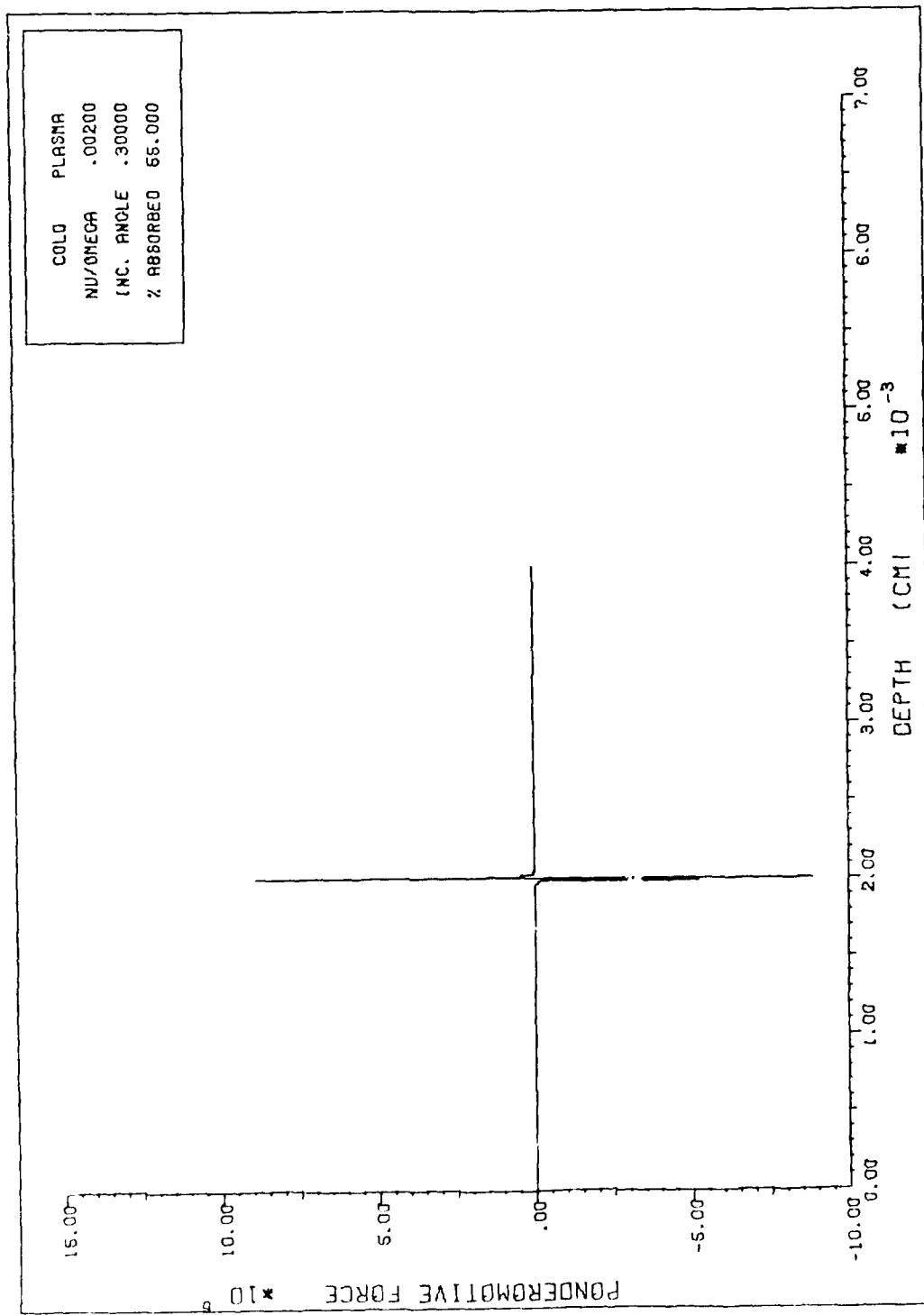


Figure 7-2.



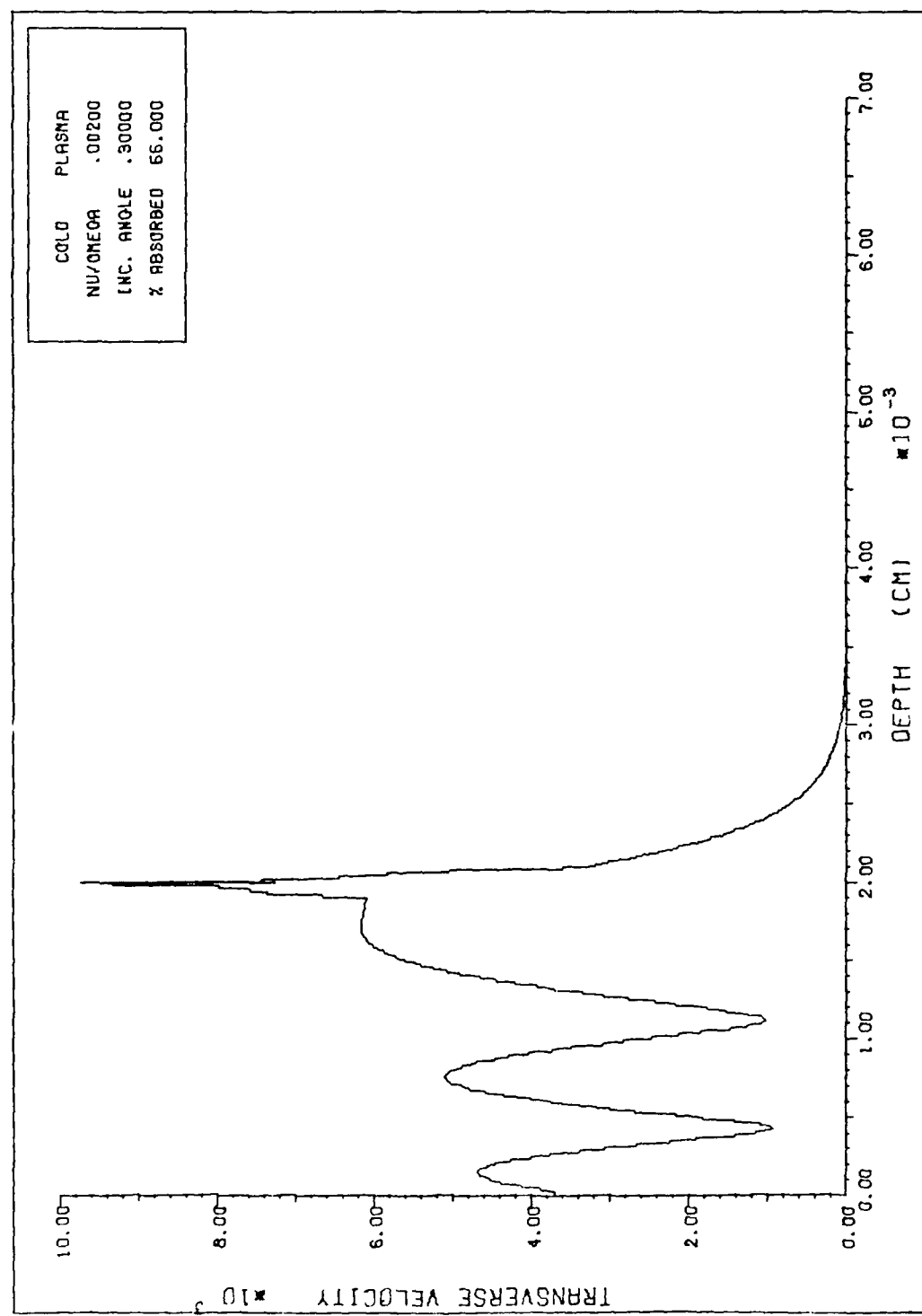
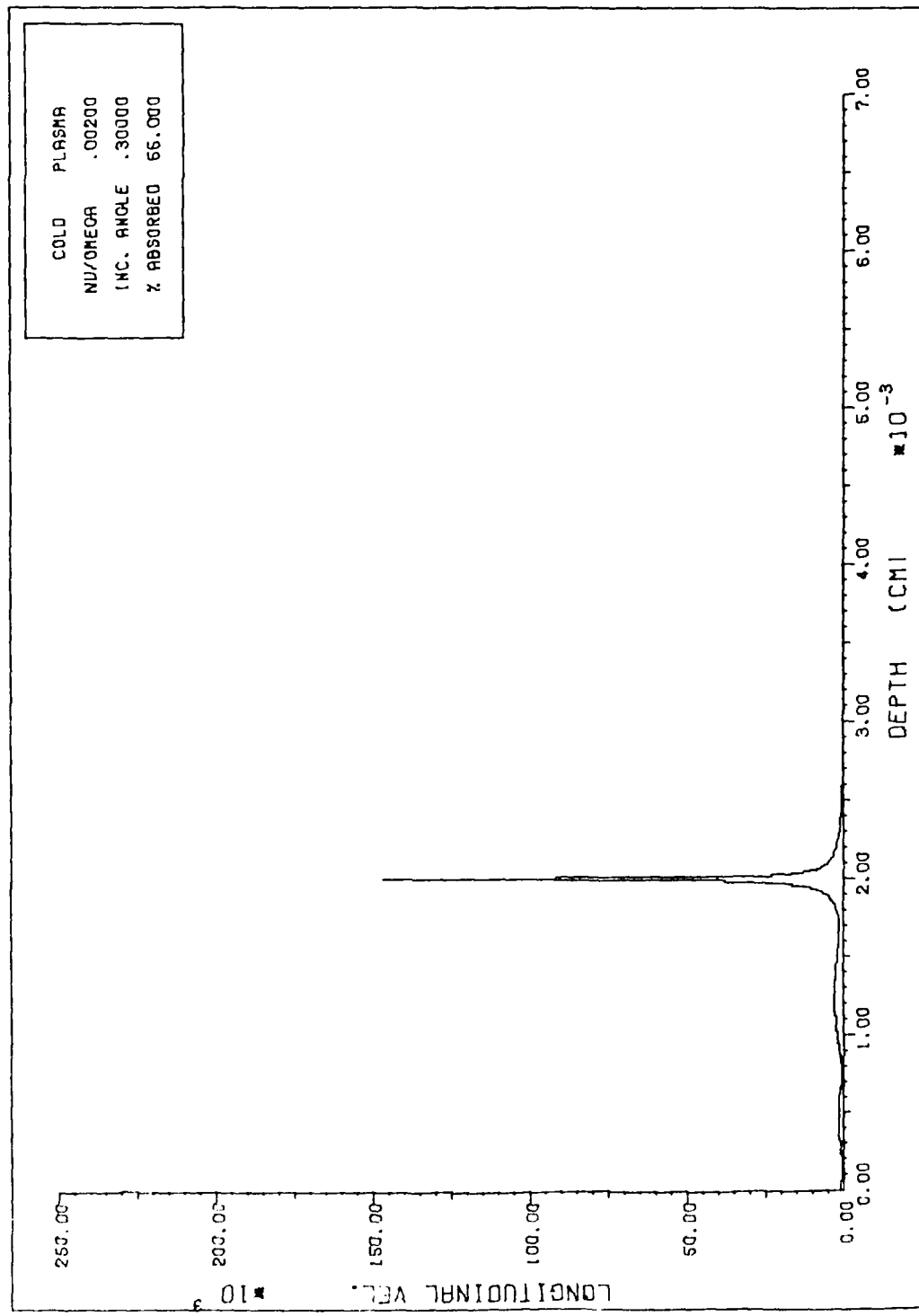


Figure 5-5.



卷之二

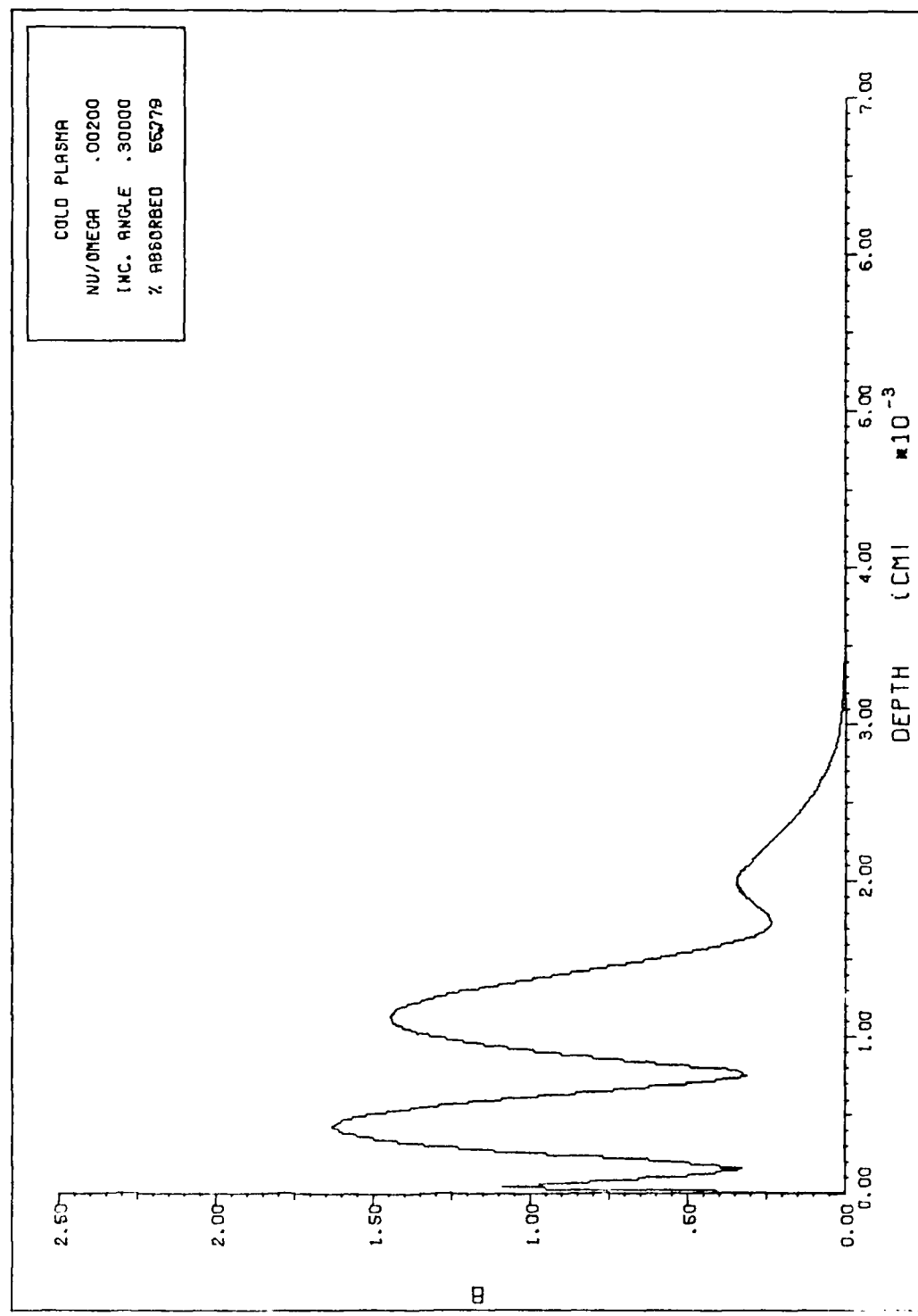


Figure E-7.

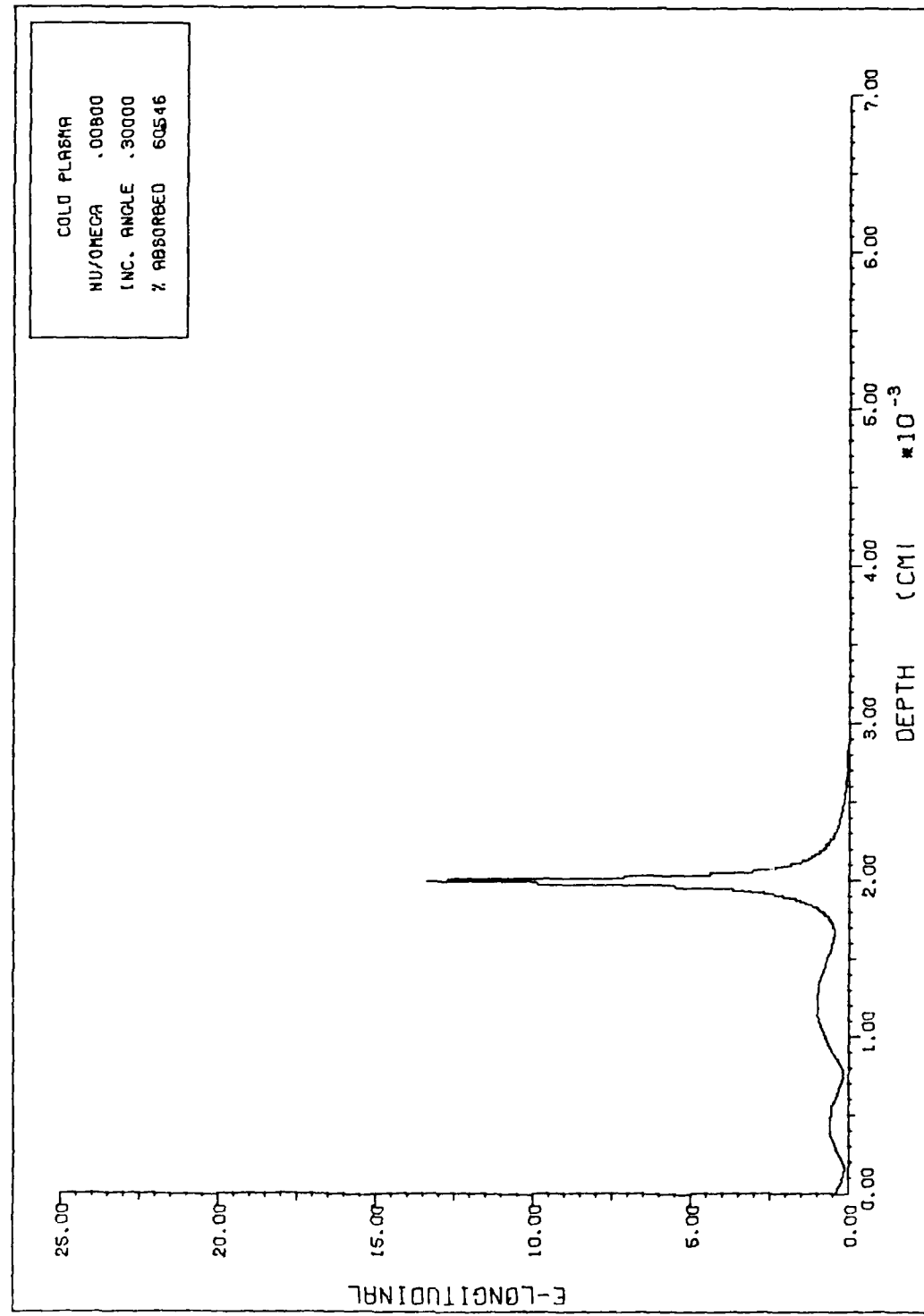


Figure 2-2.

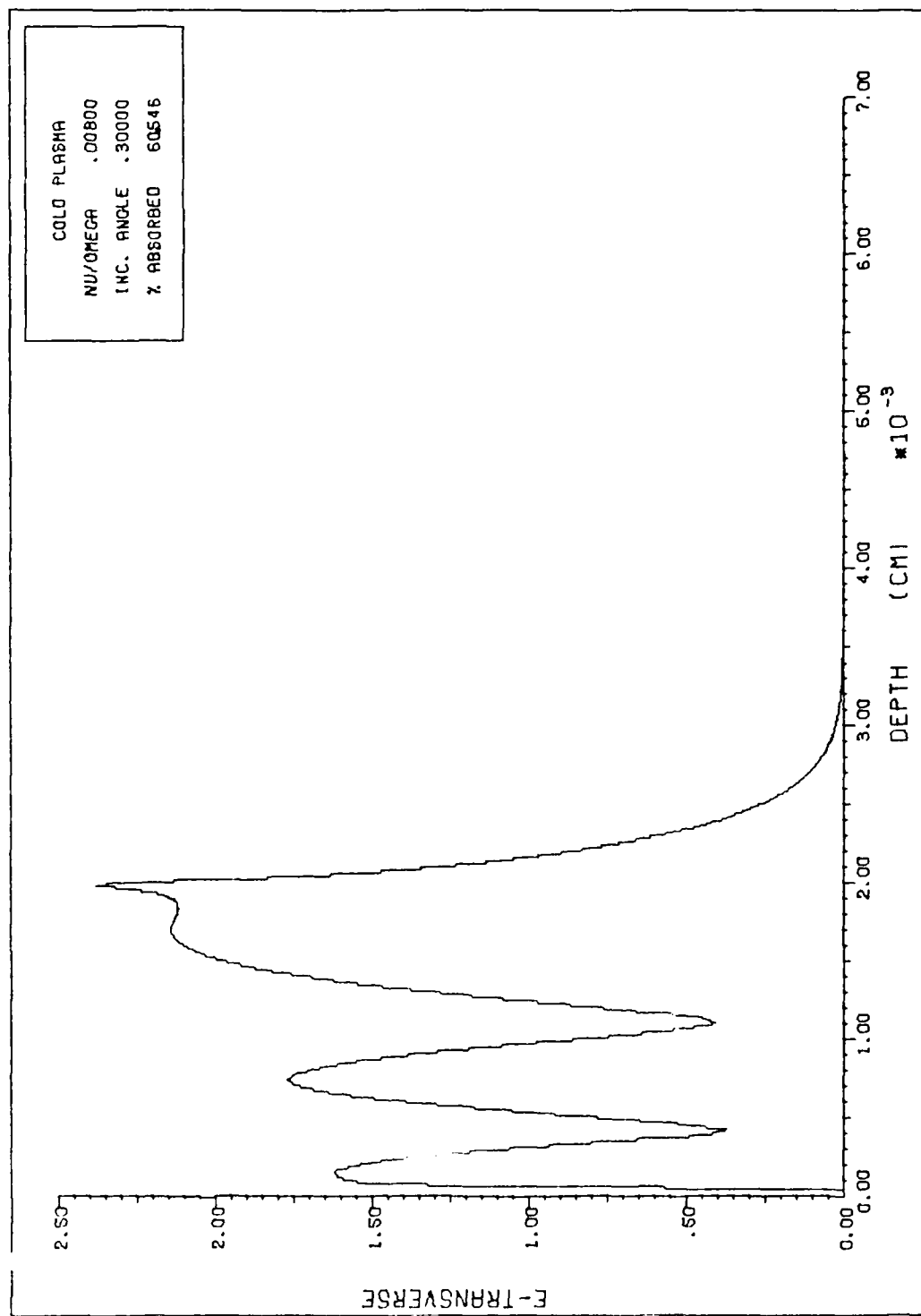


Figure 5-2.

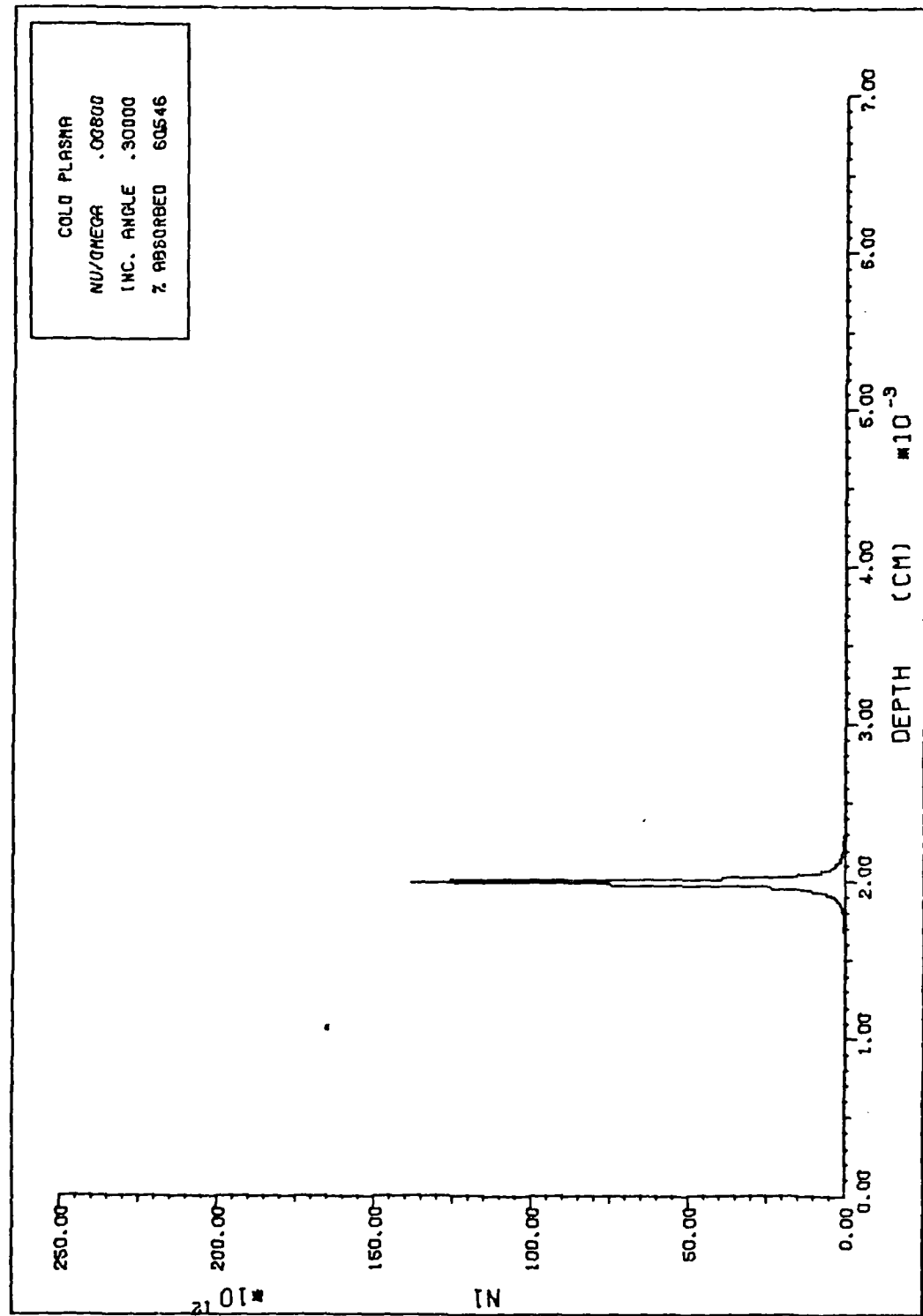


Figure 3-10.

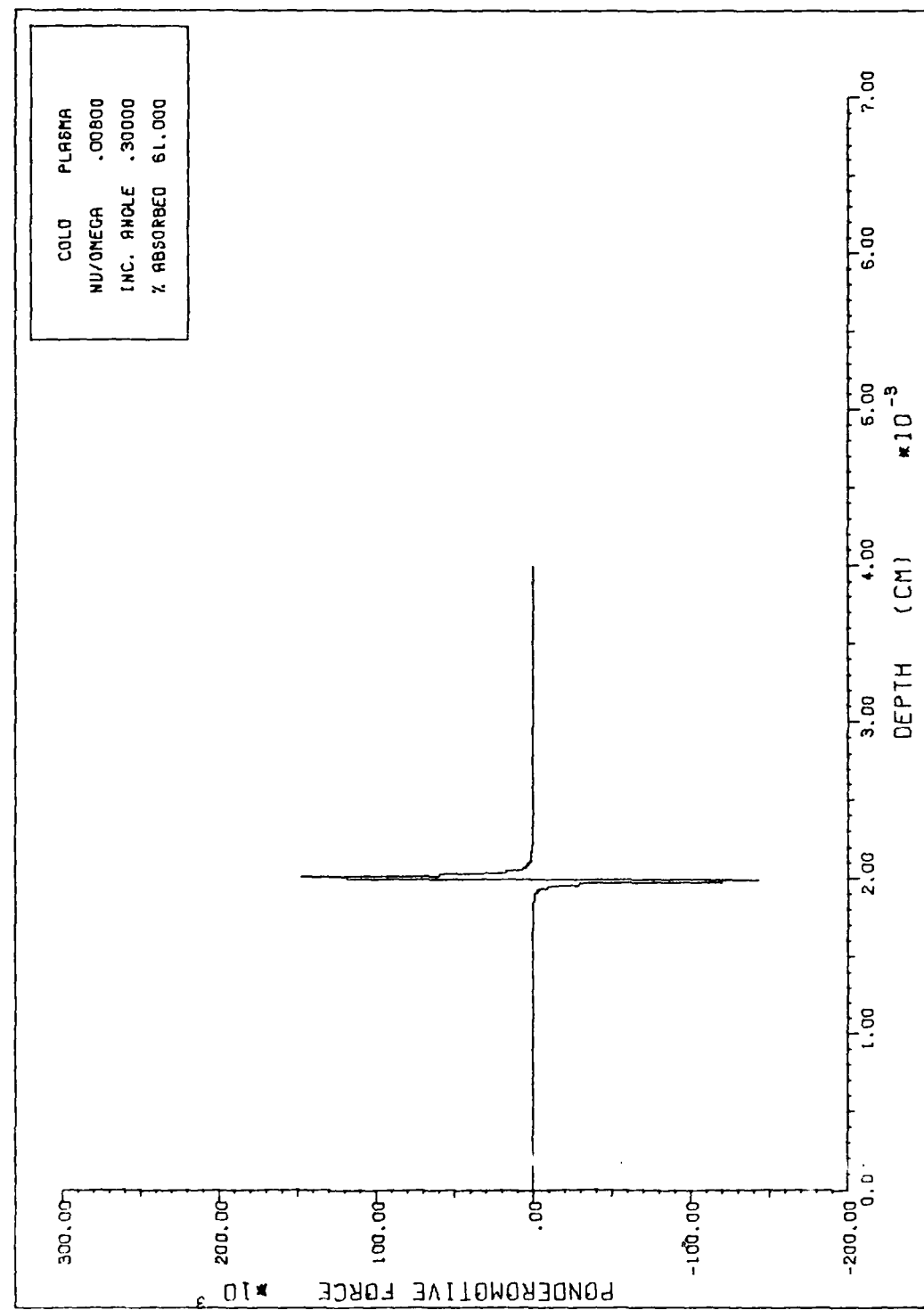


Figure B-11.

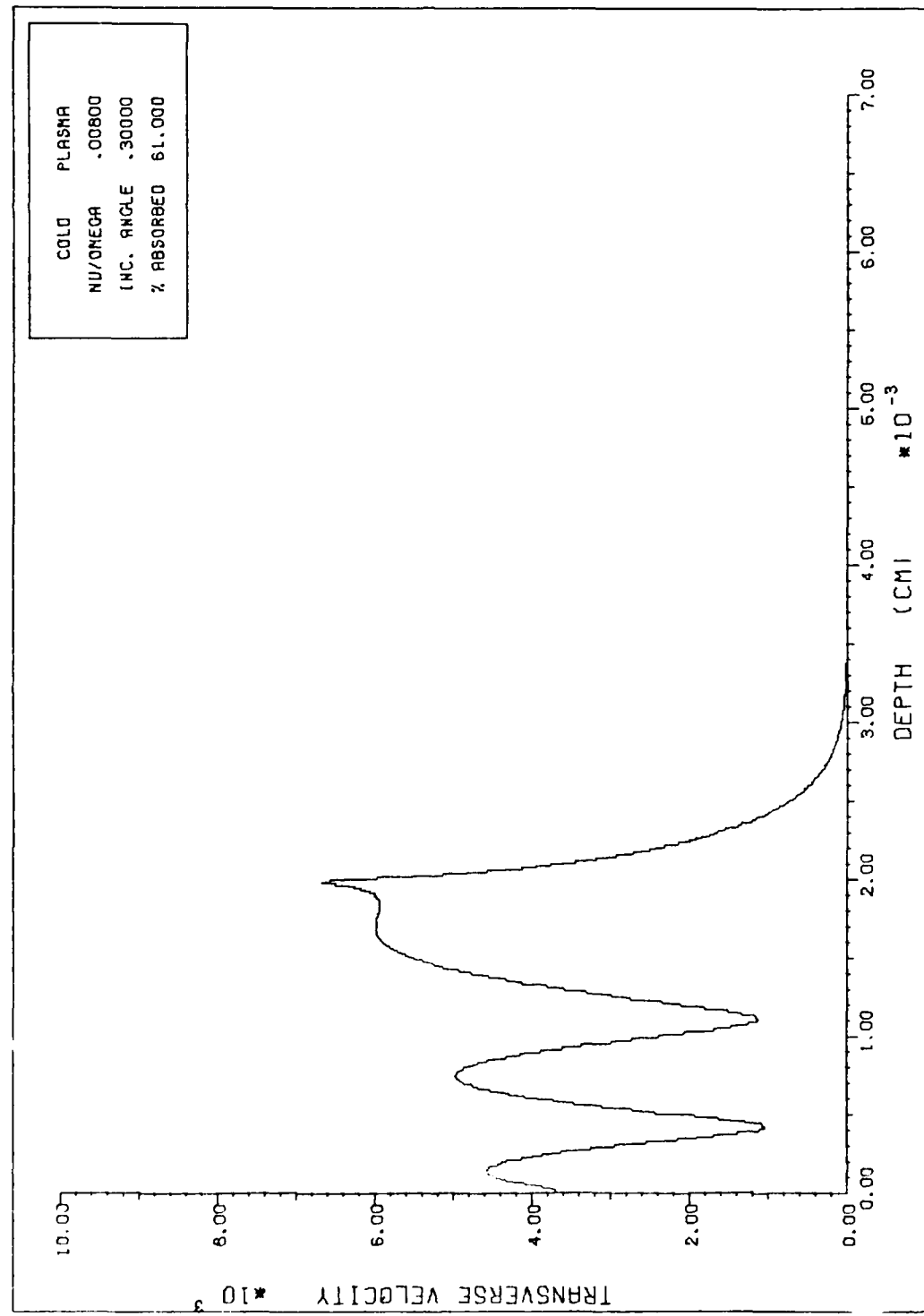


Figure 3-12.

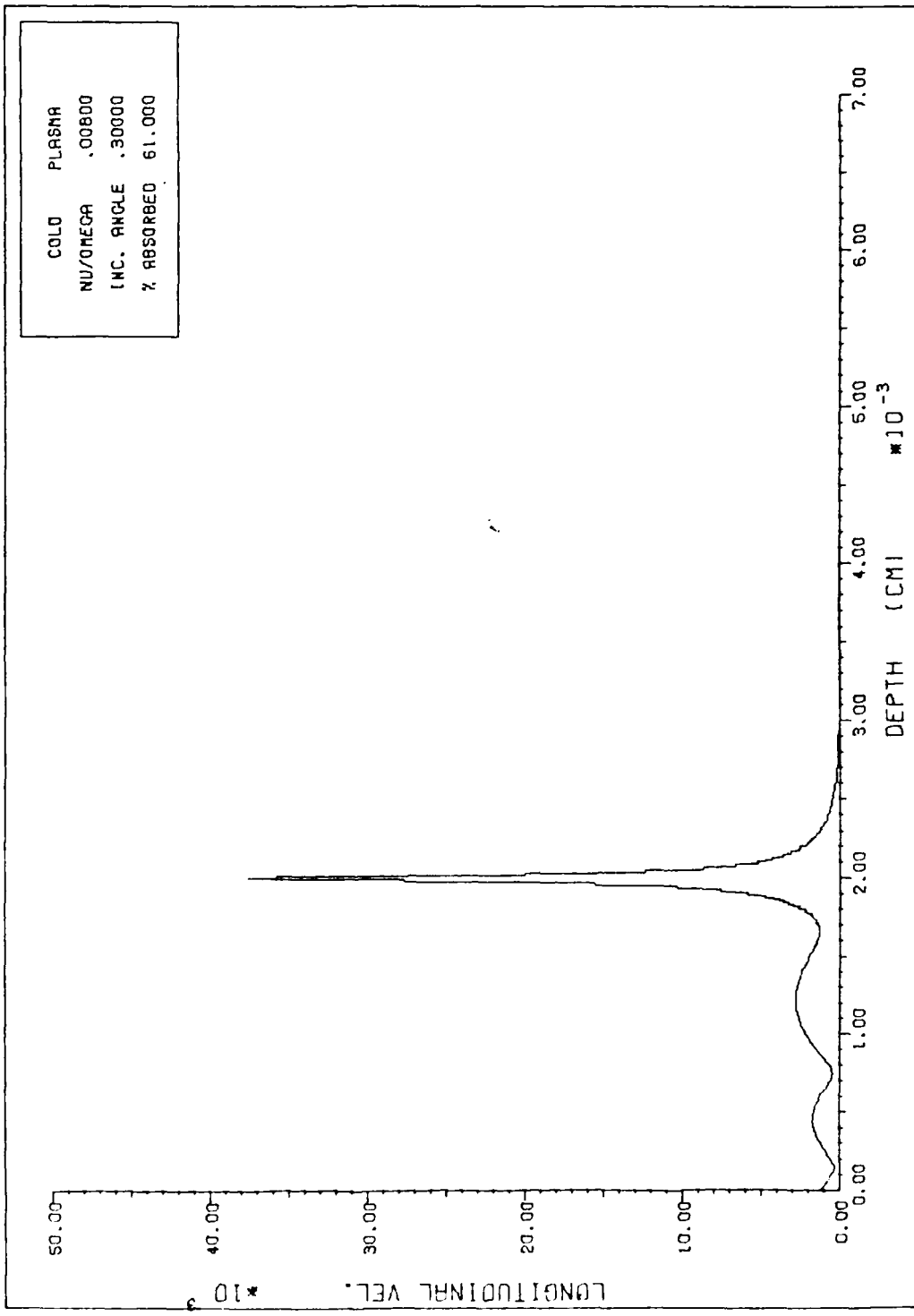


Figure 3-13.

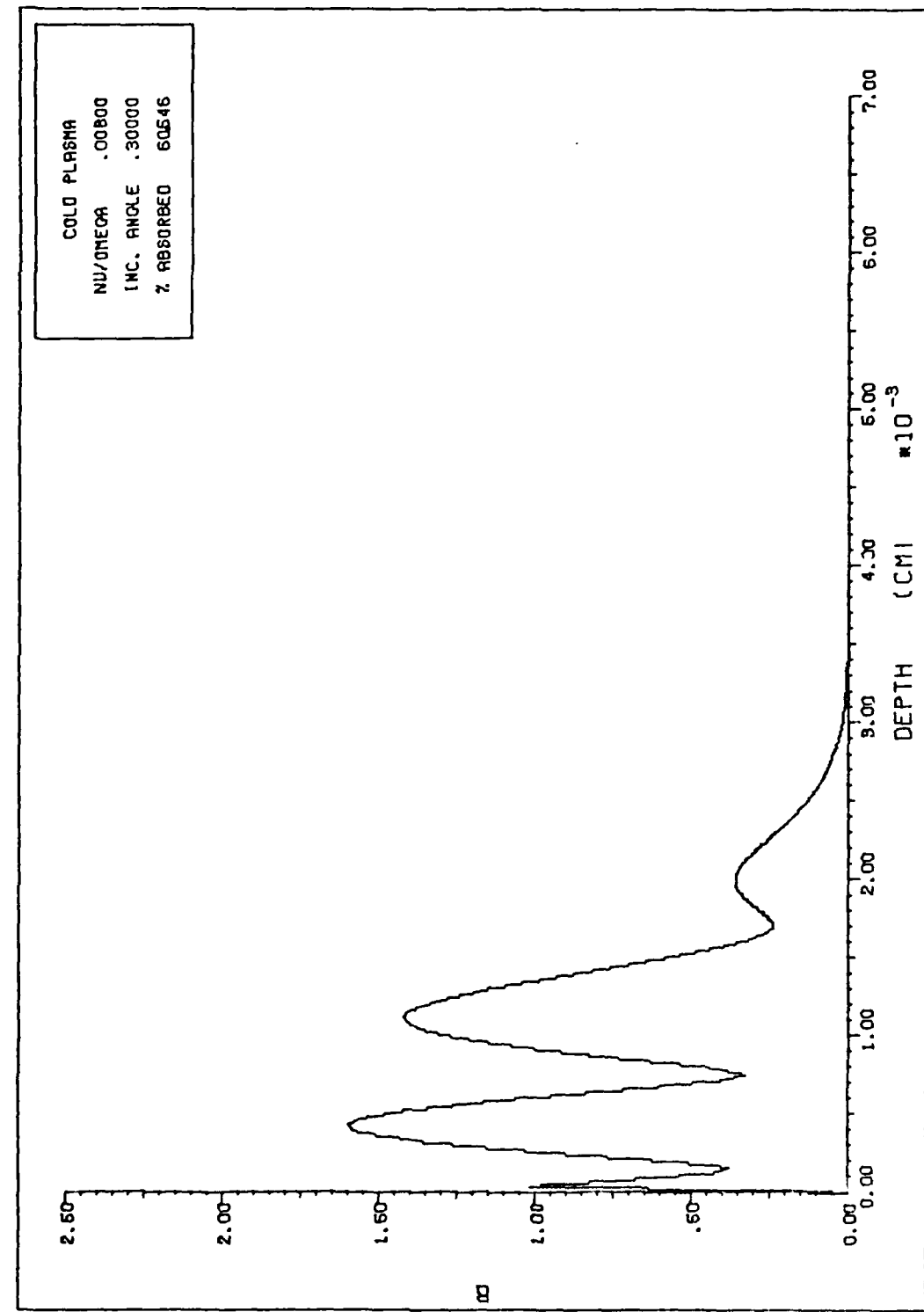


Figure 13-14.

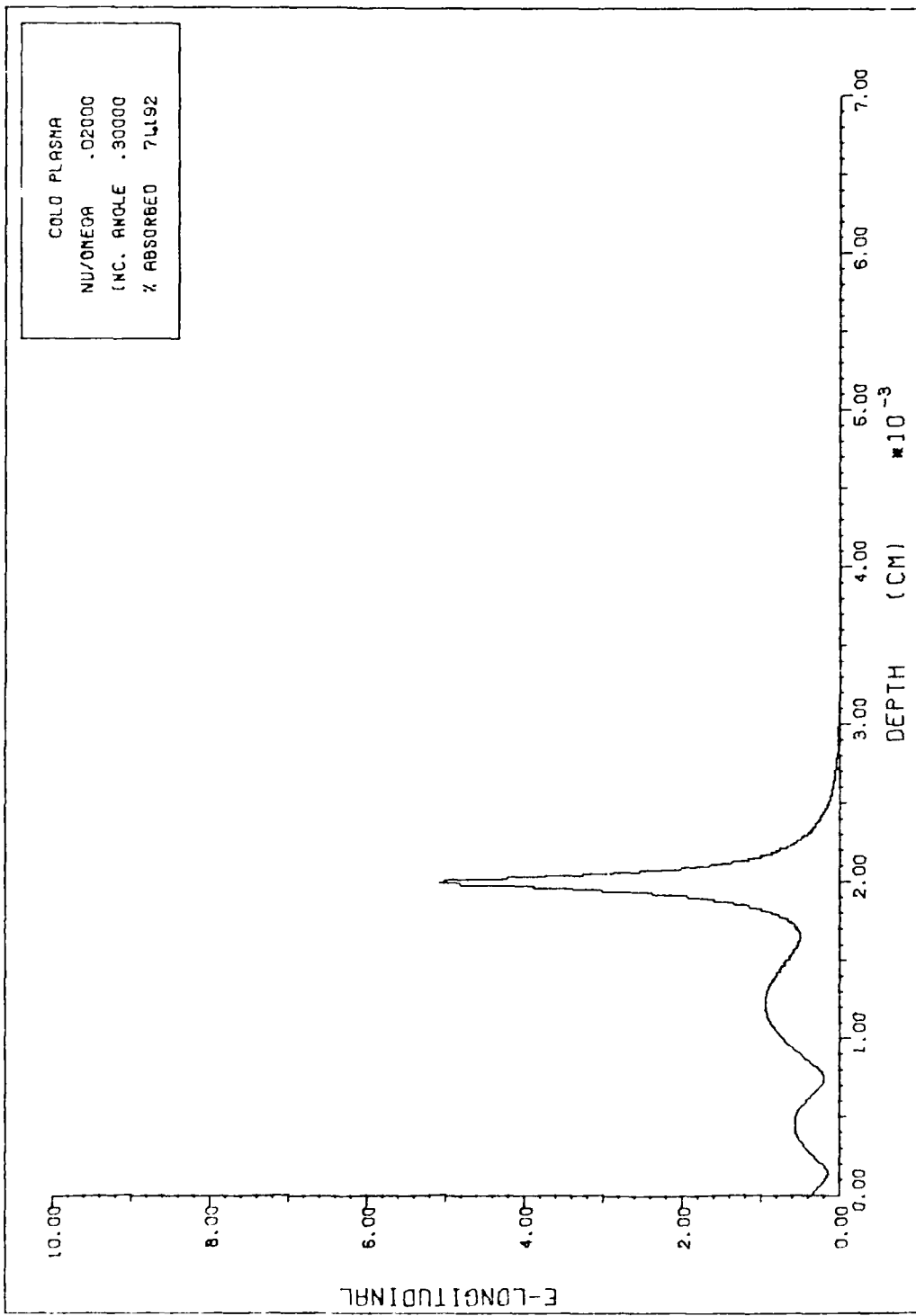


Figure 2-15.

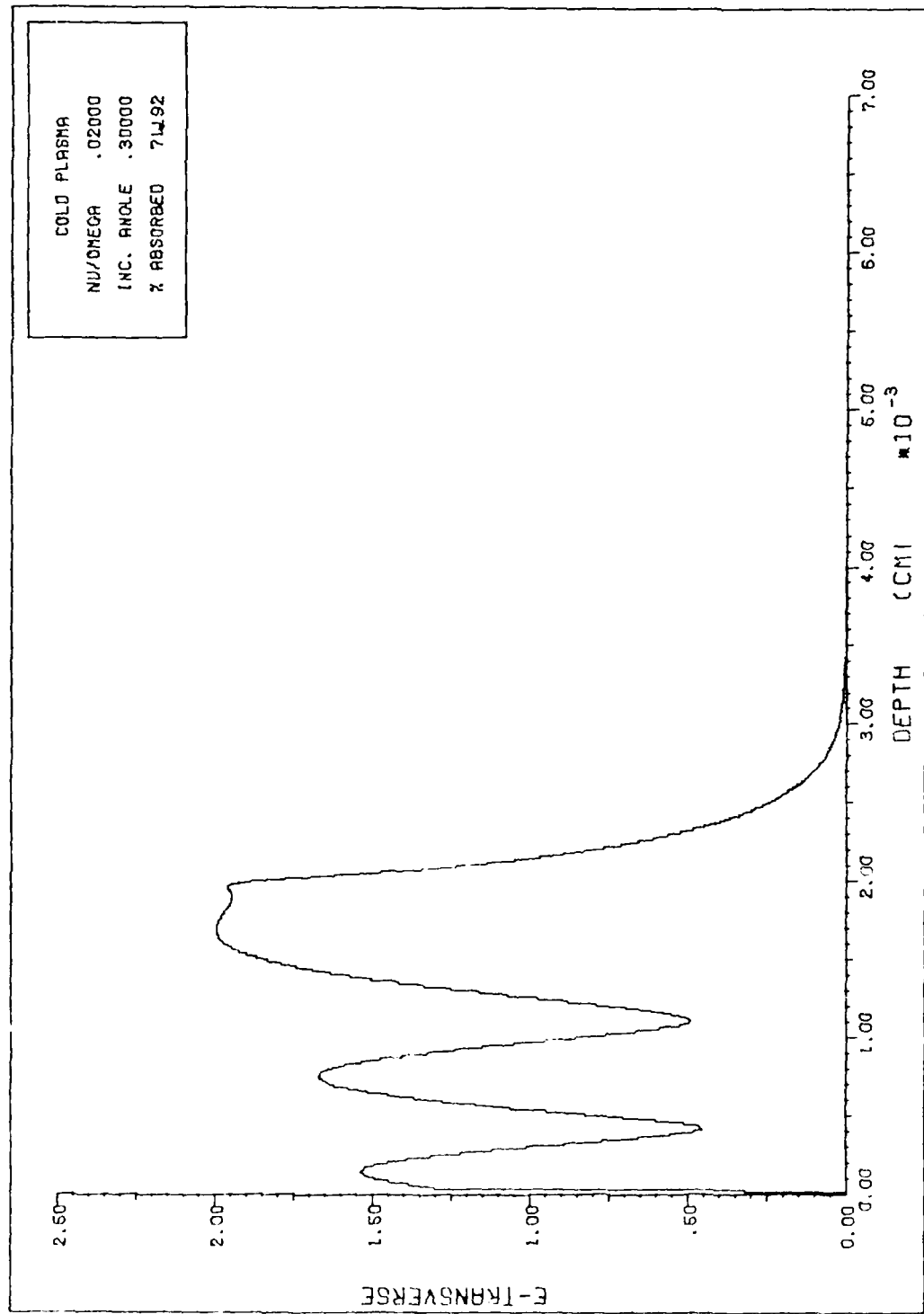


Figure 2-16.

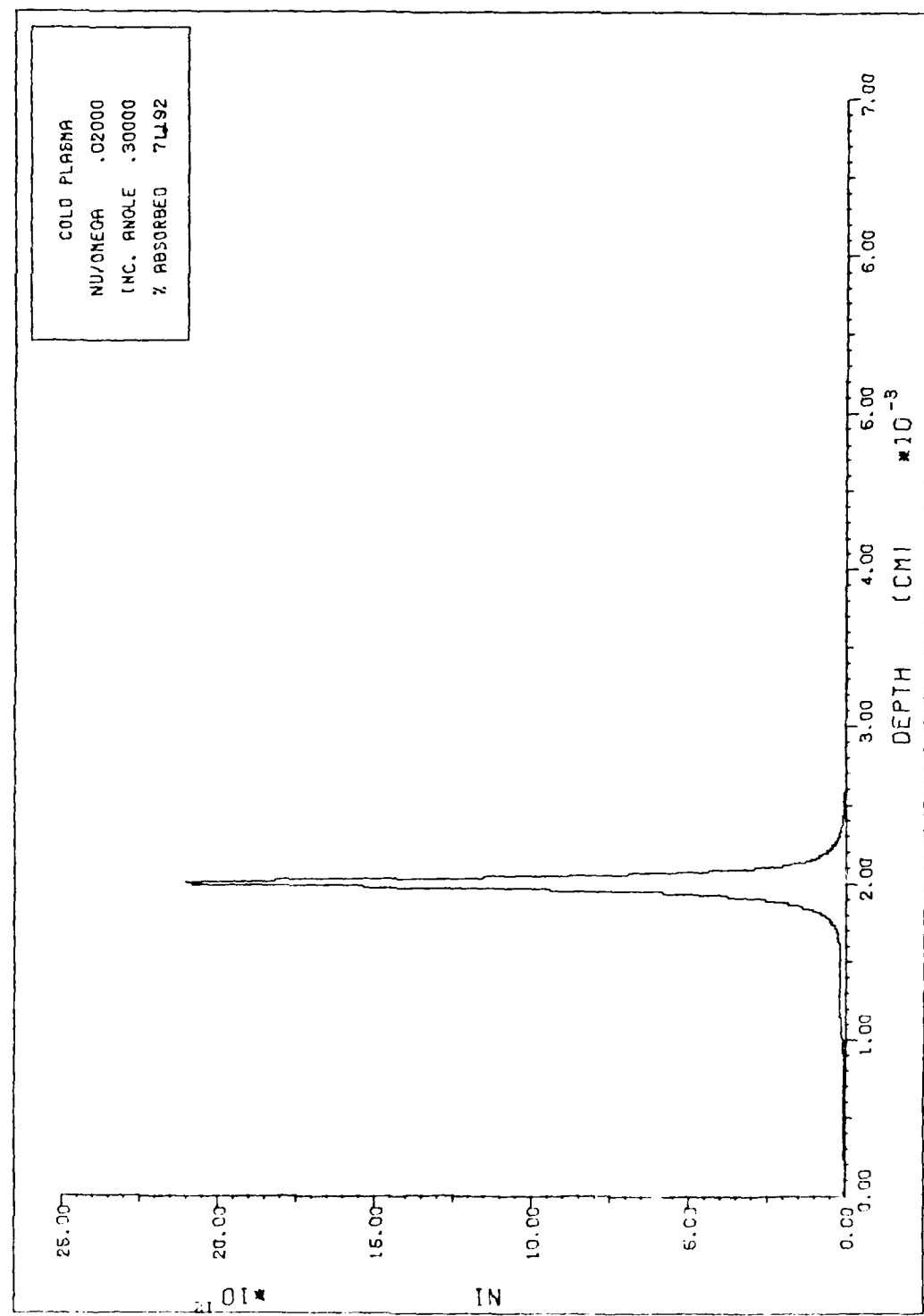


Figure 1-17.

AD-A100 802

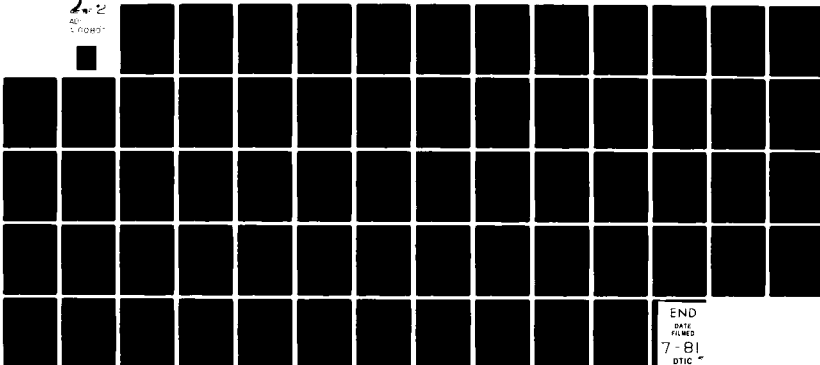
AIR FORCE INST OF TECH WRIGHT-PATTERSON AFB OH SCHOO--ETC F/G 20/9  
RESONANCE ABSORPTION OF LASER LIGHT BY WARM AND COLD PLASMAS. (U)  
MAR 81 J H RUBLE

UNCLASSIFIED

AFIT/GENE/PH/81-9

NL

1-2  
2-  
3-0085-



END  
DATE  
FILED  
7-81  
DTIC

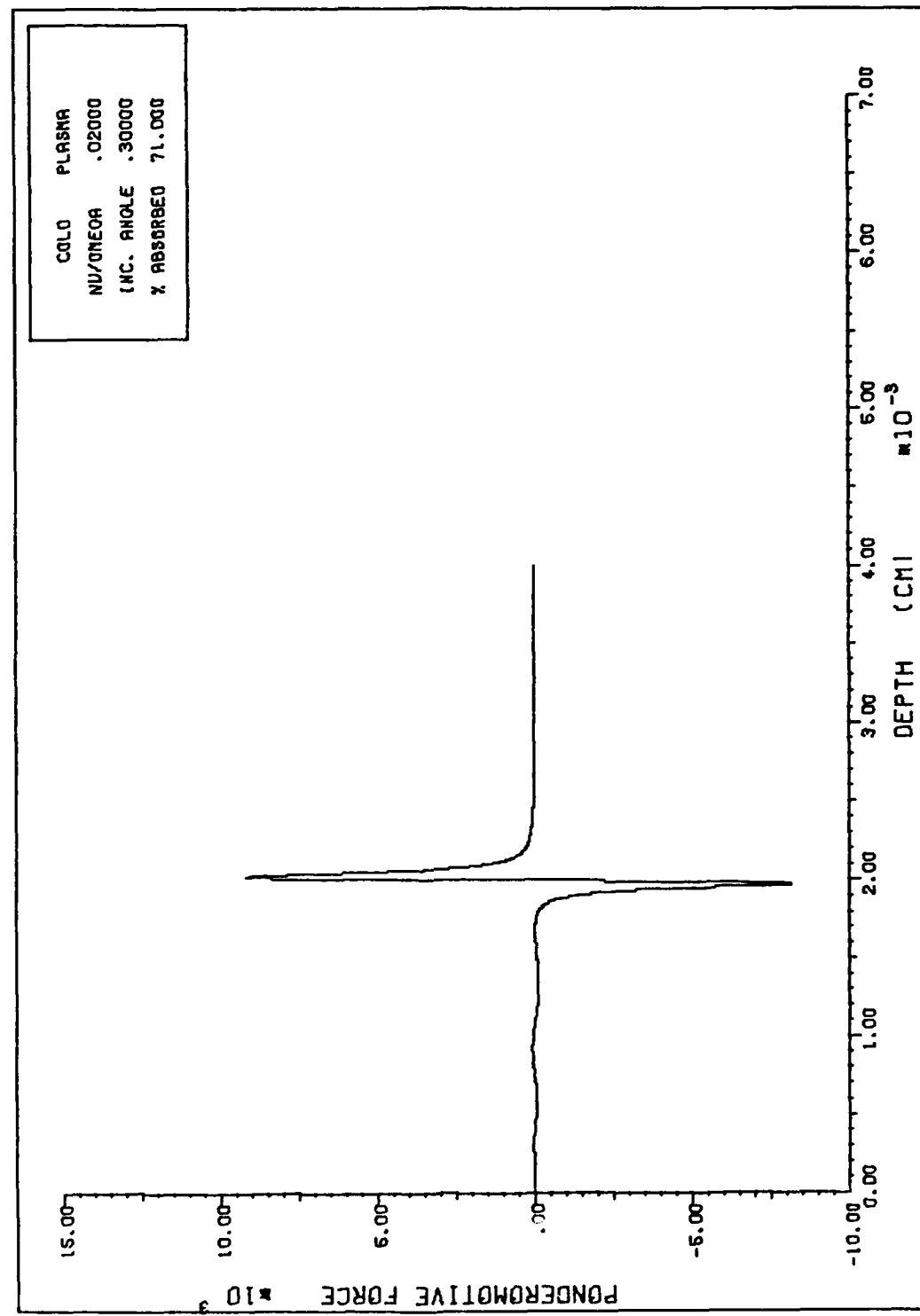


Figure 2-13.

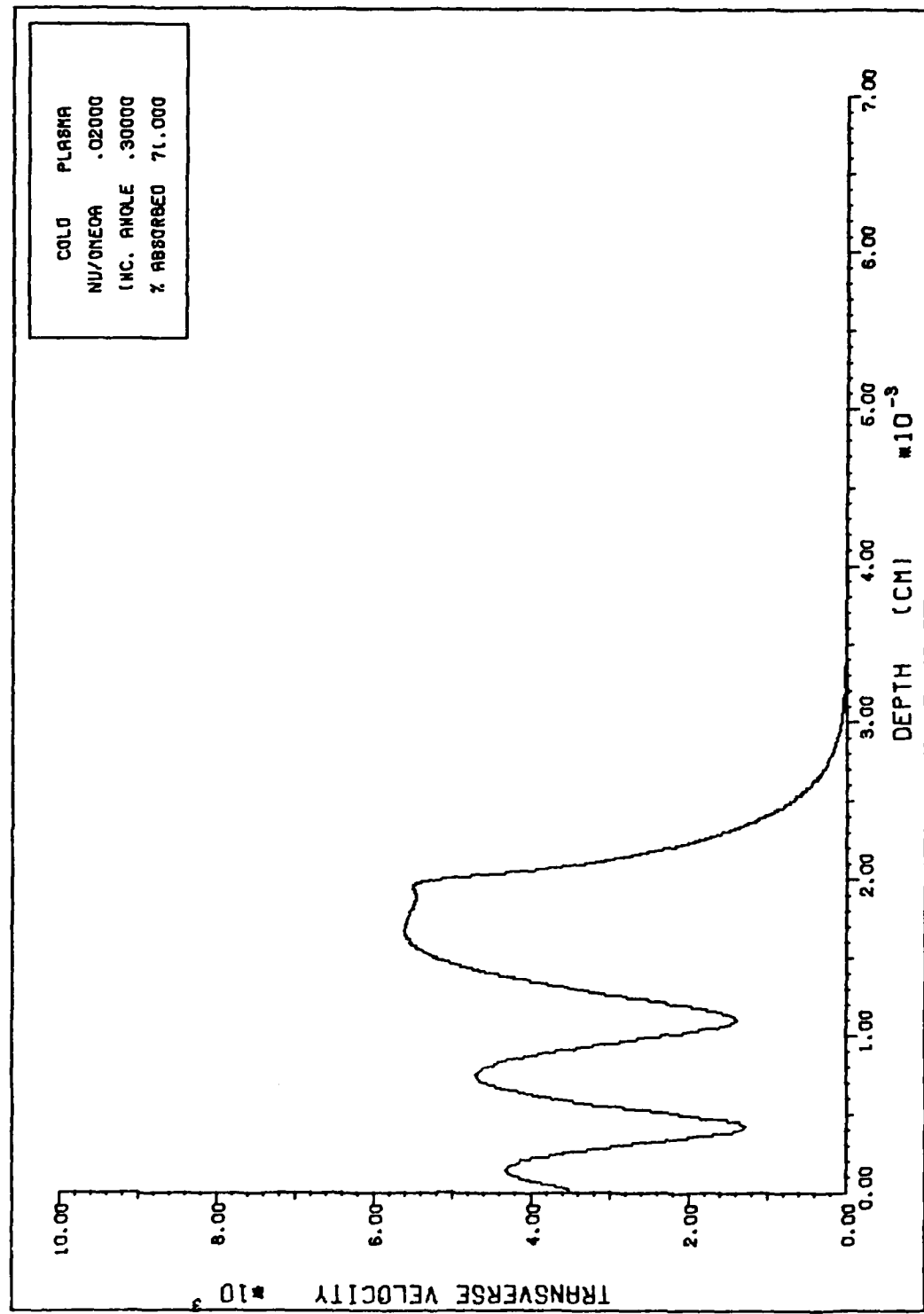


Figure B-19.

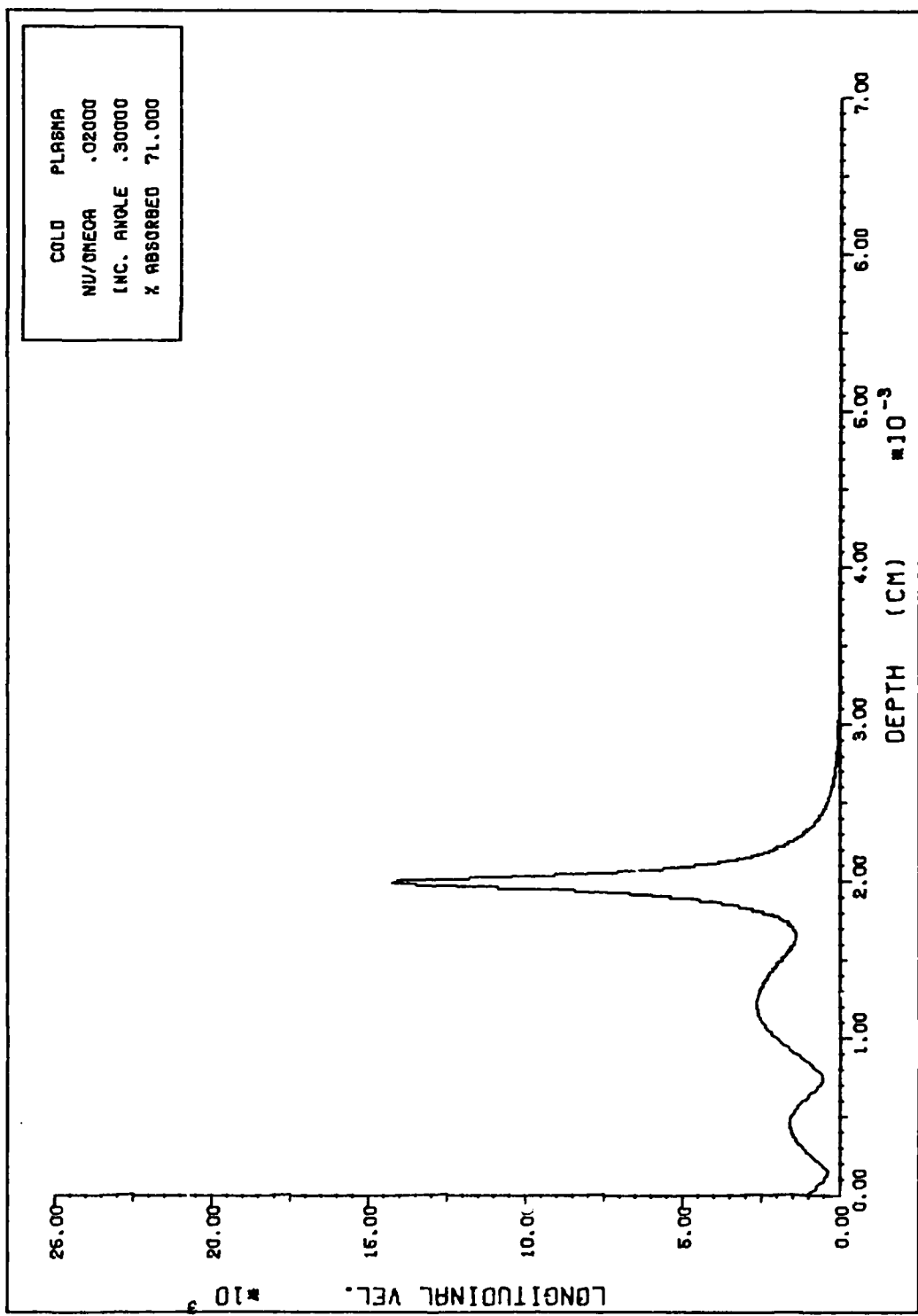
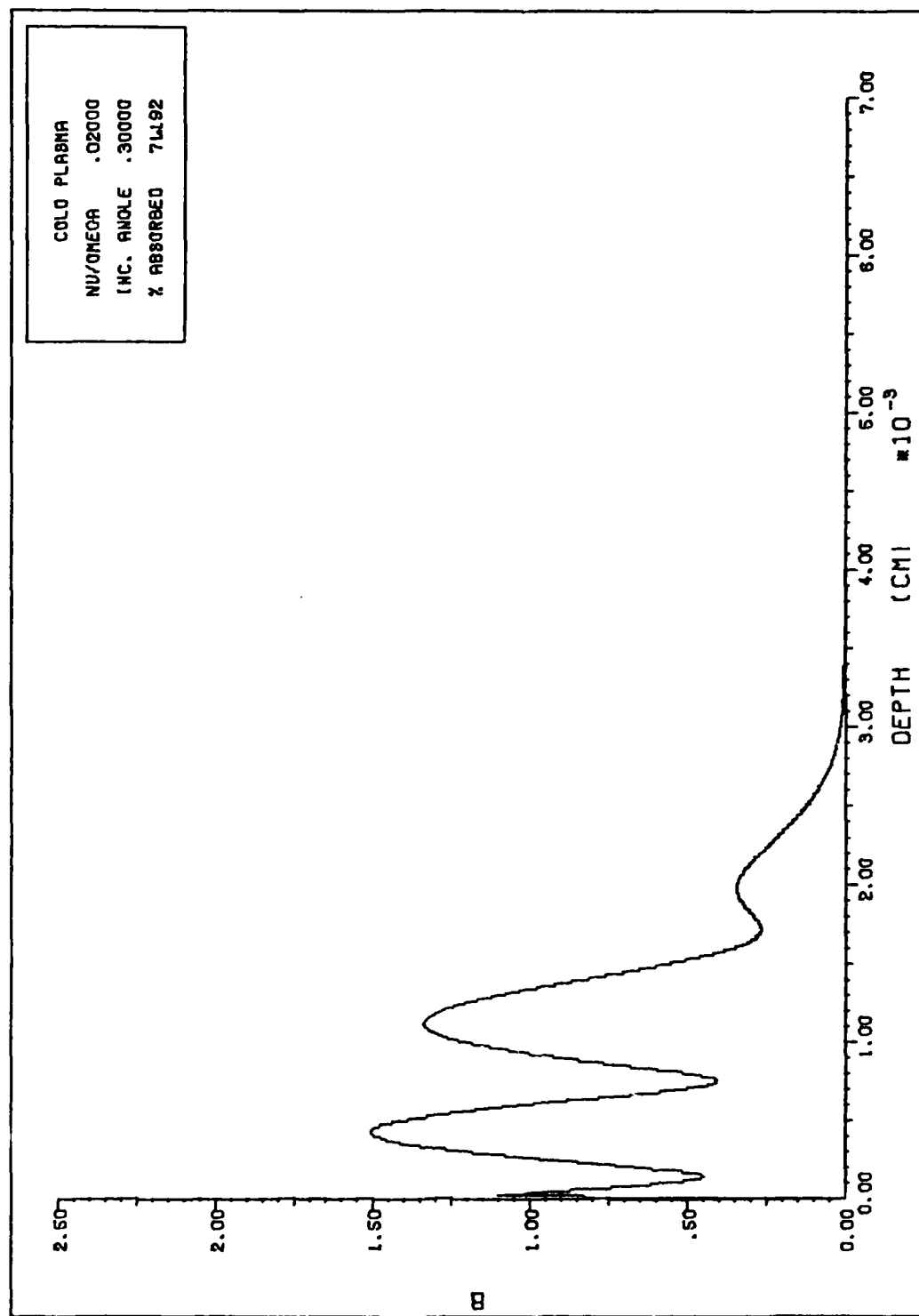


Figure B-20.

Figure B-21.



### Appendix C: Warm Plasma Data Curves

This appendix contains quantities of interest as a function of position in a warm plasma at a power of 120  $\text{W/cm}^2$ . Power scaling relationships are given in the body of the report. The curves are grouped according to the electron temperature and Landau damping coefficient (L.D.C. or  $v_L/\omega$ ) used. Each group contains:

$E_z$  (E longitudinal) in e.s.u.

$E_x$  (E transverse) in e.s.u.

$N_1/N_0$  or  $N_1/N_c$  the ratio of the hot electron number density to the initial number density or to the value of  $N_0$  at the critical surface ( $1.12 \times 10^{19}$ )

$F_{NL}$  the Ponderomotive force per cubic centimeter

$v_{transverse}$  the velocity of the hot electrons in the x-direction cm/sec

$v_{longitudinal}$  the velocity of the hot electrons in the z-direction cm/sec

$B$  the magnetic field in Gauss

Note that  $v_{os}$  used in the report is the square root of the sum of the squares of  $v_{transverse}$  and  $v_{longitudinal}$ . Since each set of figures is the same except for the value of  $v_L/\omega$  and the temperature, collective figure titles will be given and the figures simply numbered. The following are the titles:

Figures C-1 - C-7; Data for  $v_L/\omega = .1$  and  $T/mc^2 = .0005$

Figures C-8 - C-14; Data for  $v_L/\omega = .-9$  and  $T/mc^2 = .00125$

Figures C-15 - C-21; Data for  $v_L/\omega = .1$  and  $T/mc^2 = .005$

Figures C-22 - C-28; Data for  $v_L/\omega = .1$  and  $T/mc^2 = .05$

Figures C-29 - C-35; Data for  $v_L/\omega = .67$  and  $T/mc^2 = .00125$

Figures C-36 - C-42; Data for  $v_L/\omega = .67$  and  $T/mc^2 = .005$

Figures C-43 - C-49; Data for  $v_L/\omega = .67$  and  $T/mc^2 = .01$

Figures C-50 - C-56; Data for  $v_L/\omega = .67$  and  $T/mc^2 = .1$

Please note that the legend of each figure contains additional information.

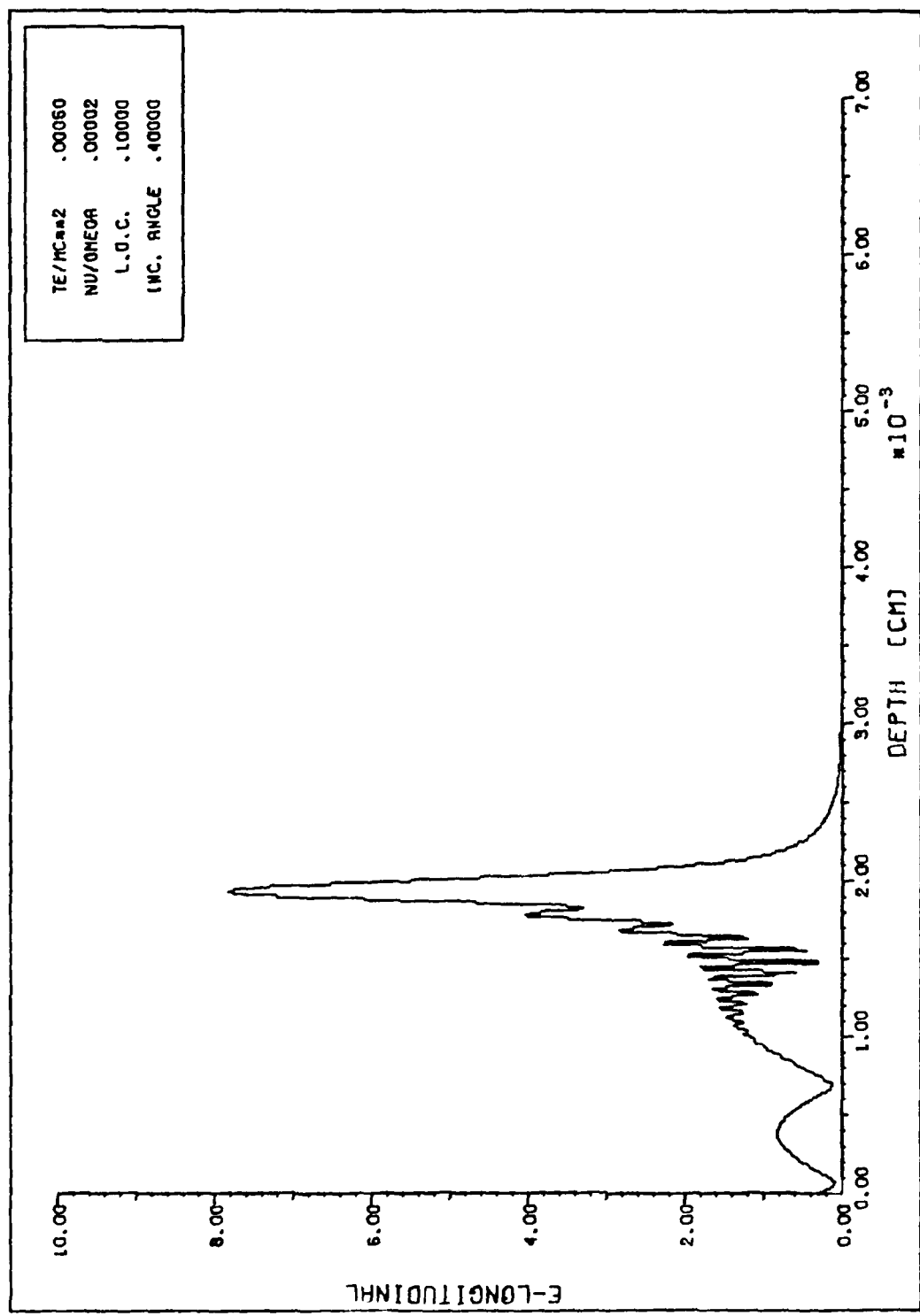
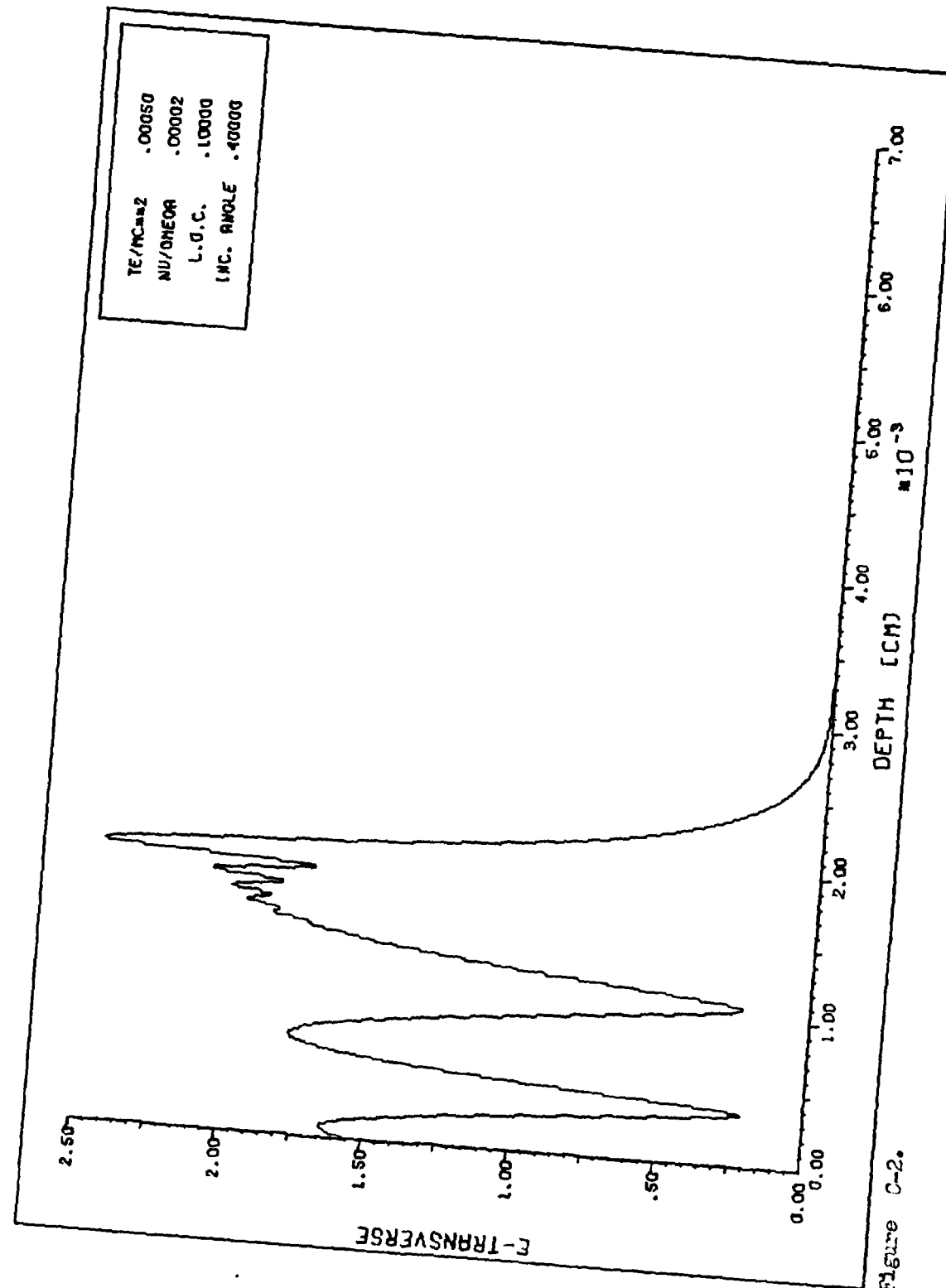


Figure C-1.



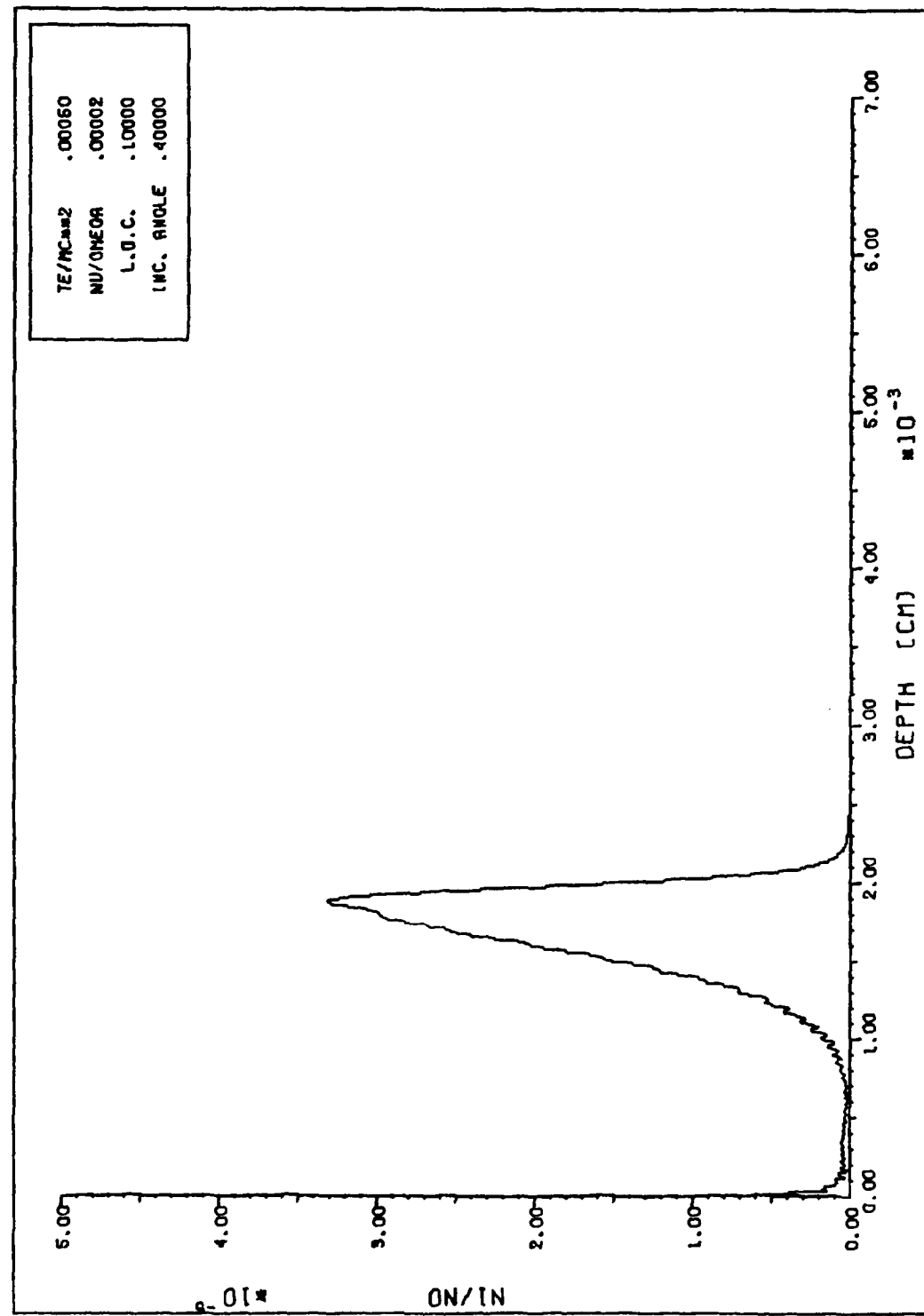


Figure C-3.

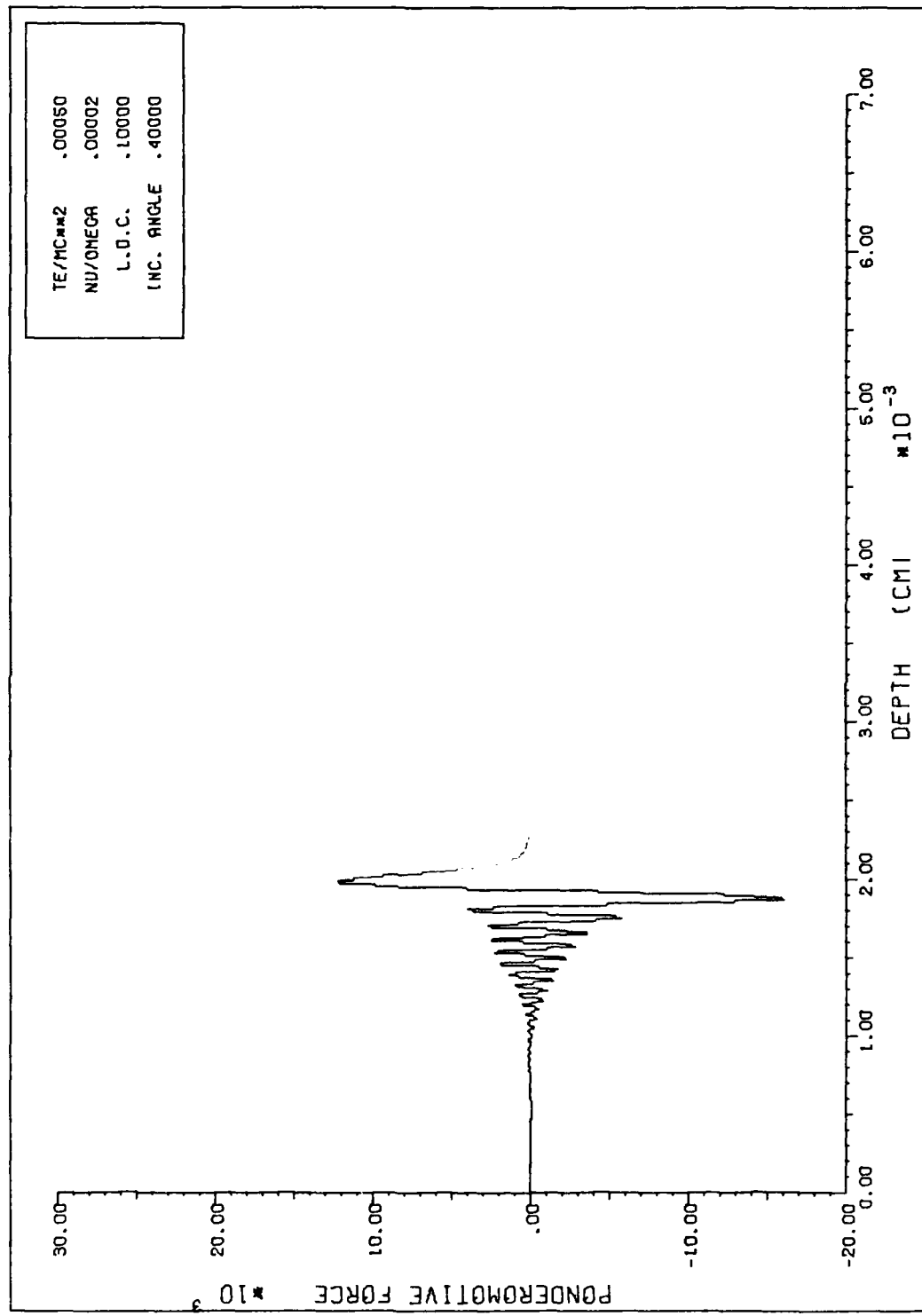


Figure C-4.

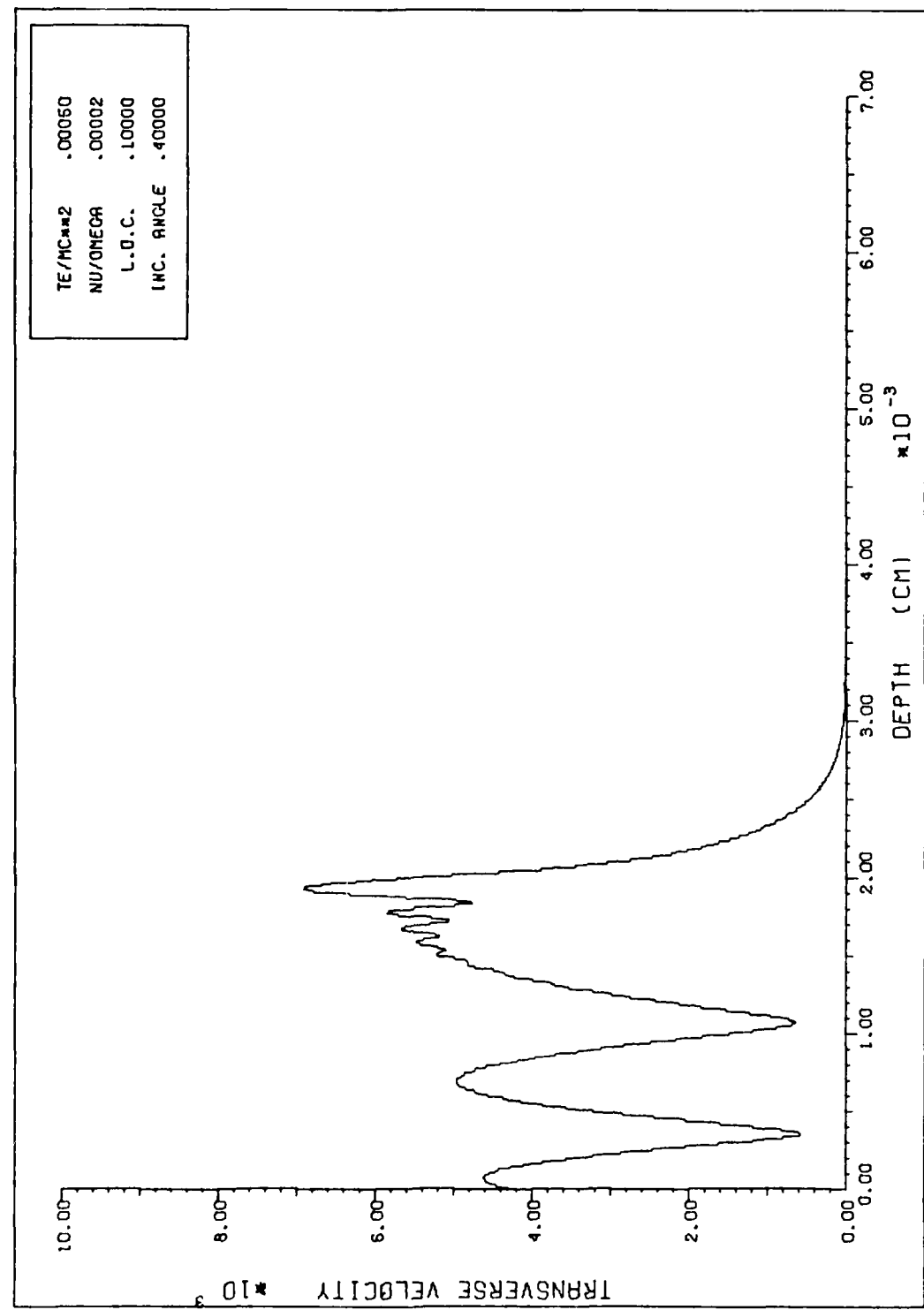


Figure C-5.

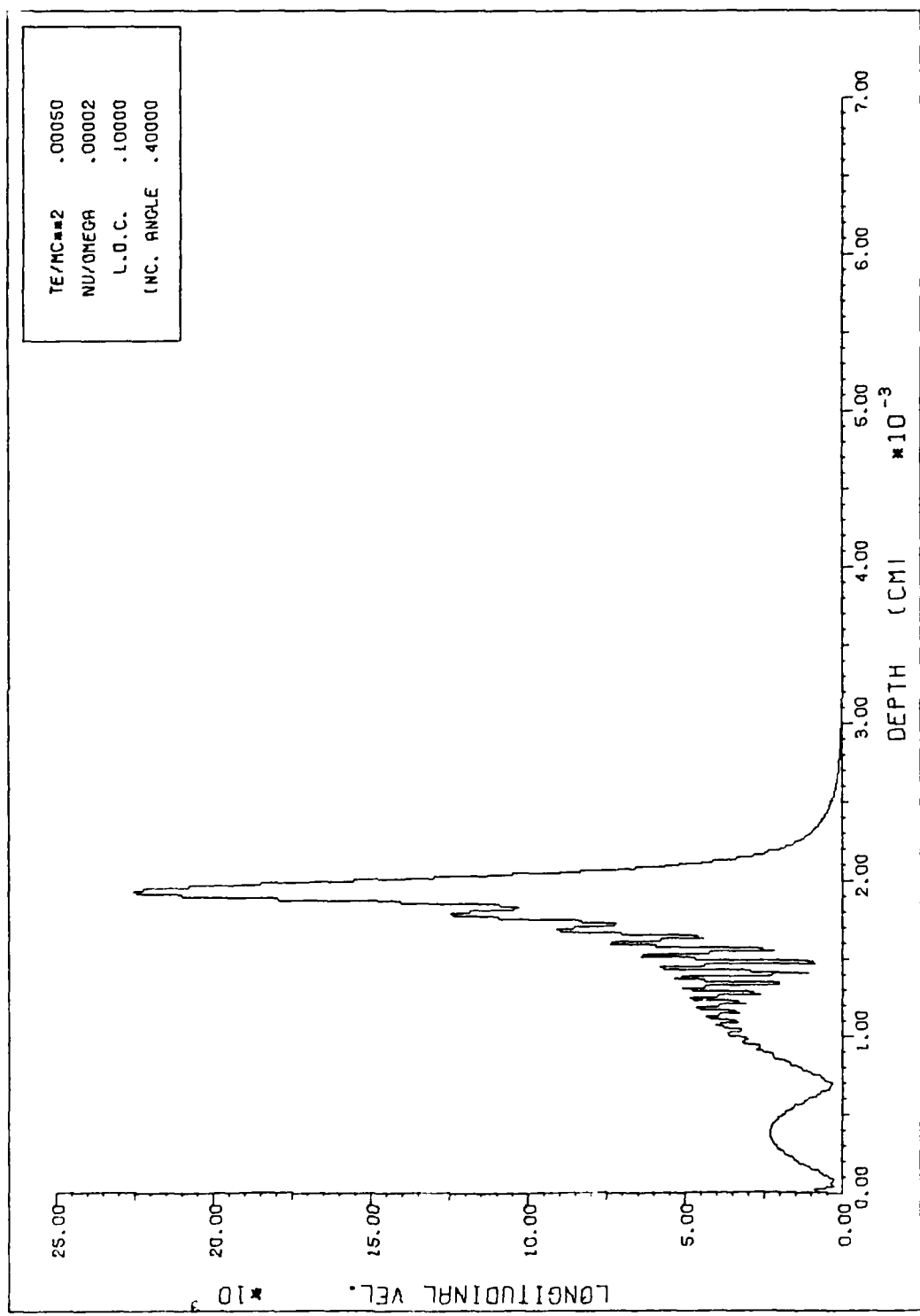
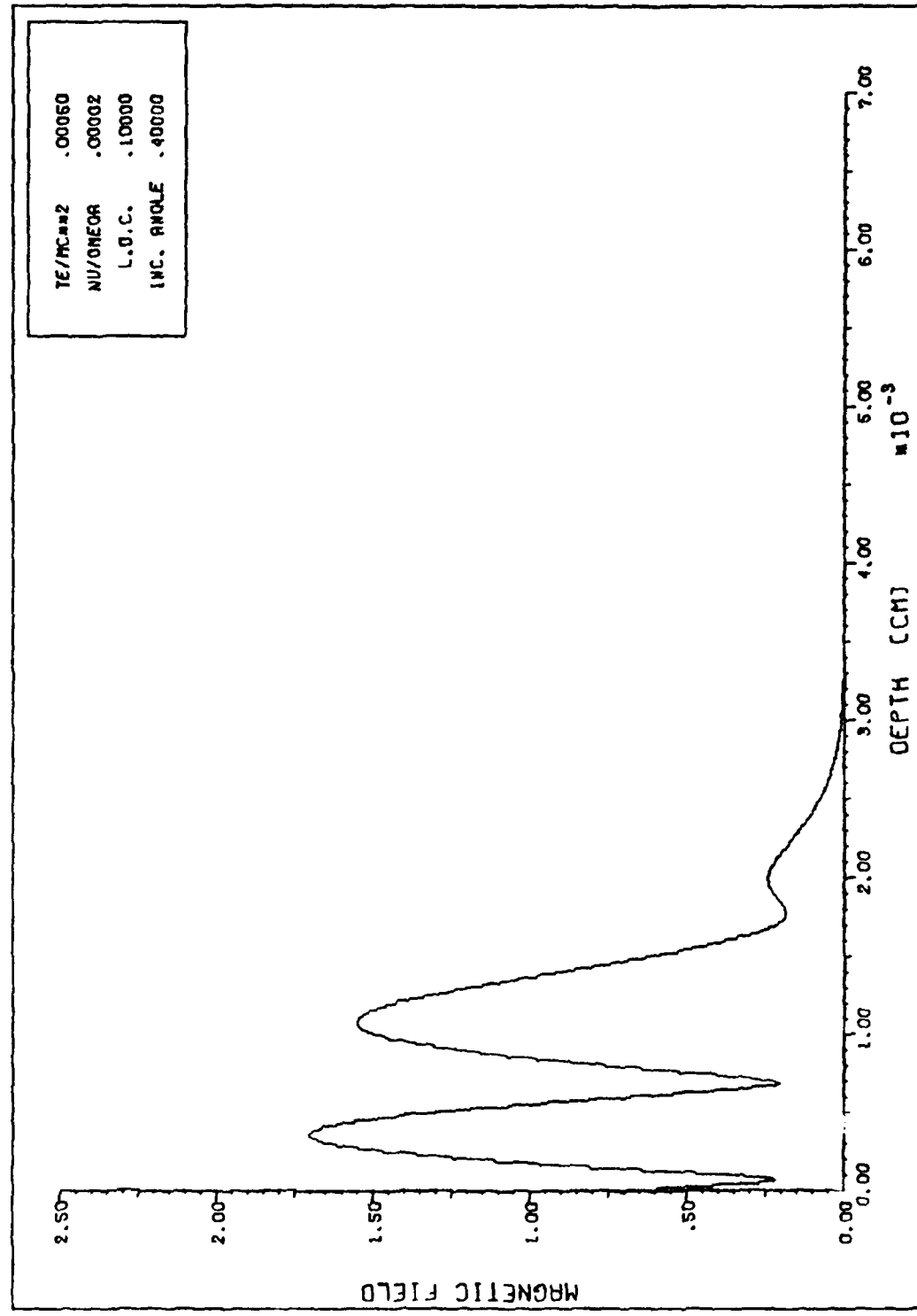


Figure 3-6.



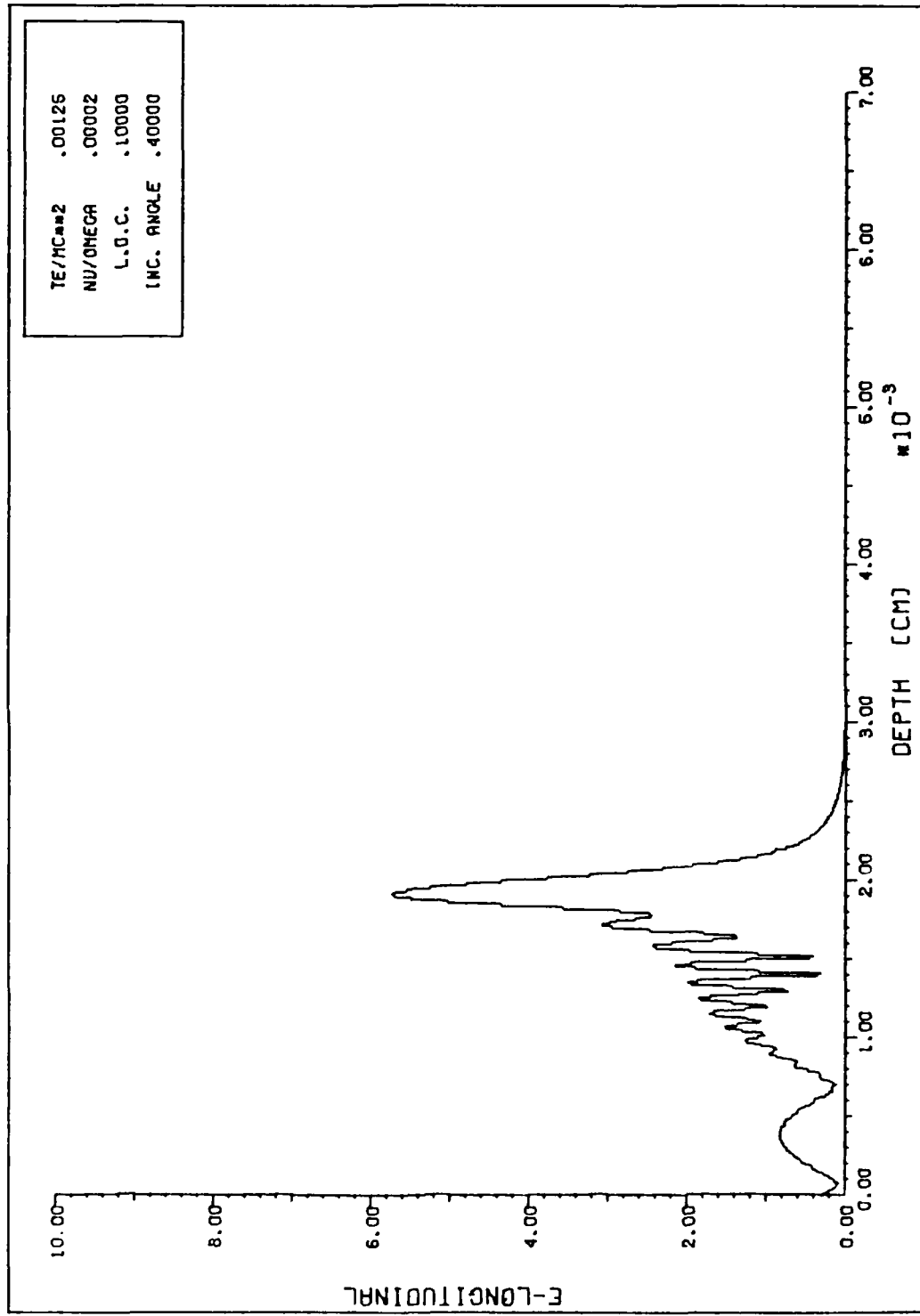


Figure 3-3.

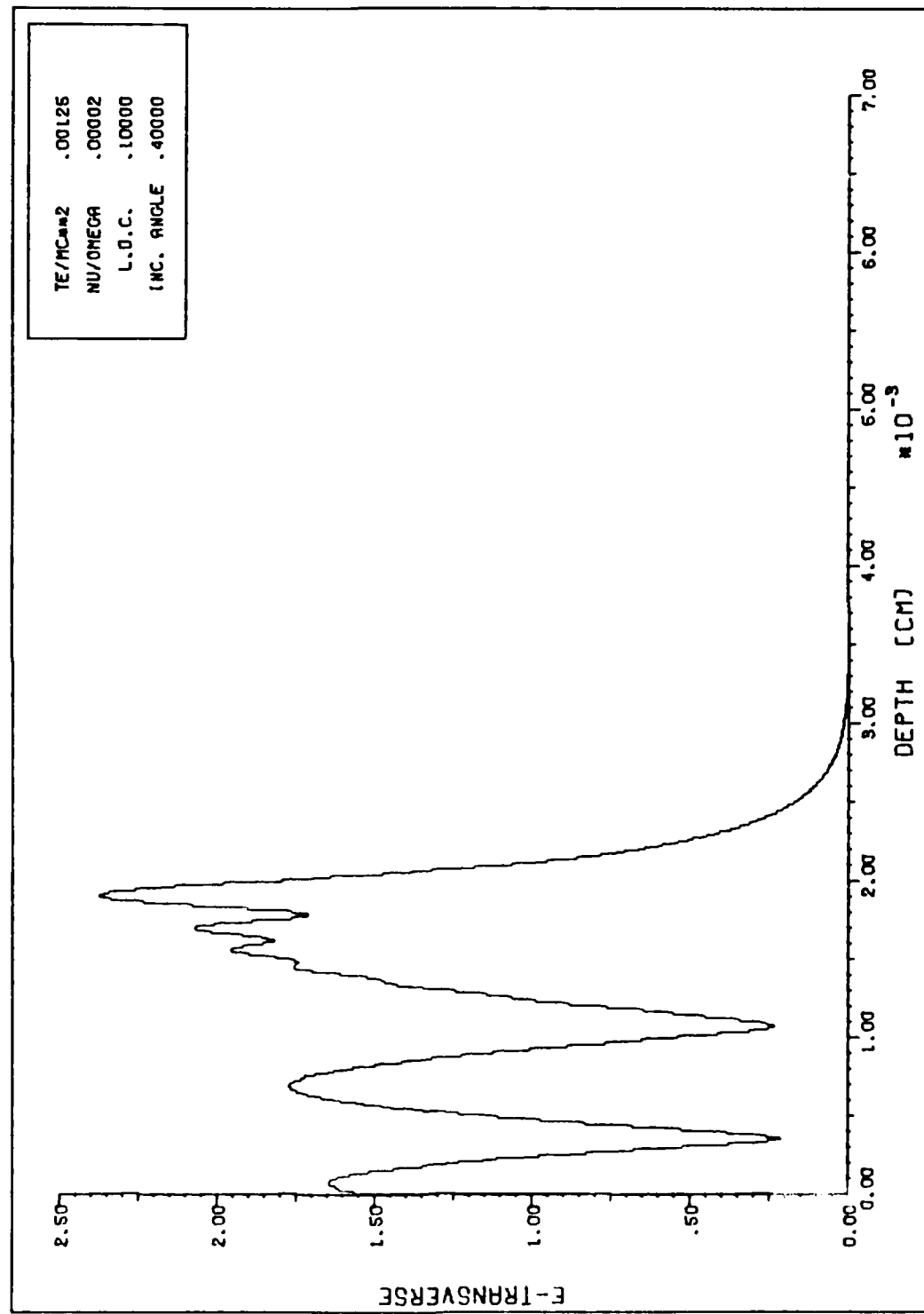
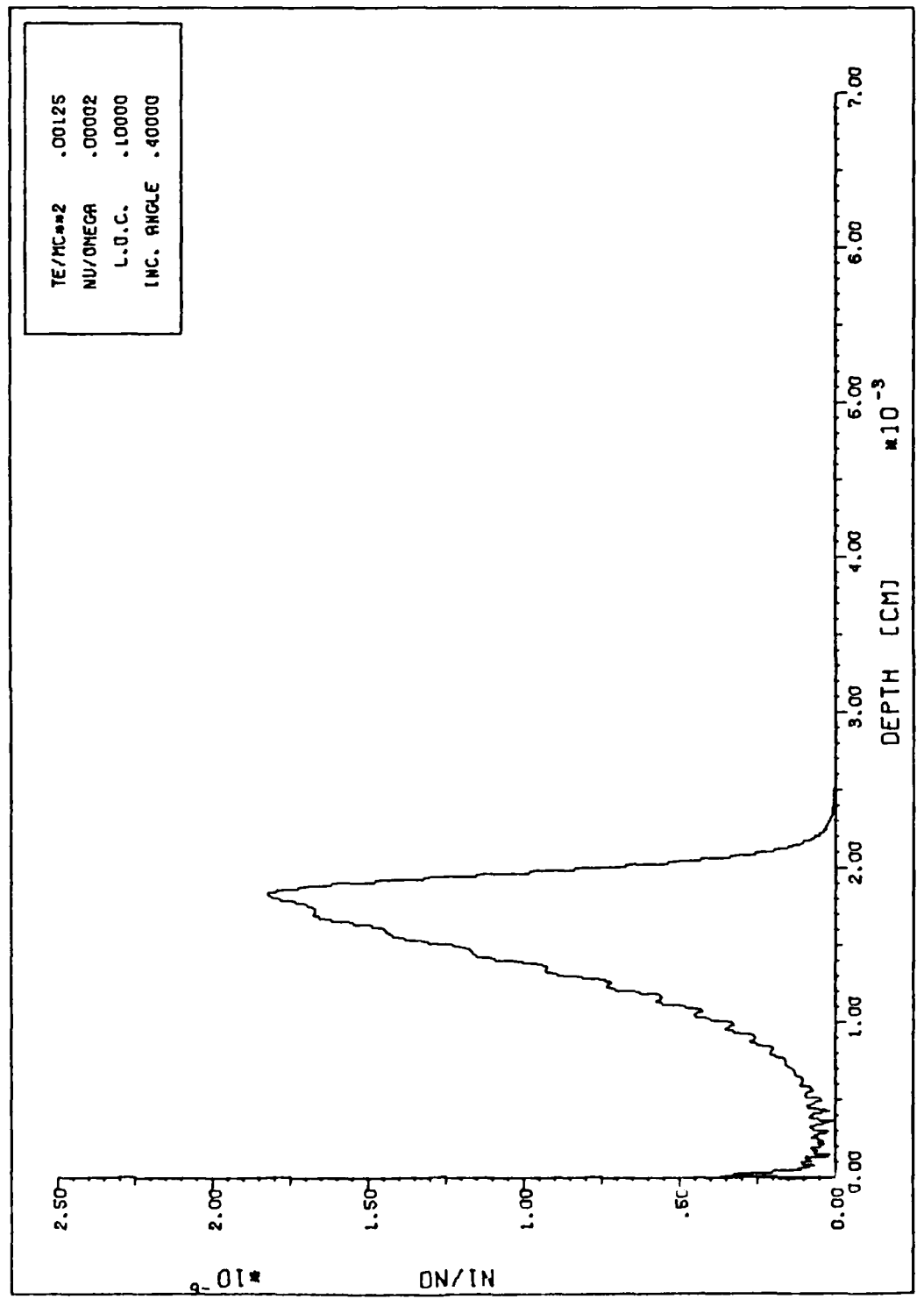


Figure 3-7.



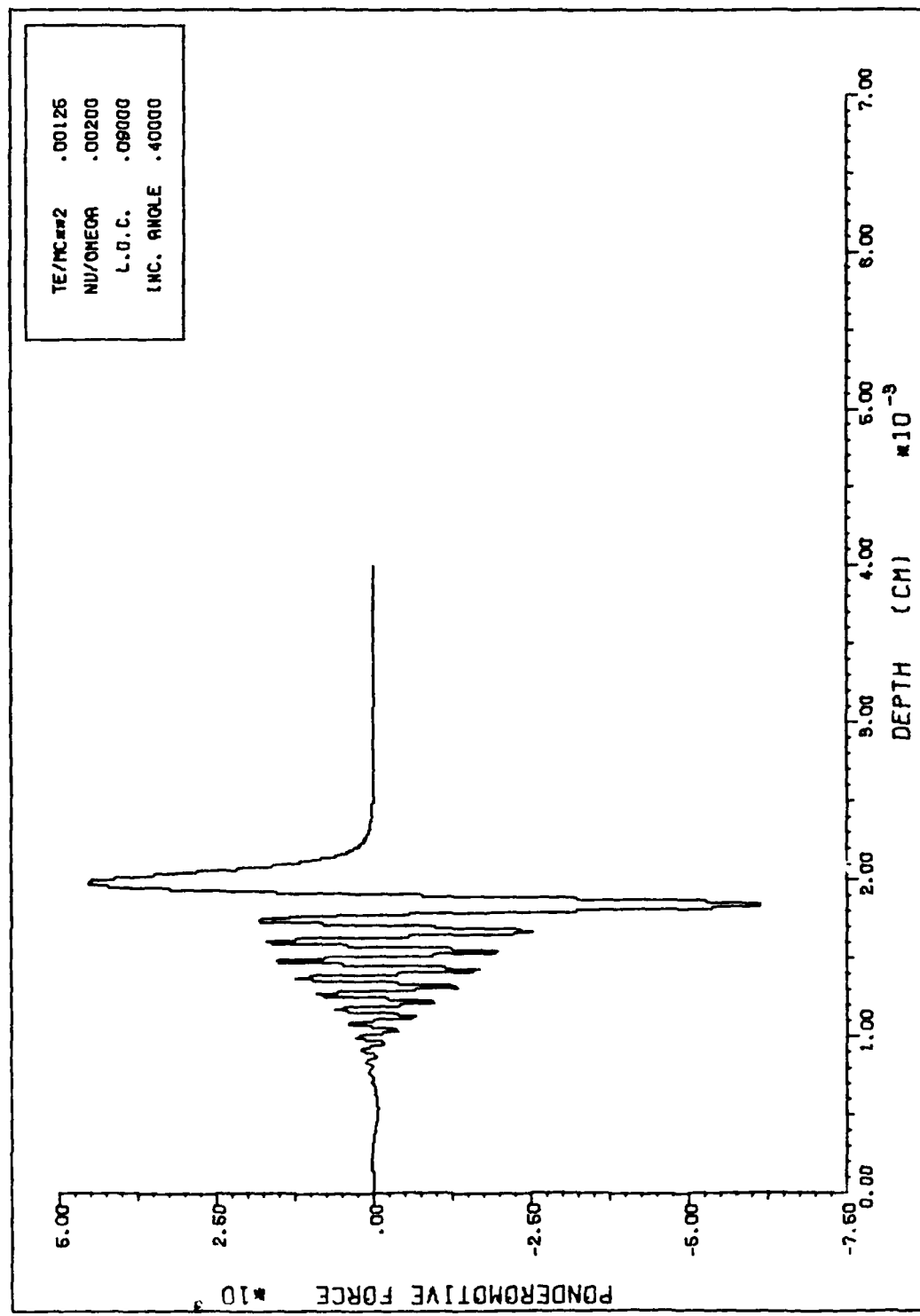


FIGURE C-11.

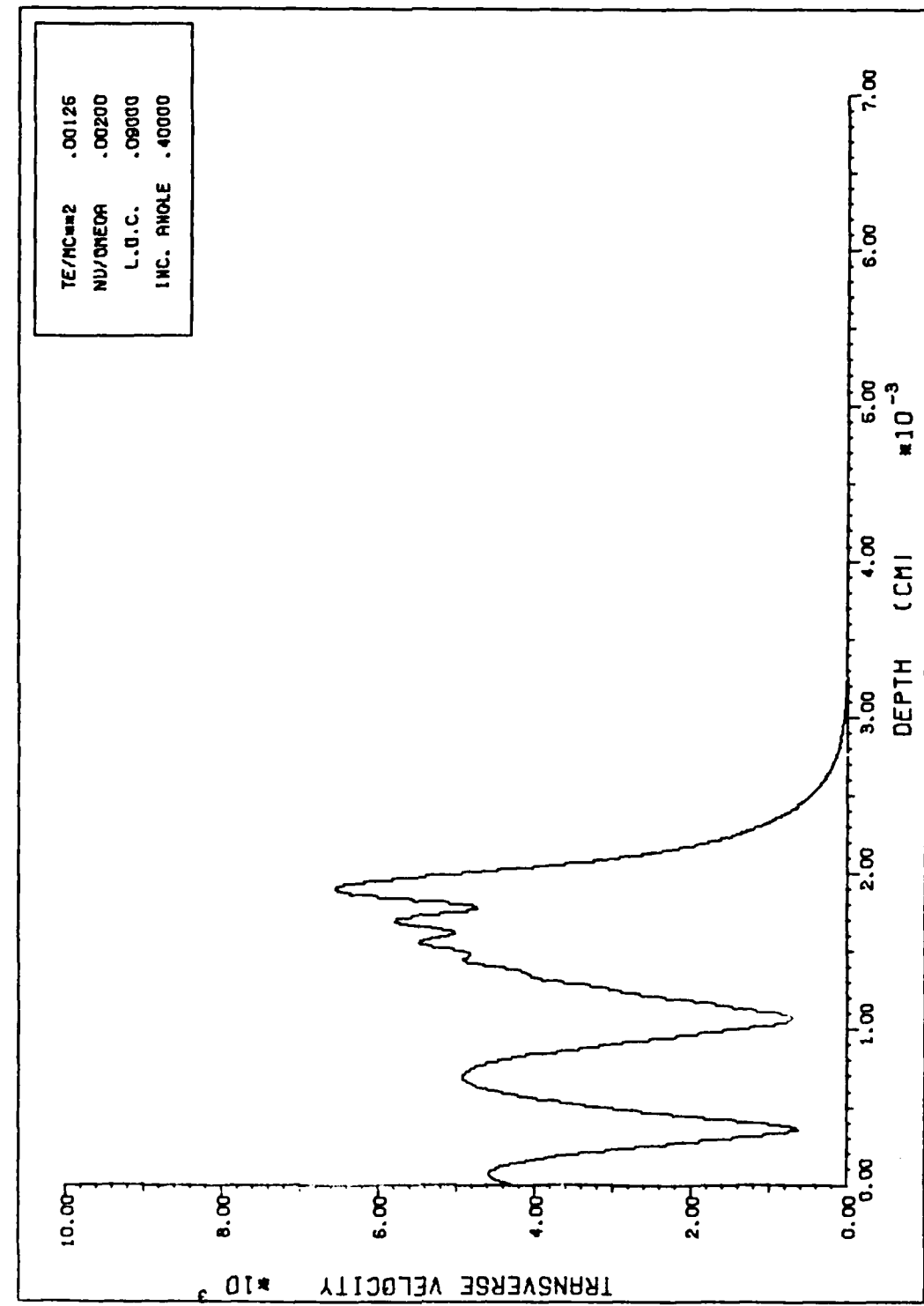


Figure C-12.

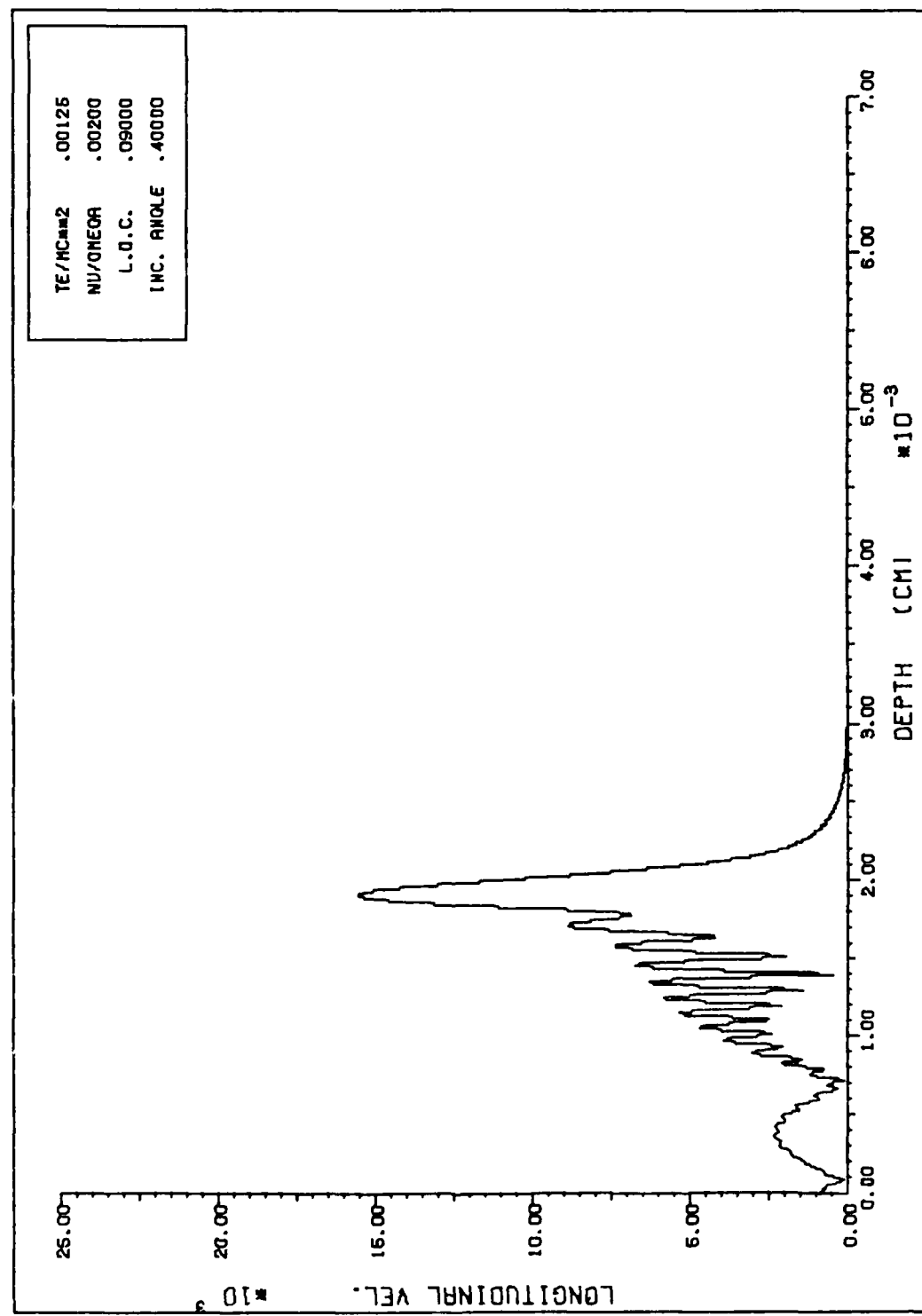


Figure C-13.

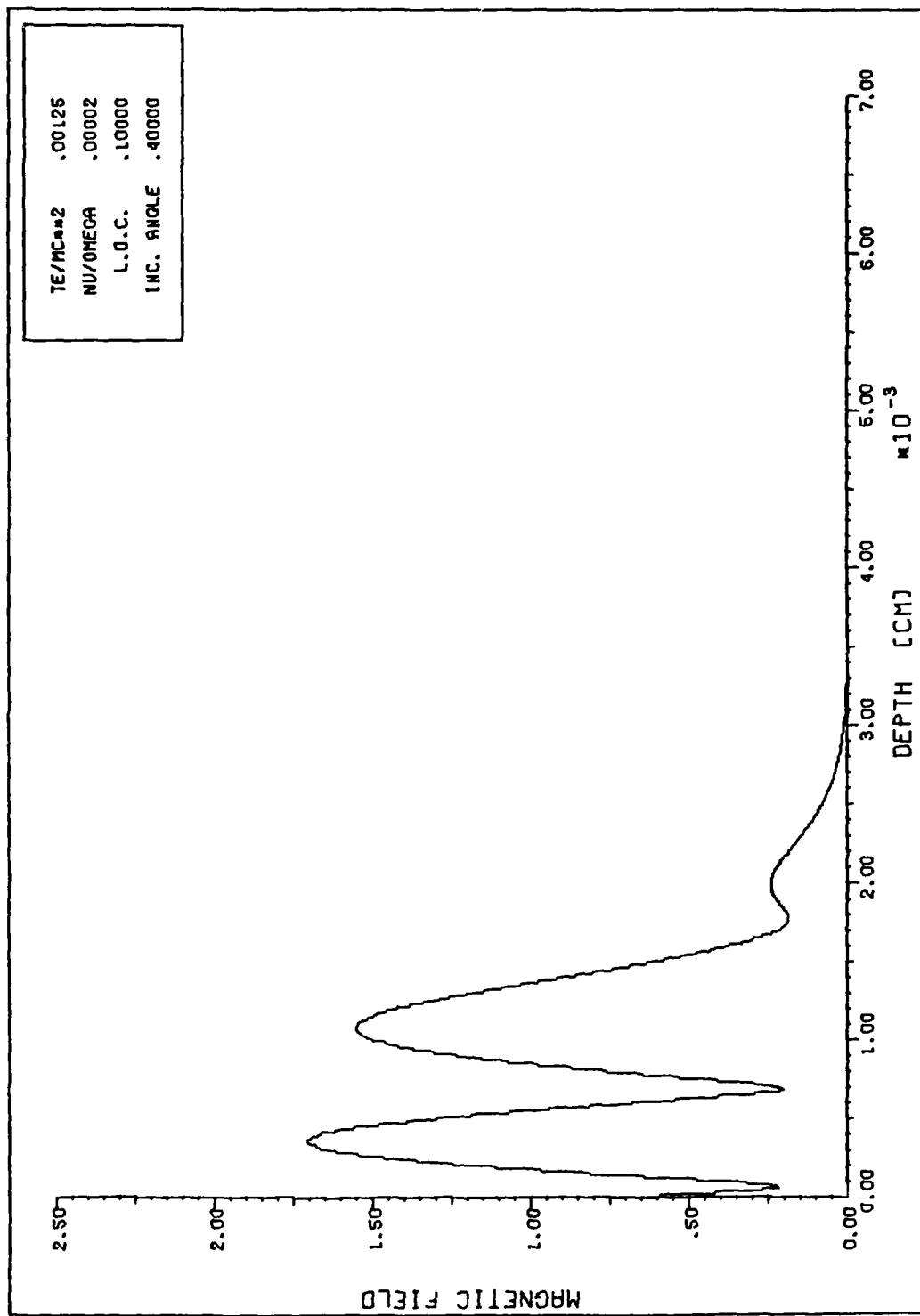


Figure 3-14.

CUT

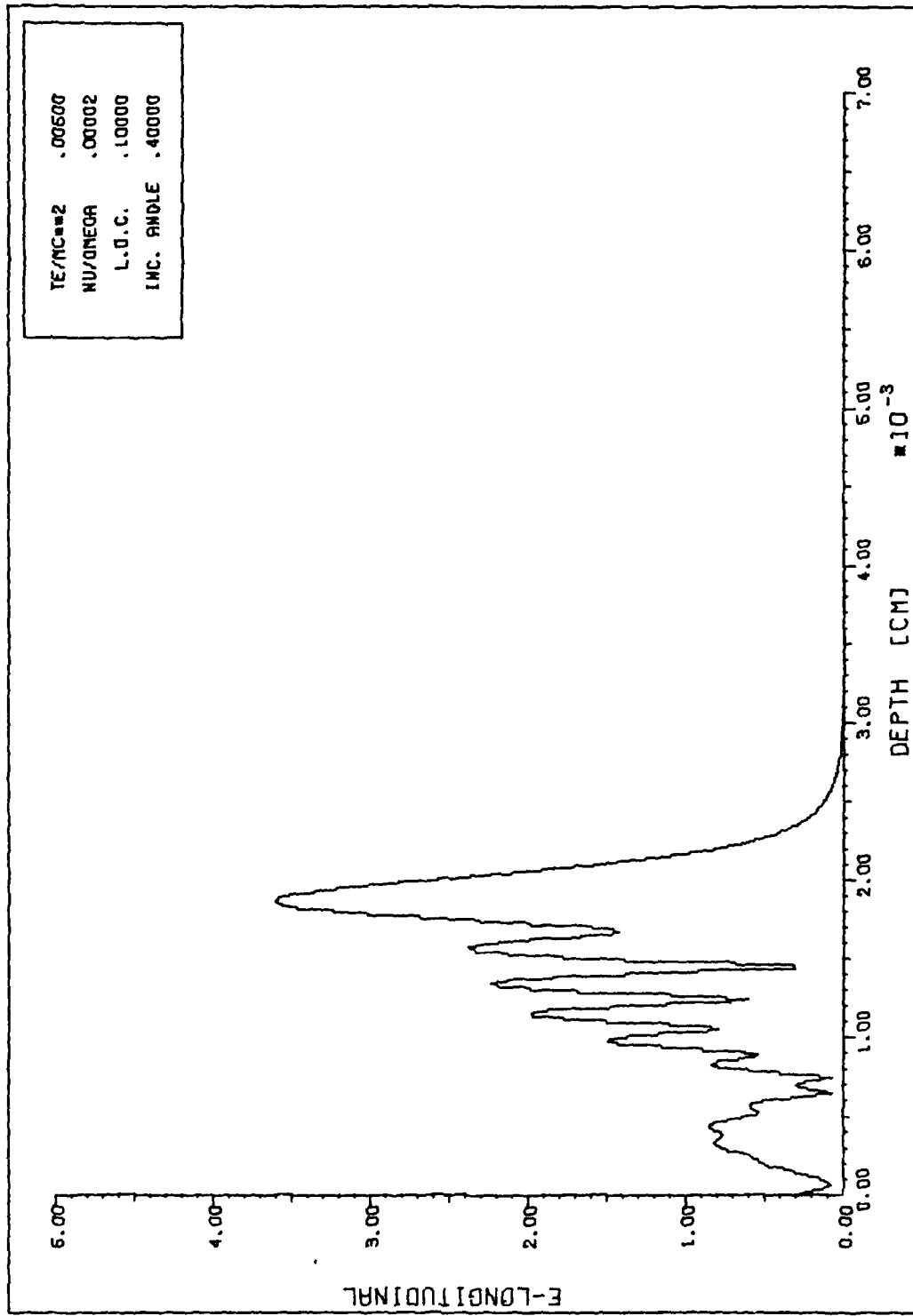
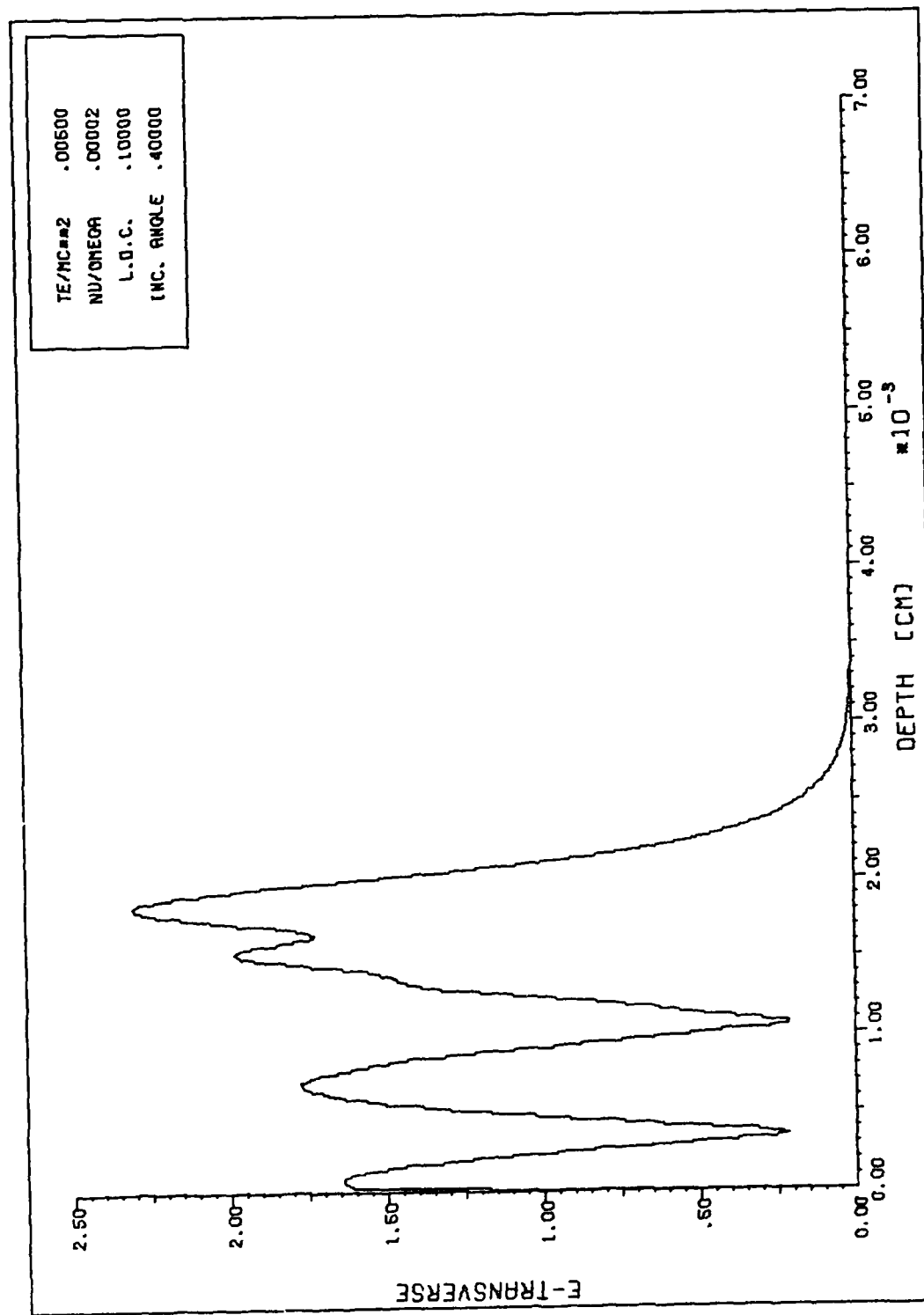


Figure 3-15.



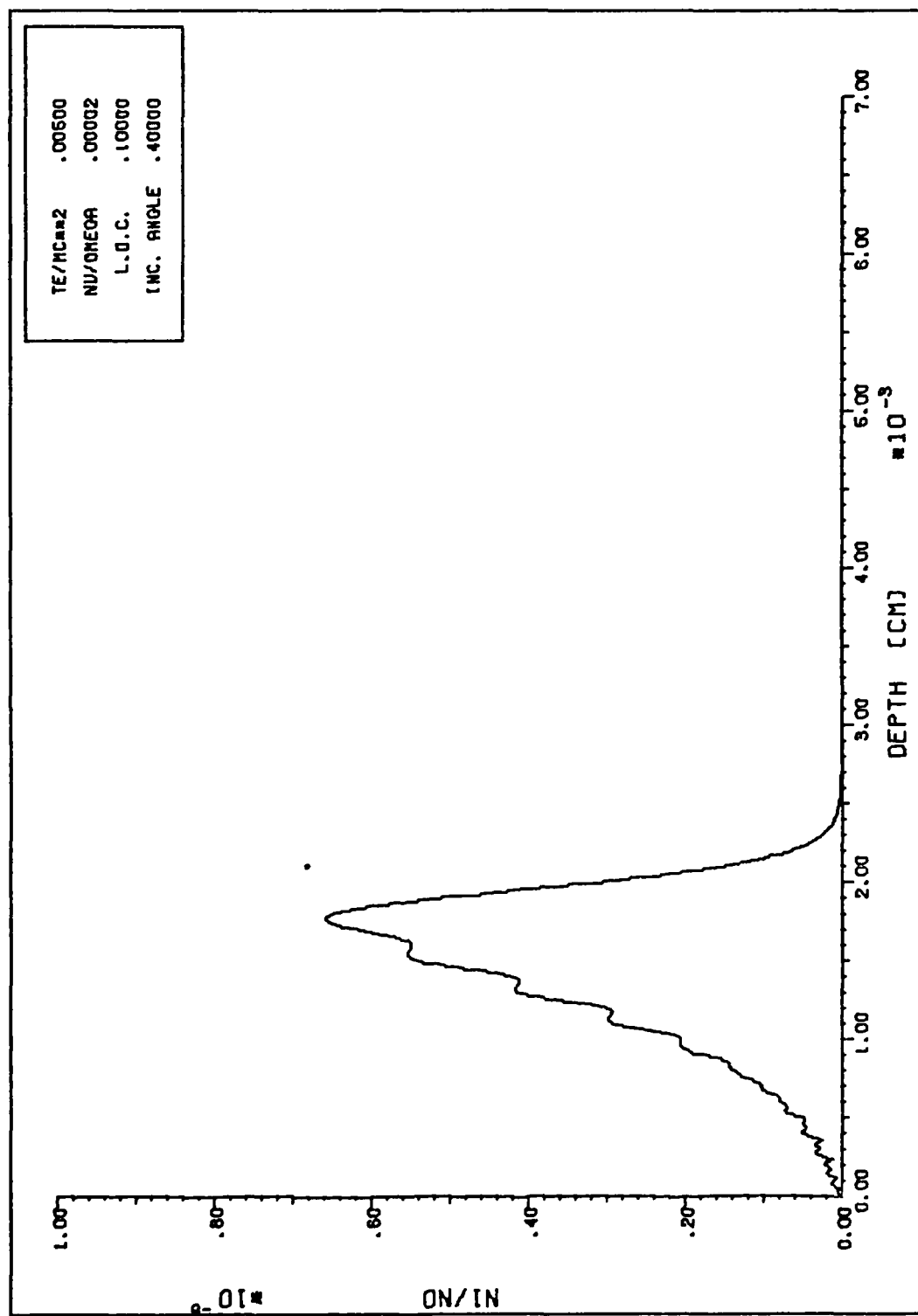


Figure C-17.

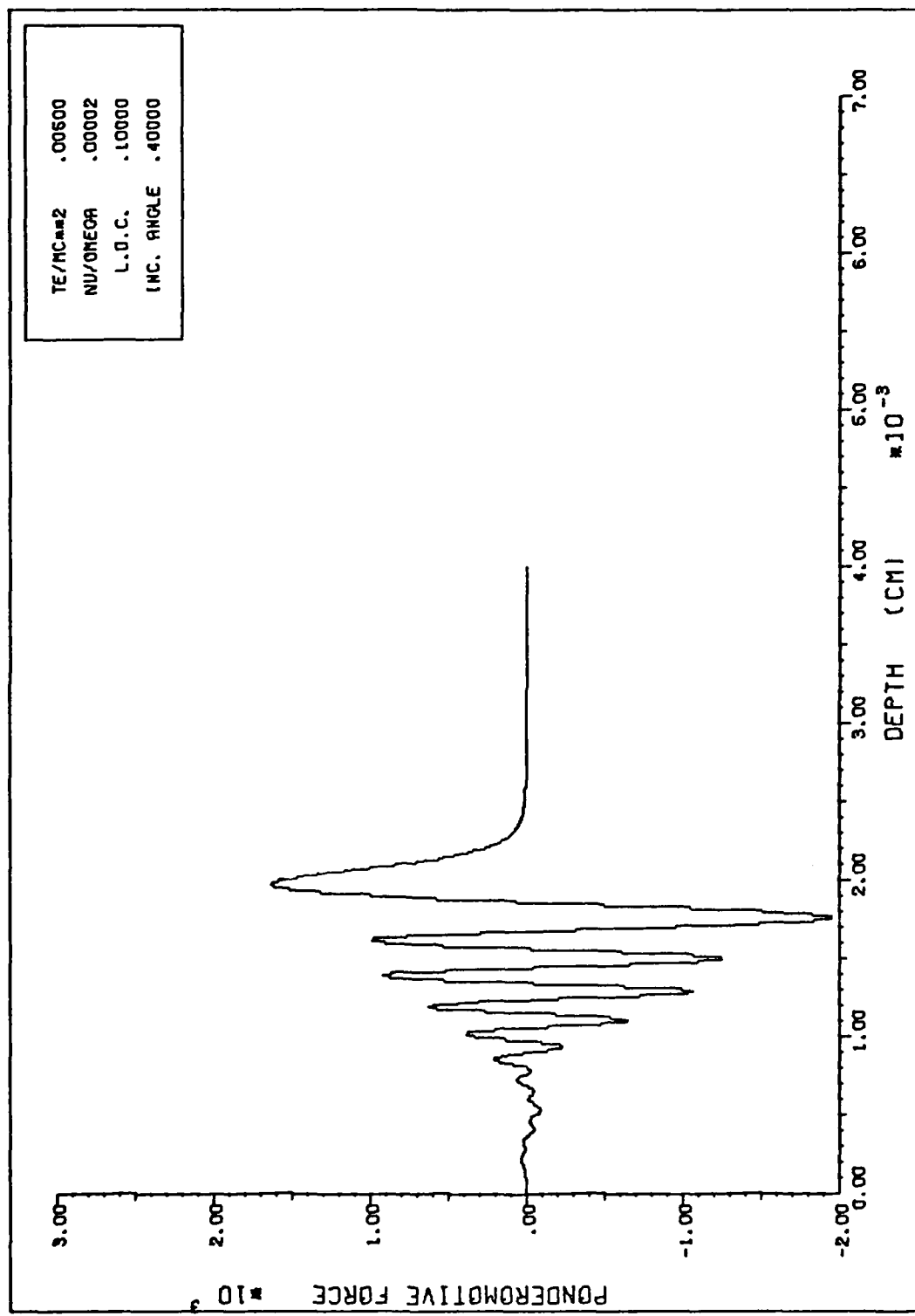


Figure C-18.

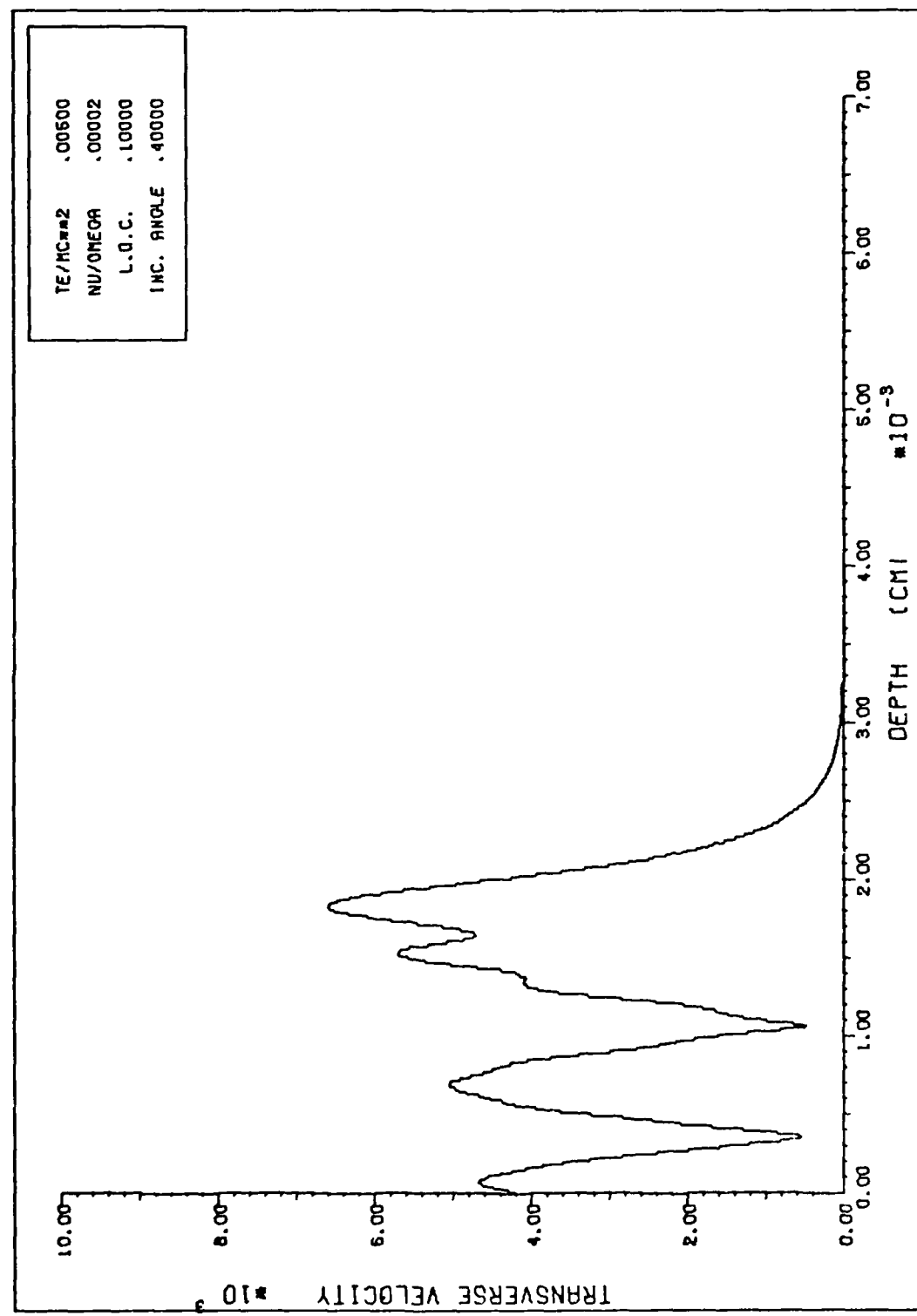


Figure C-19.

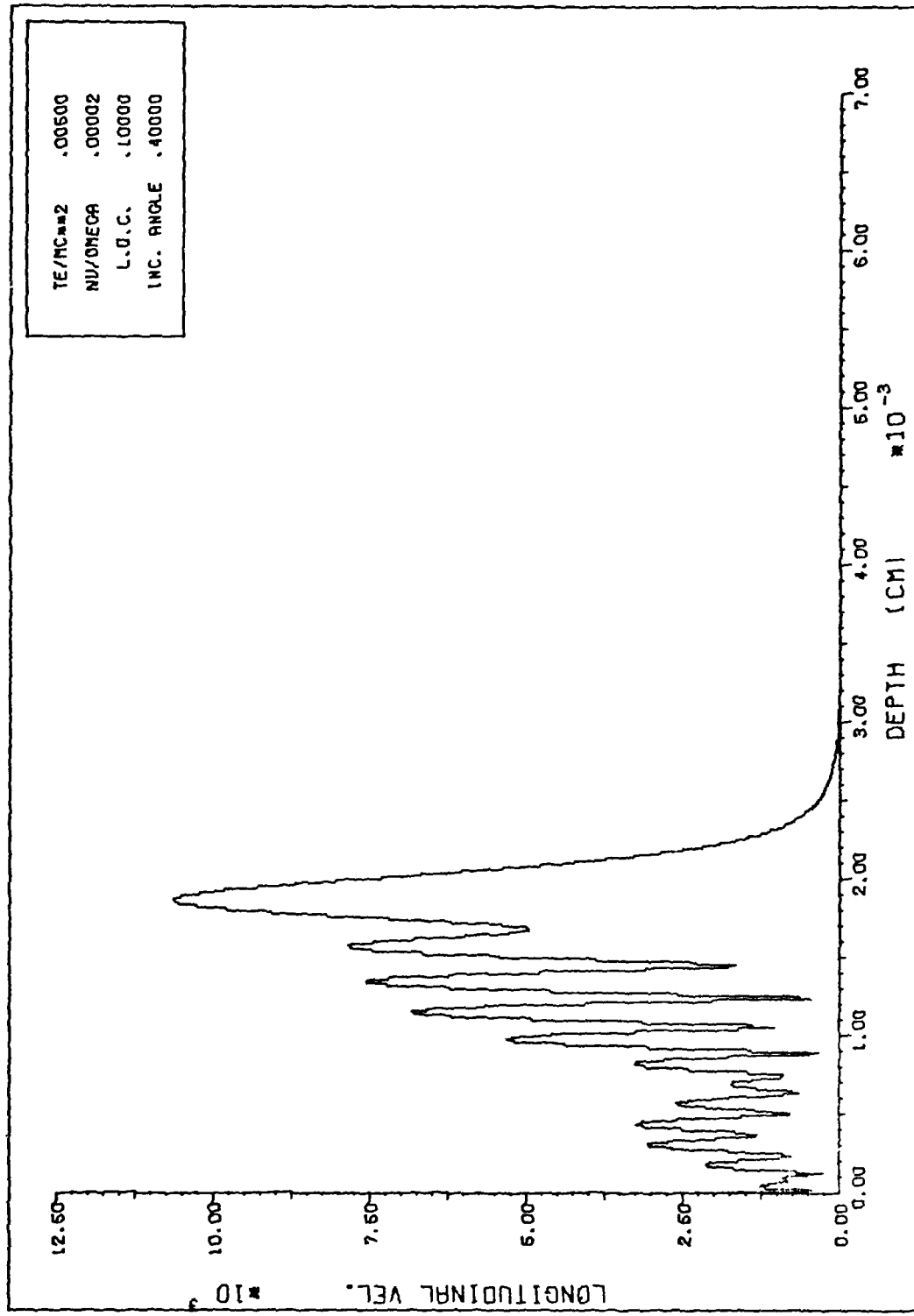


Figure C-20.

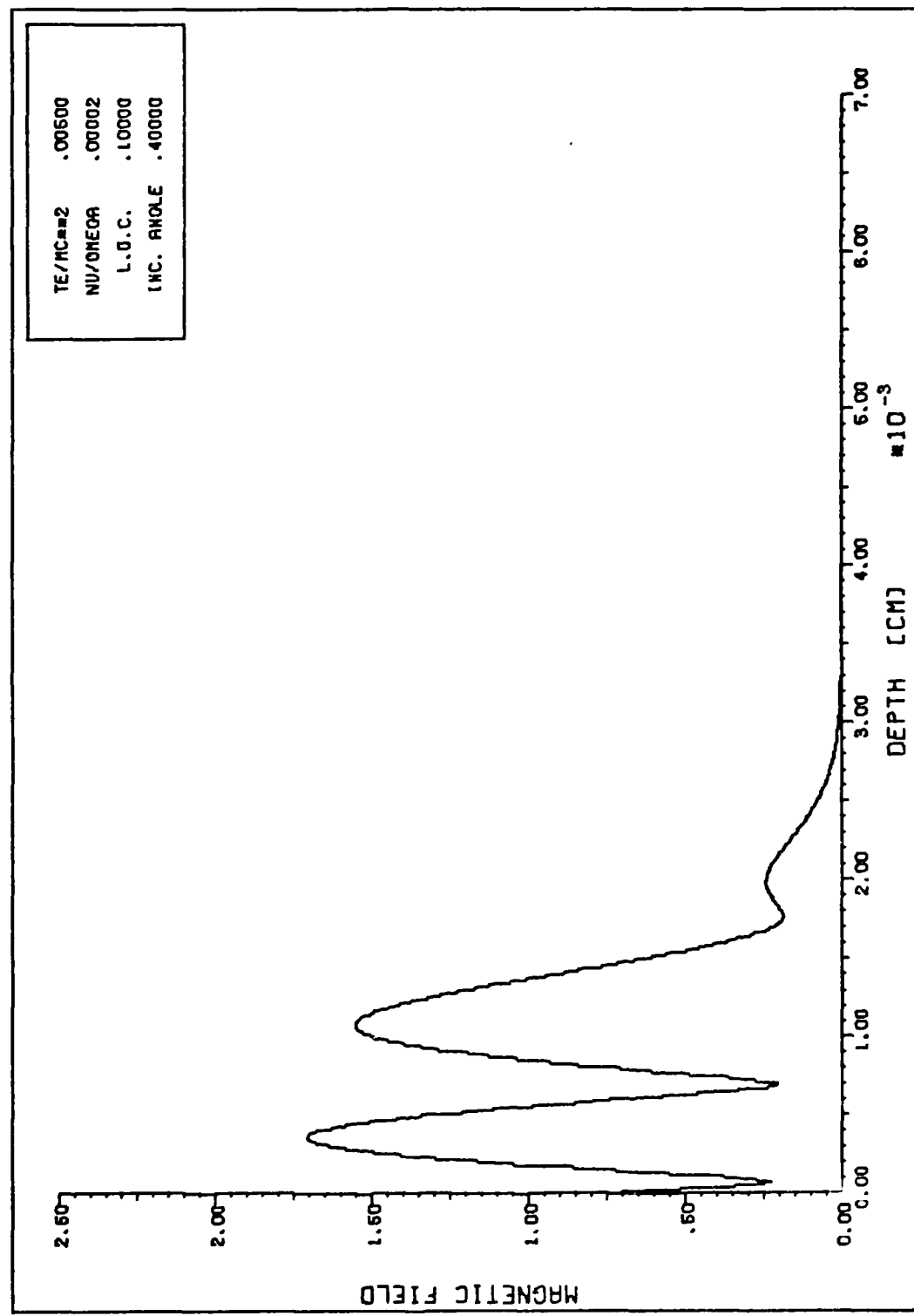
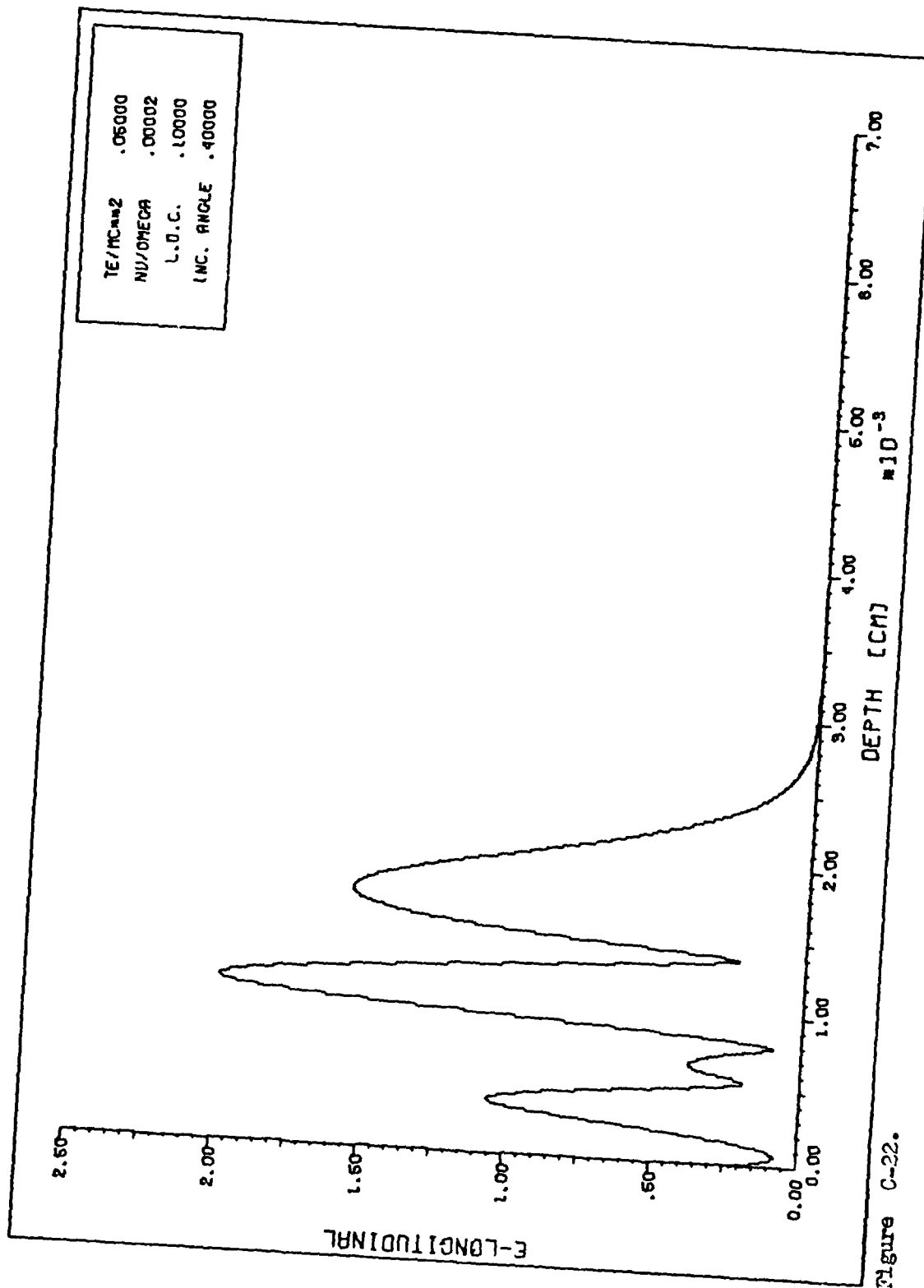


Figure C-21.



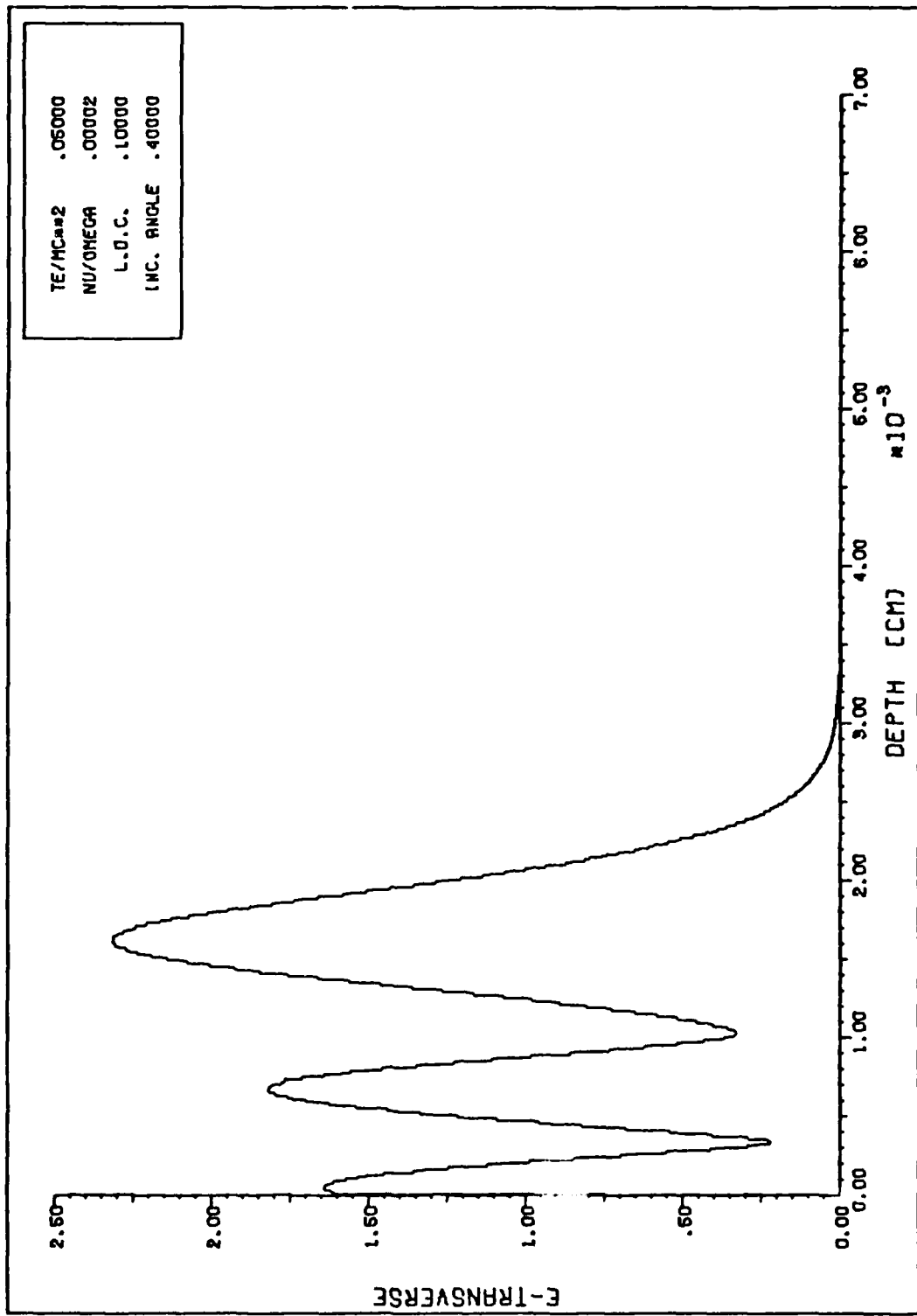


Figure C-23.

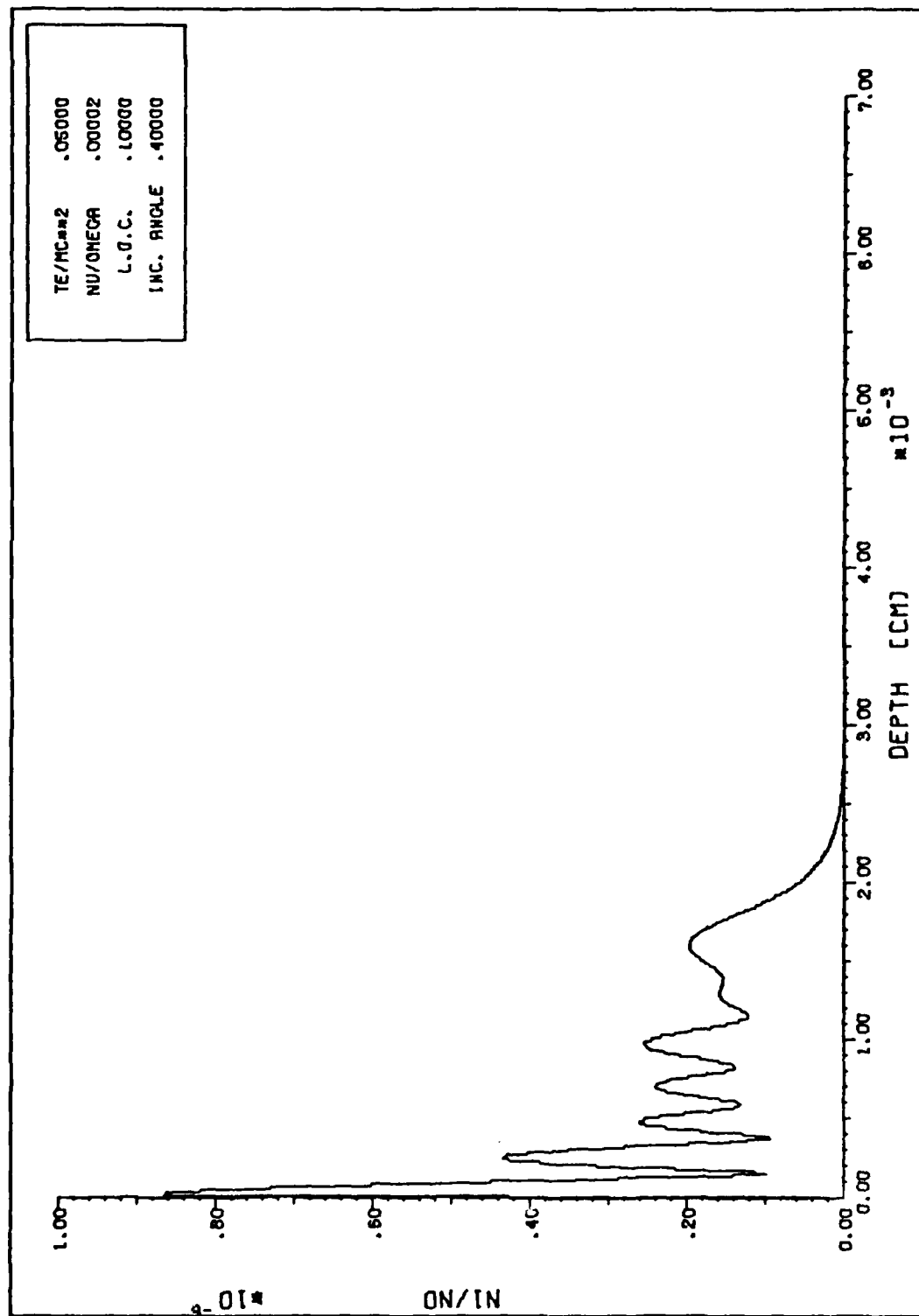
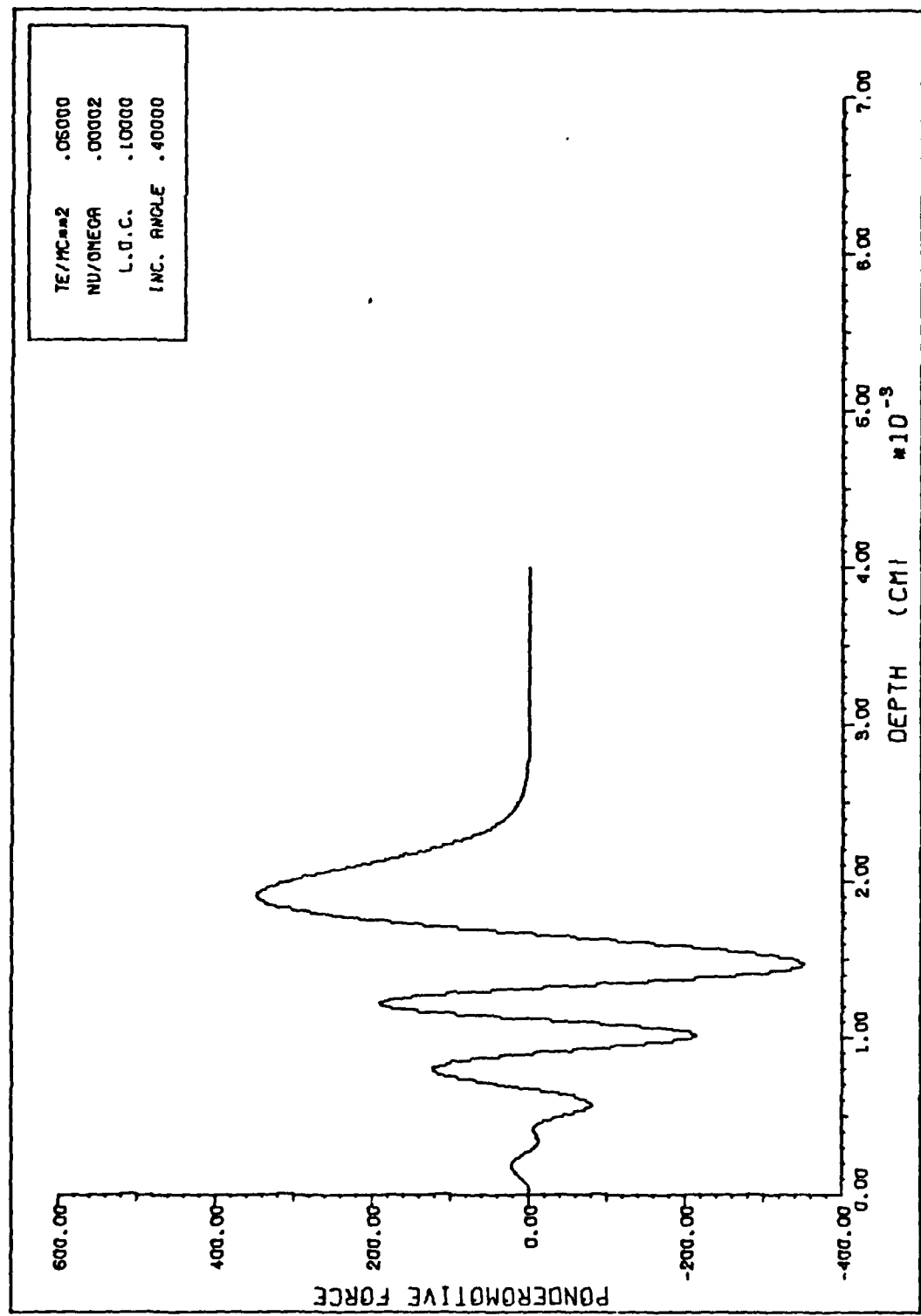
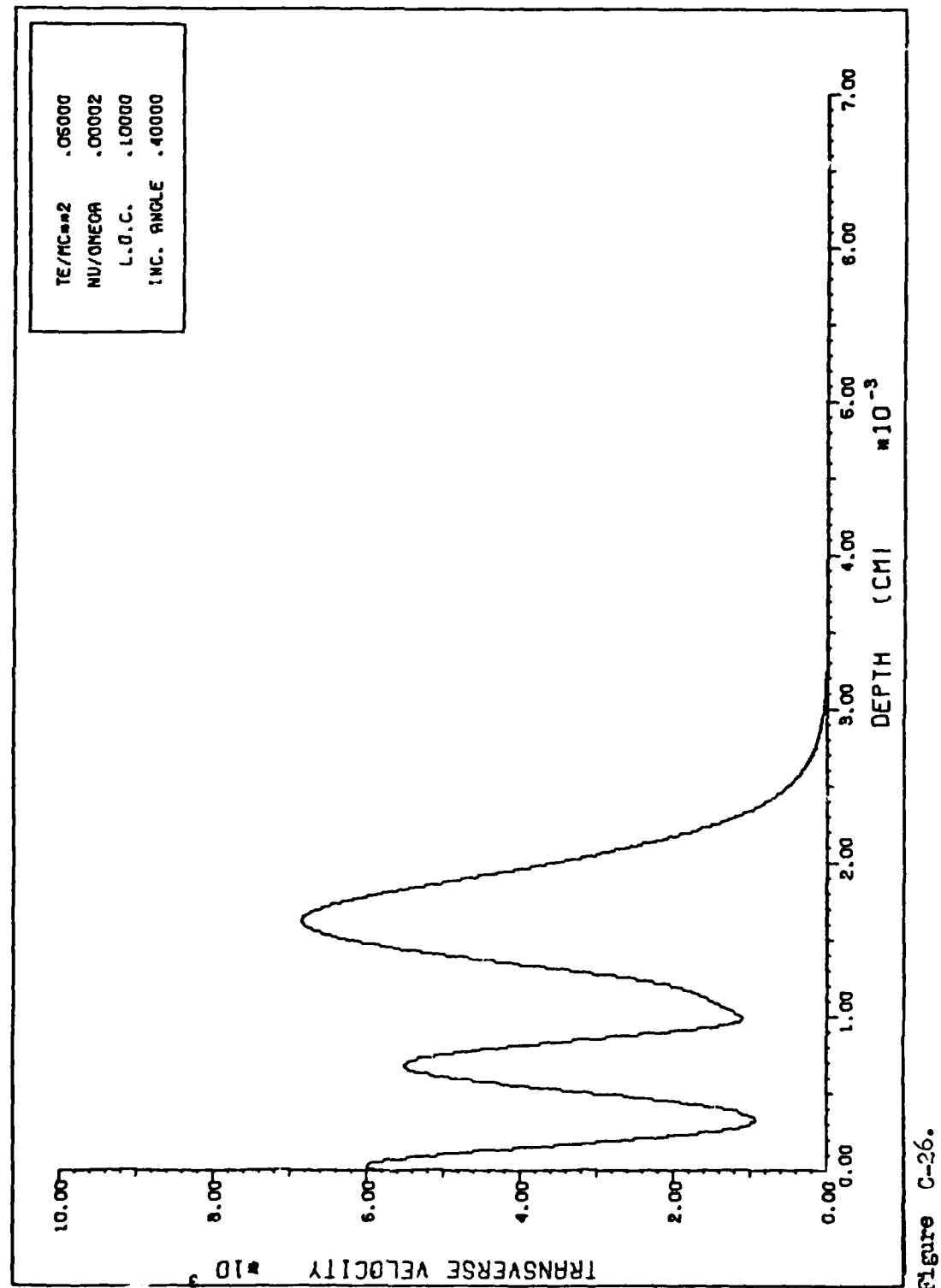


Figure C-24.





211

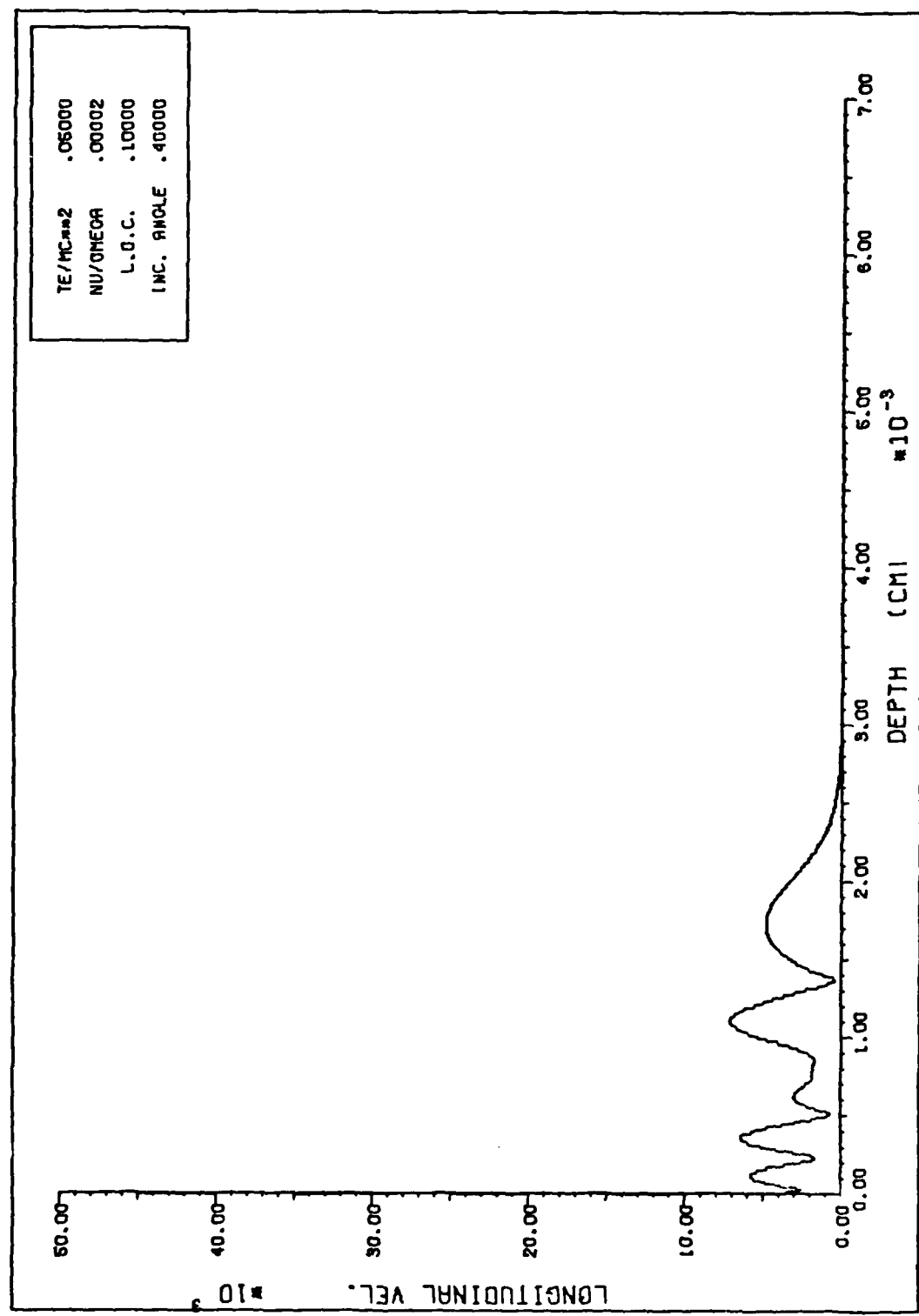


Figure C-27.

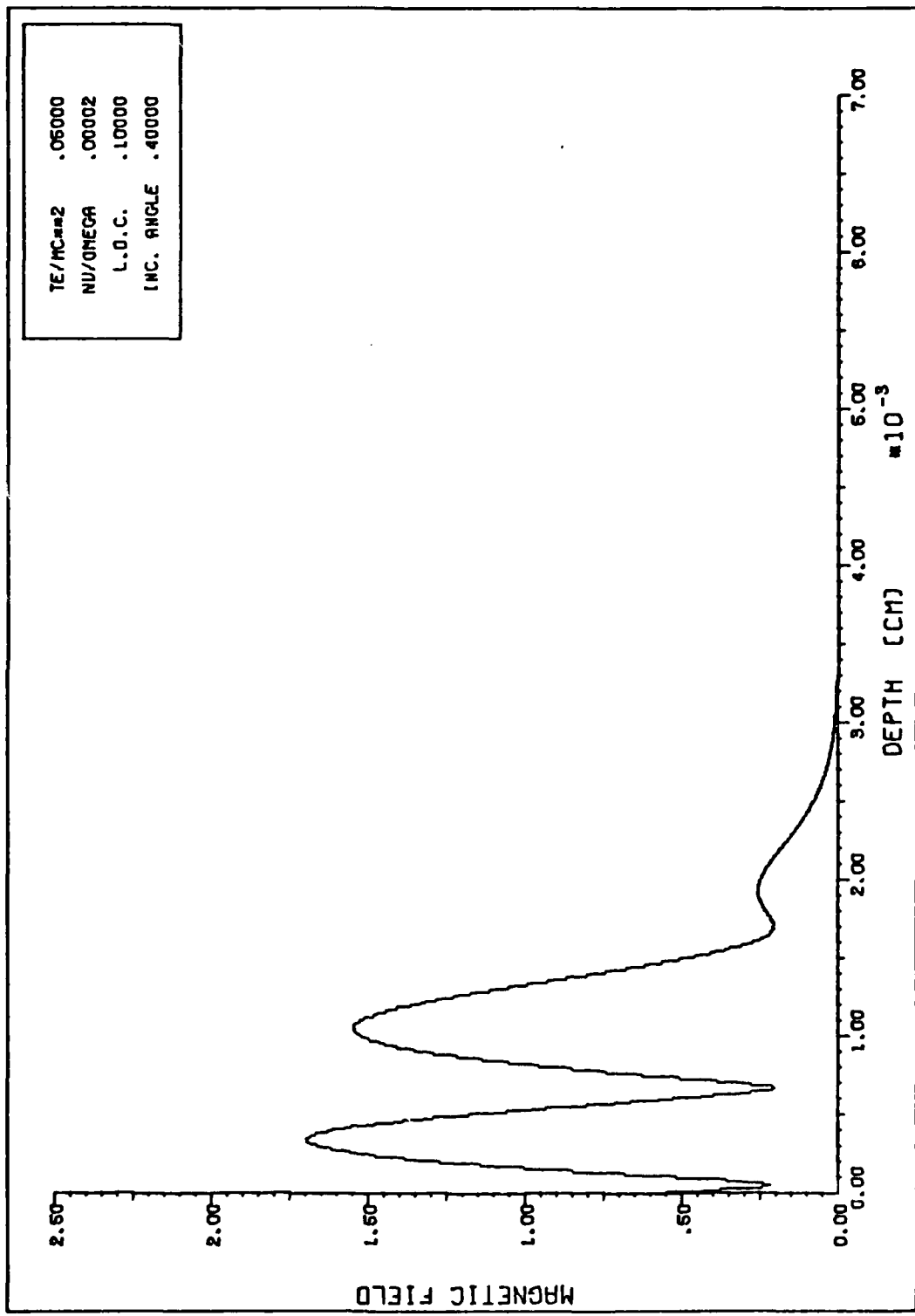


Figure C-23.

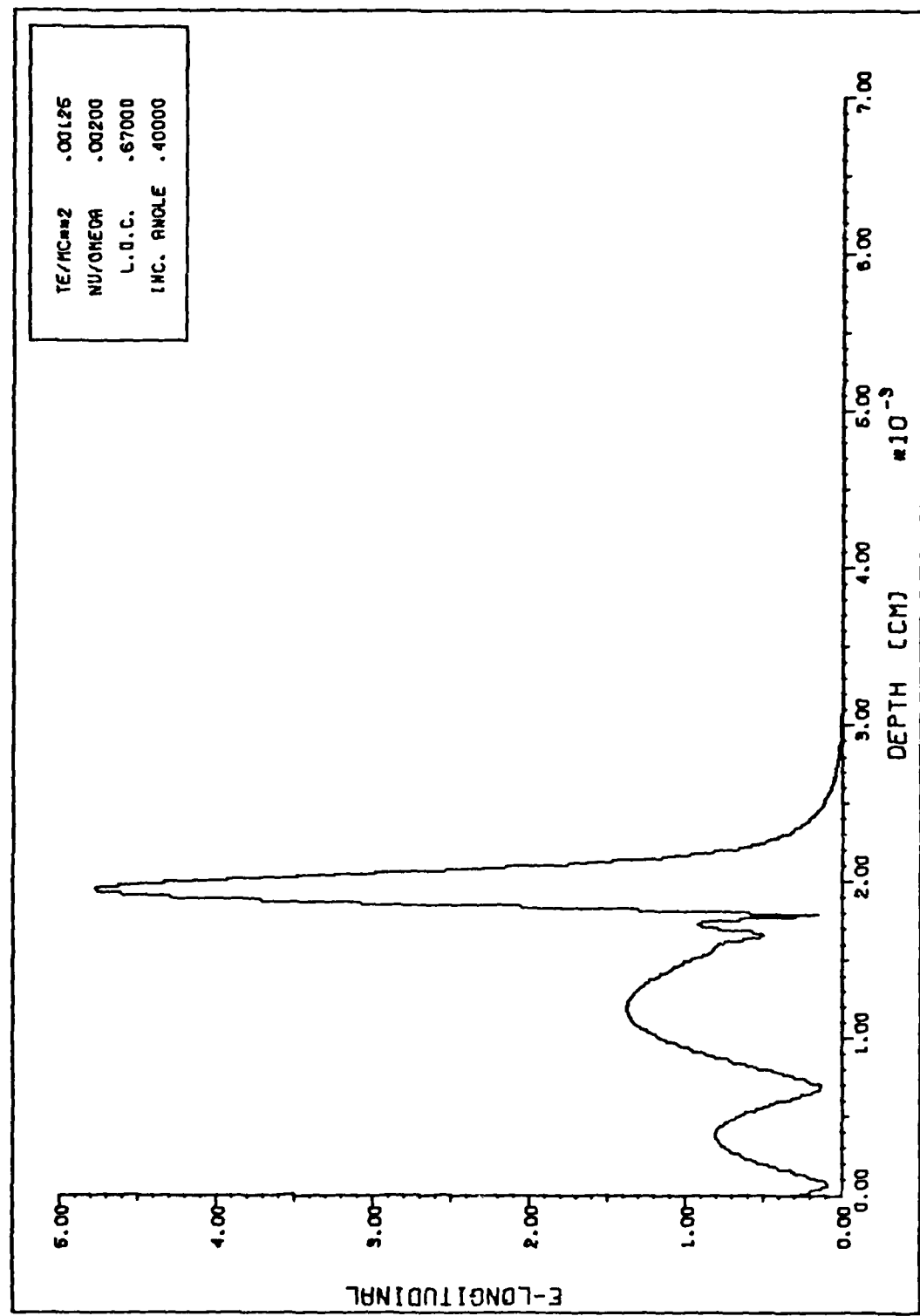


Figure C-29.

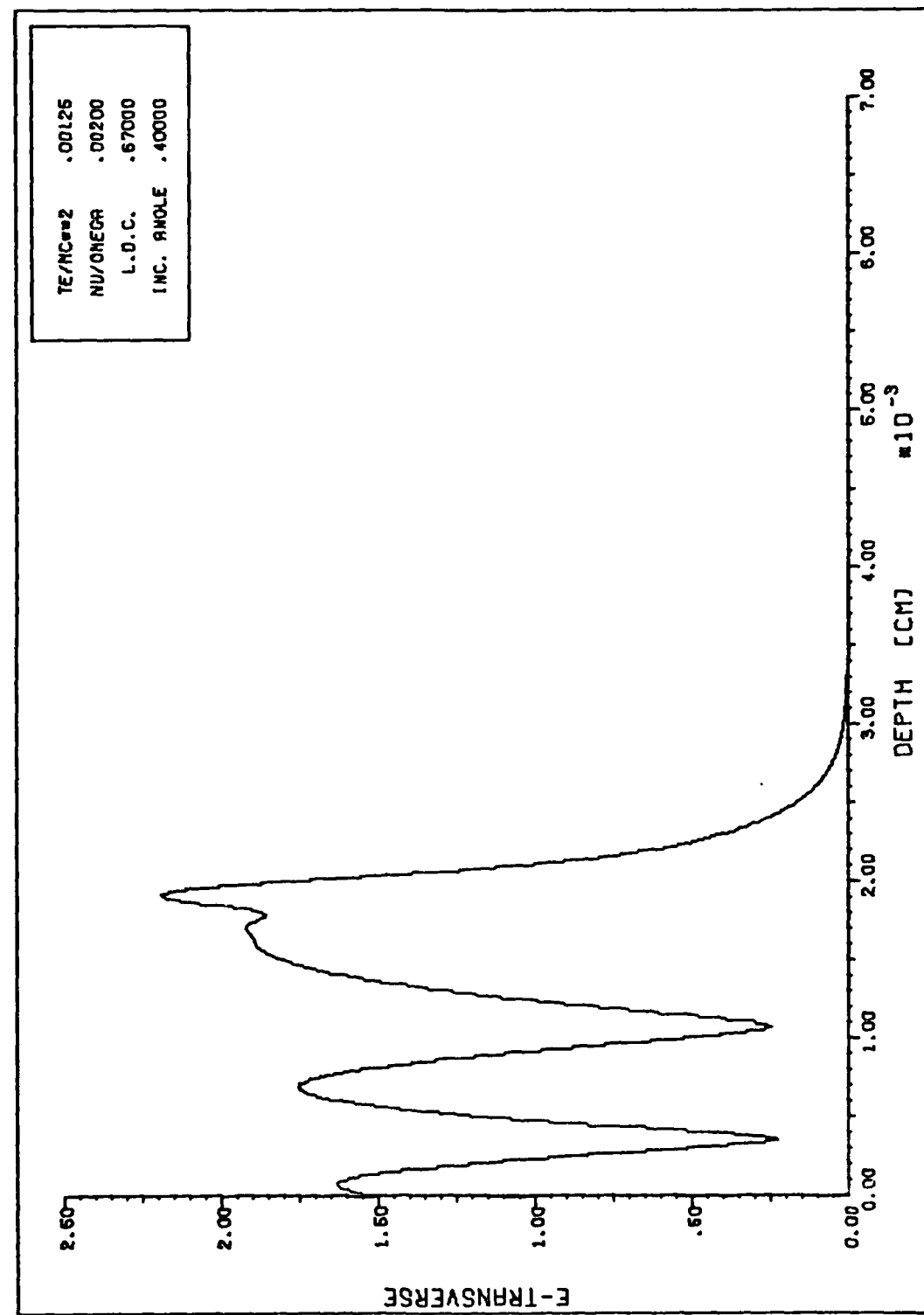


Figure C-30.

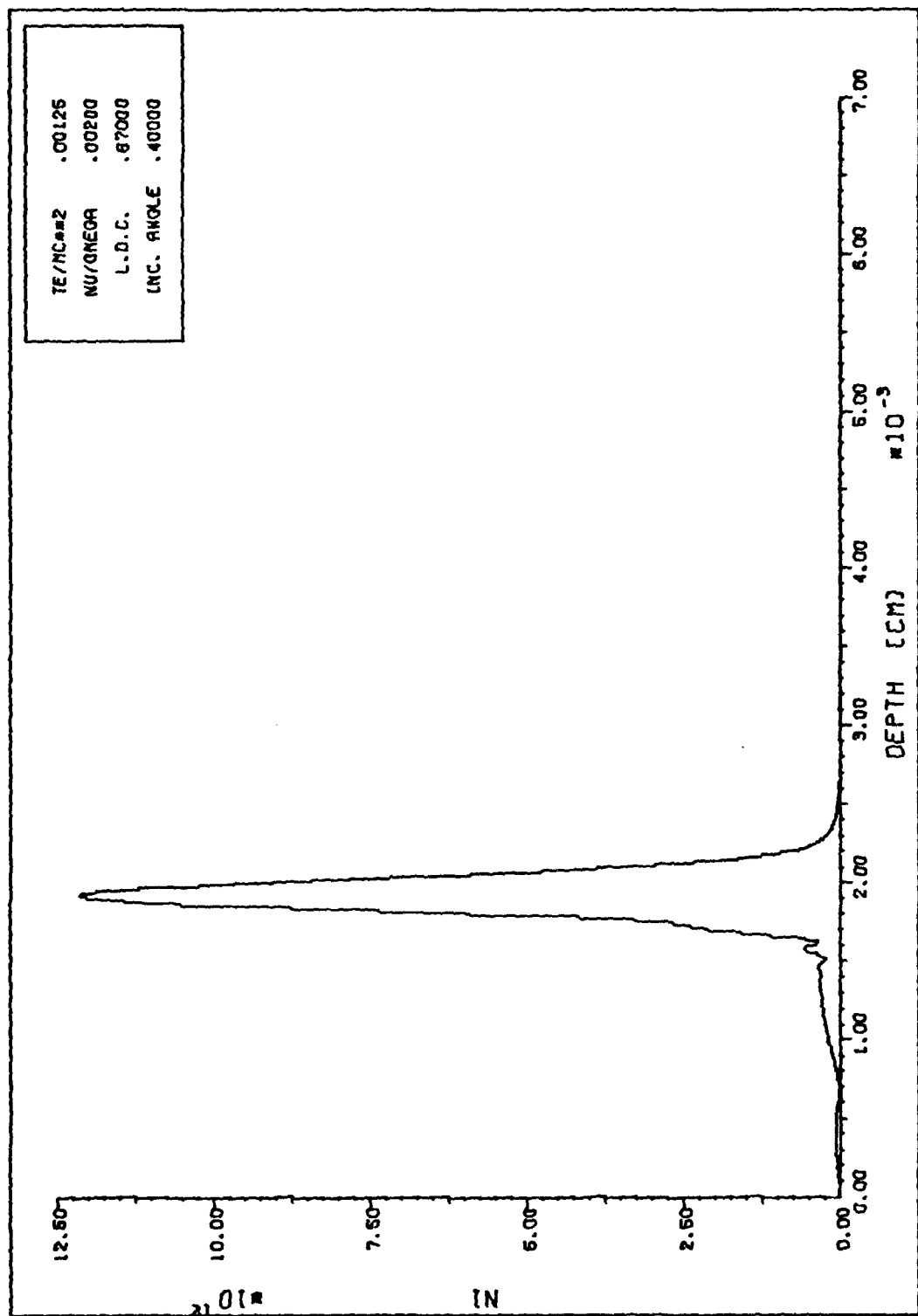


Figure C-31.

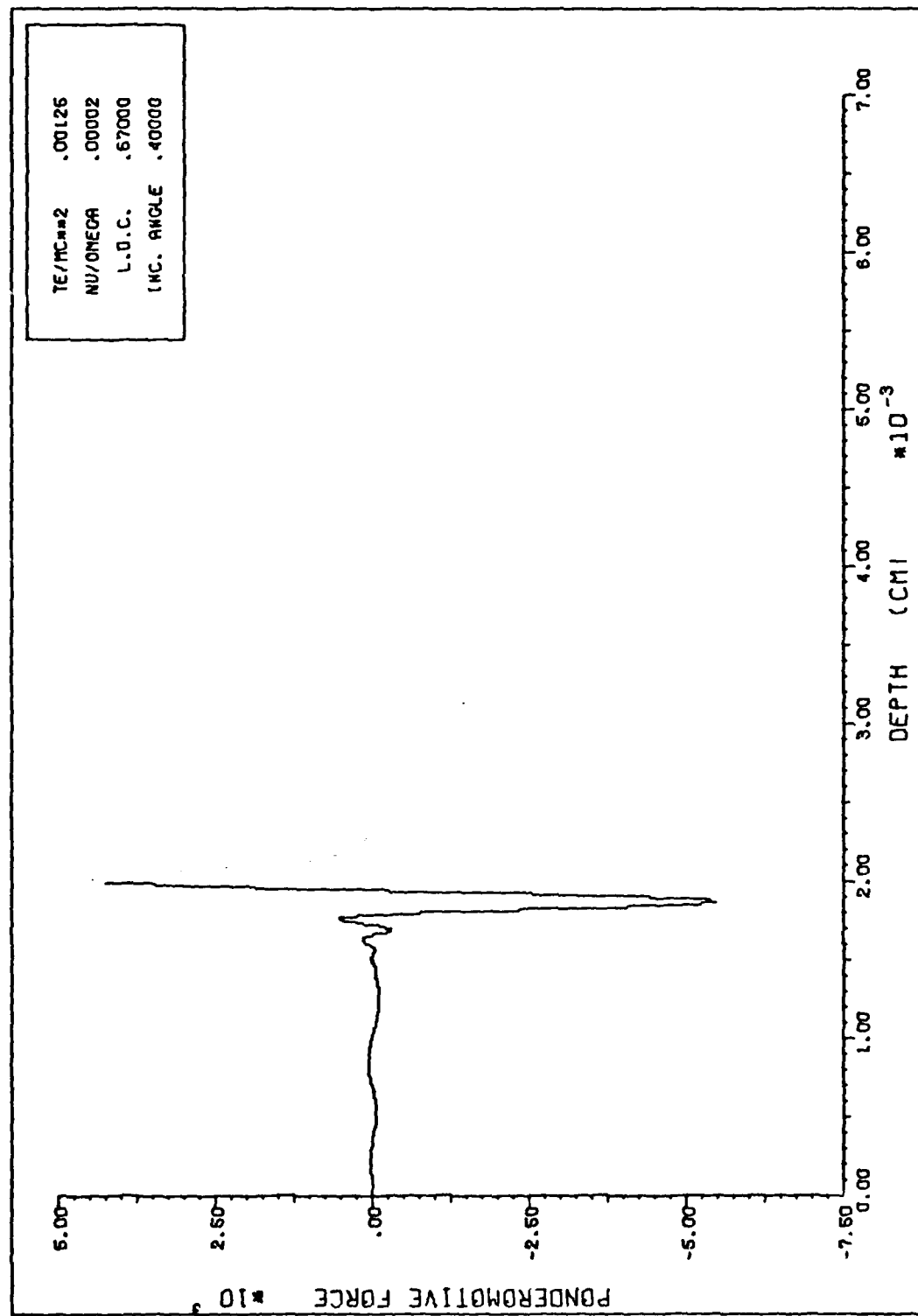


Figure C-32.

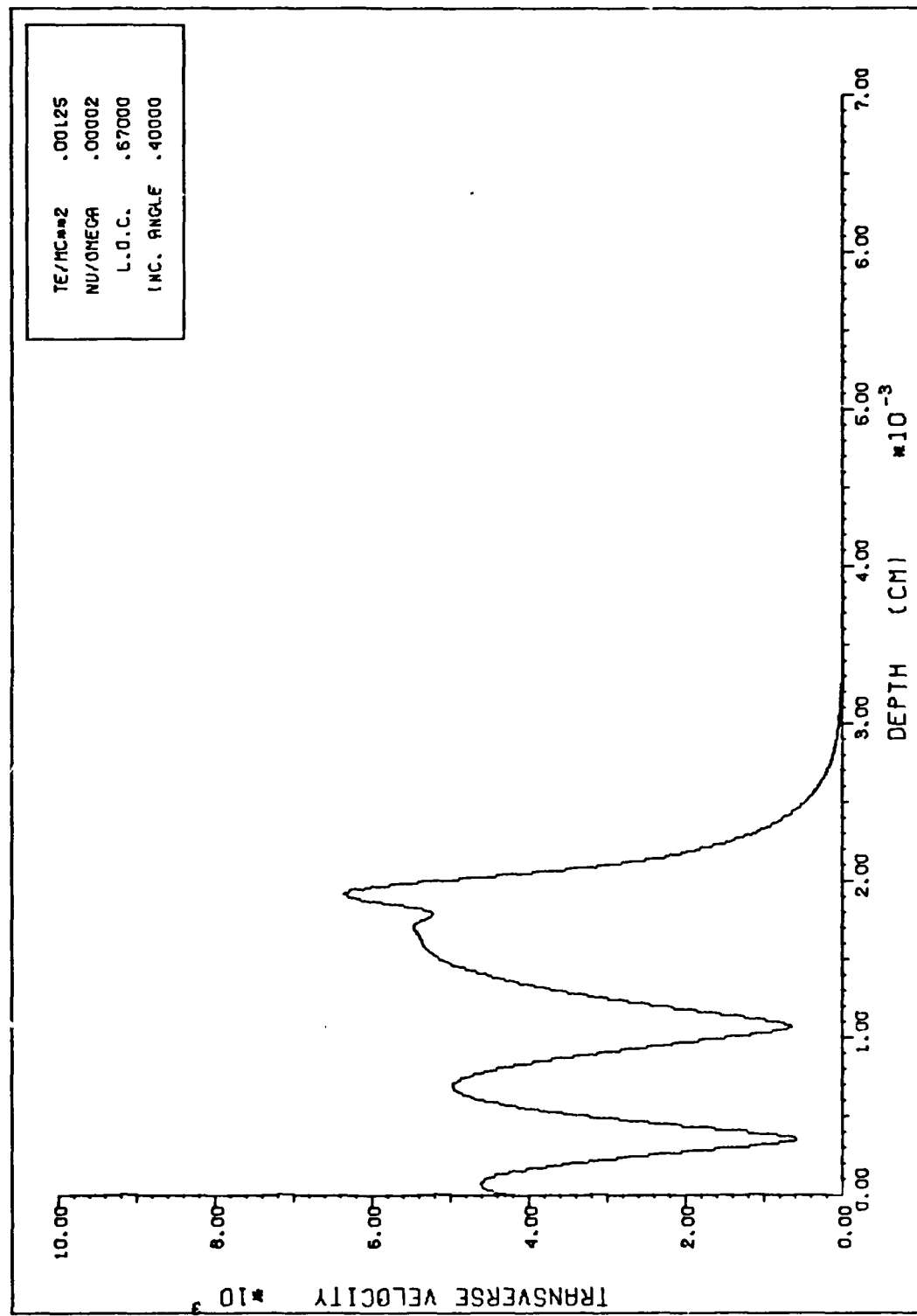


Figure C-33.

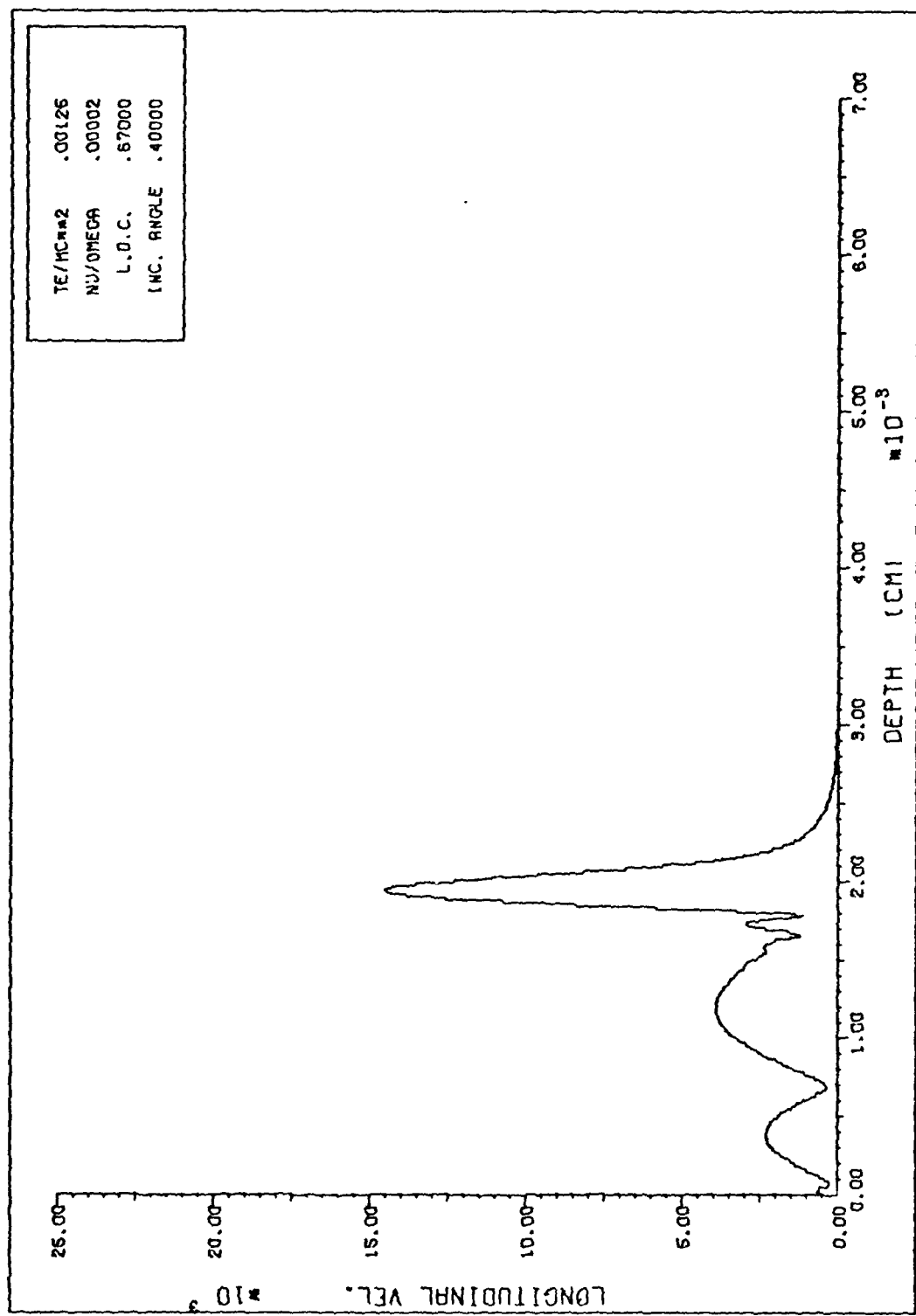


Figure C-34.

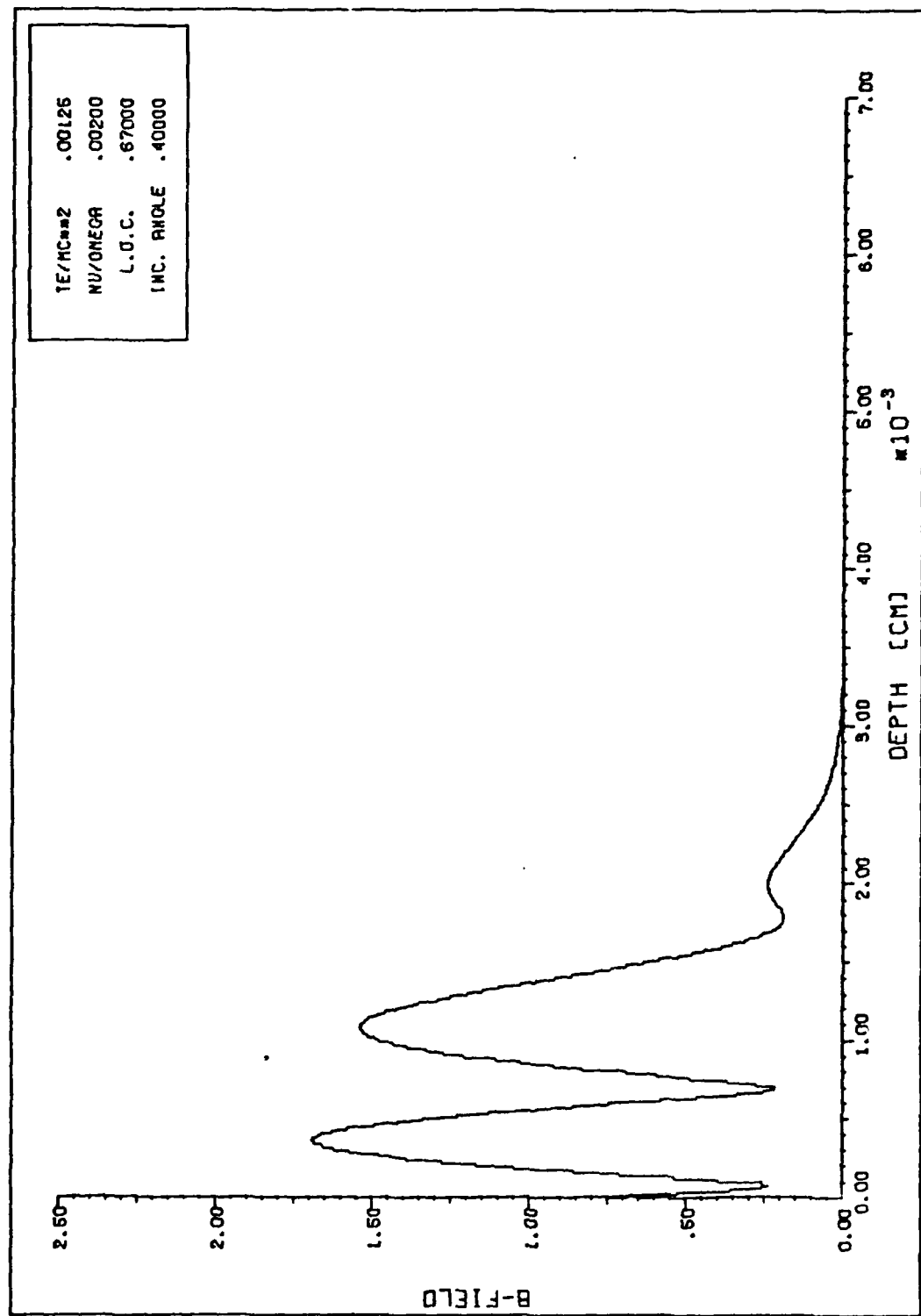


Figure C-35.

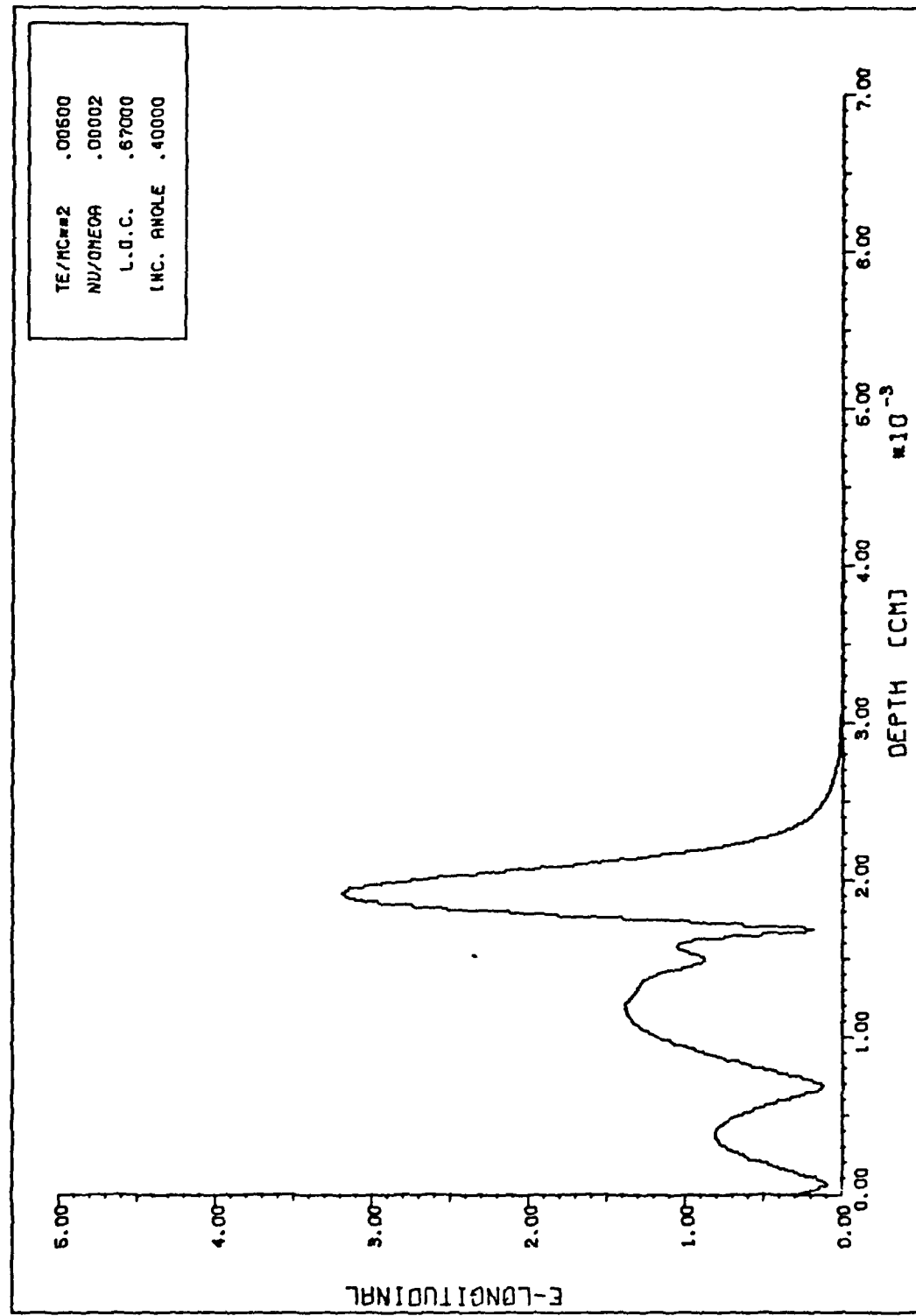


Figure C-36.

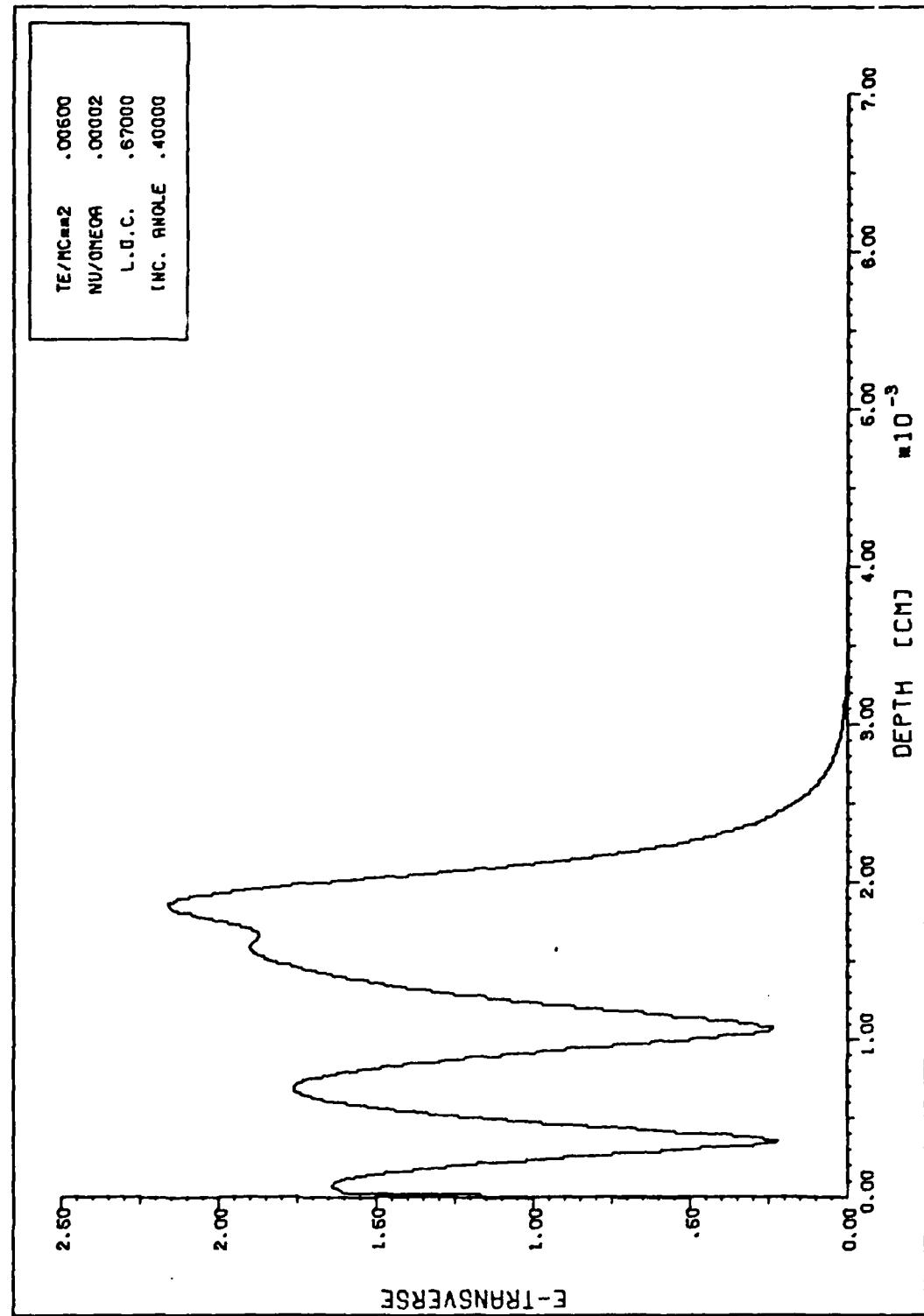


Figure C-37.

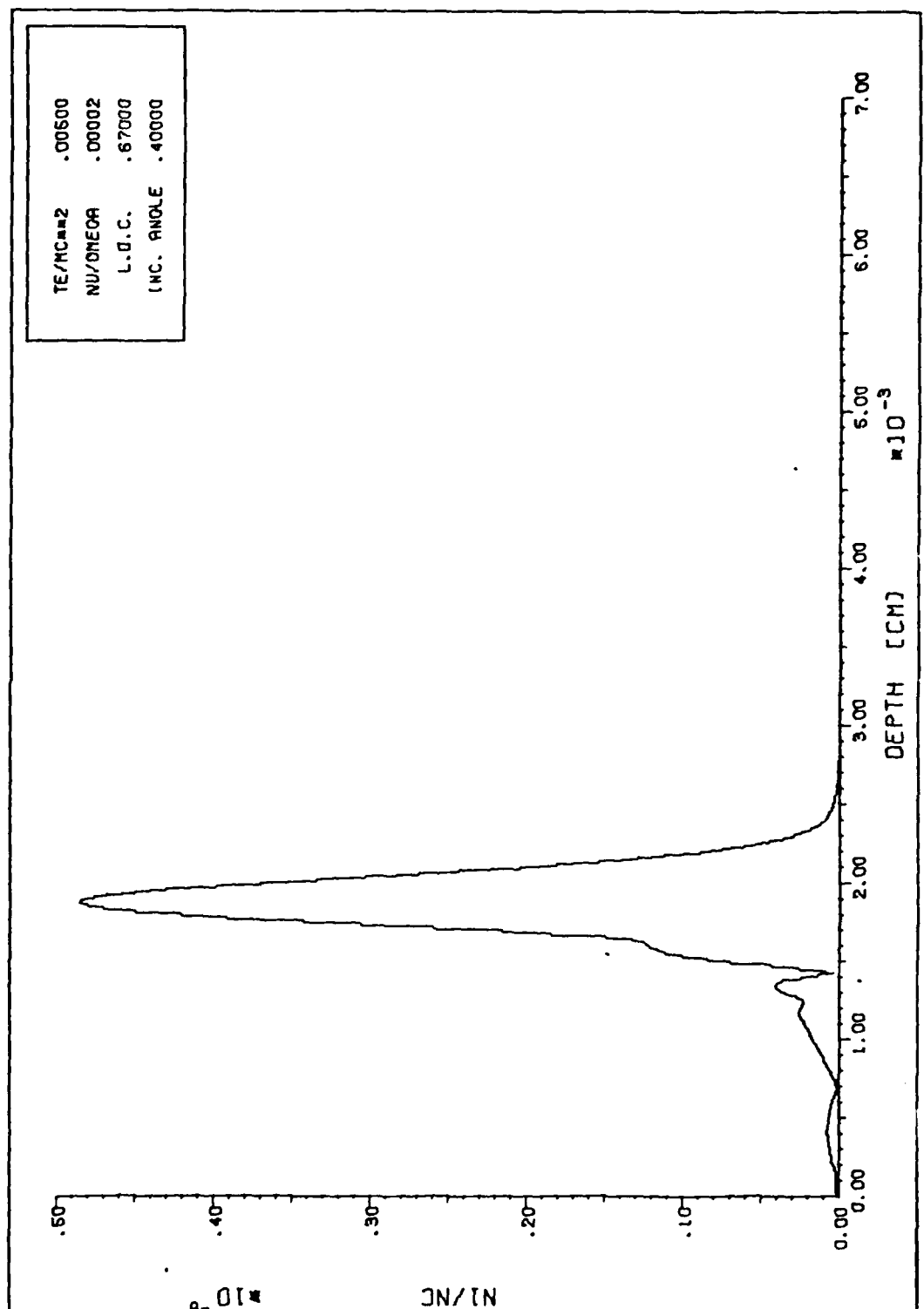
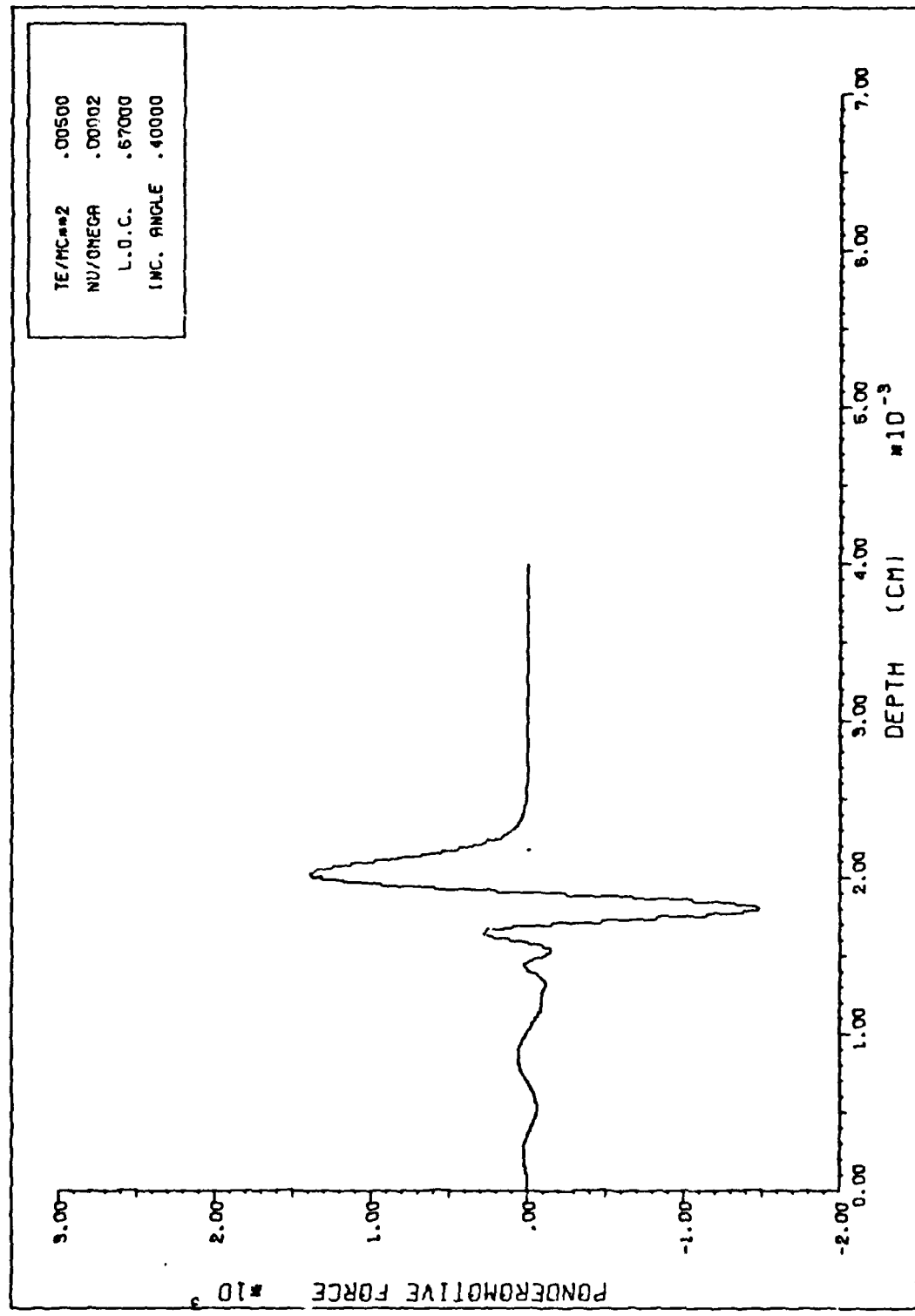


Figure C-38.



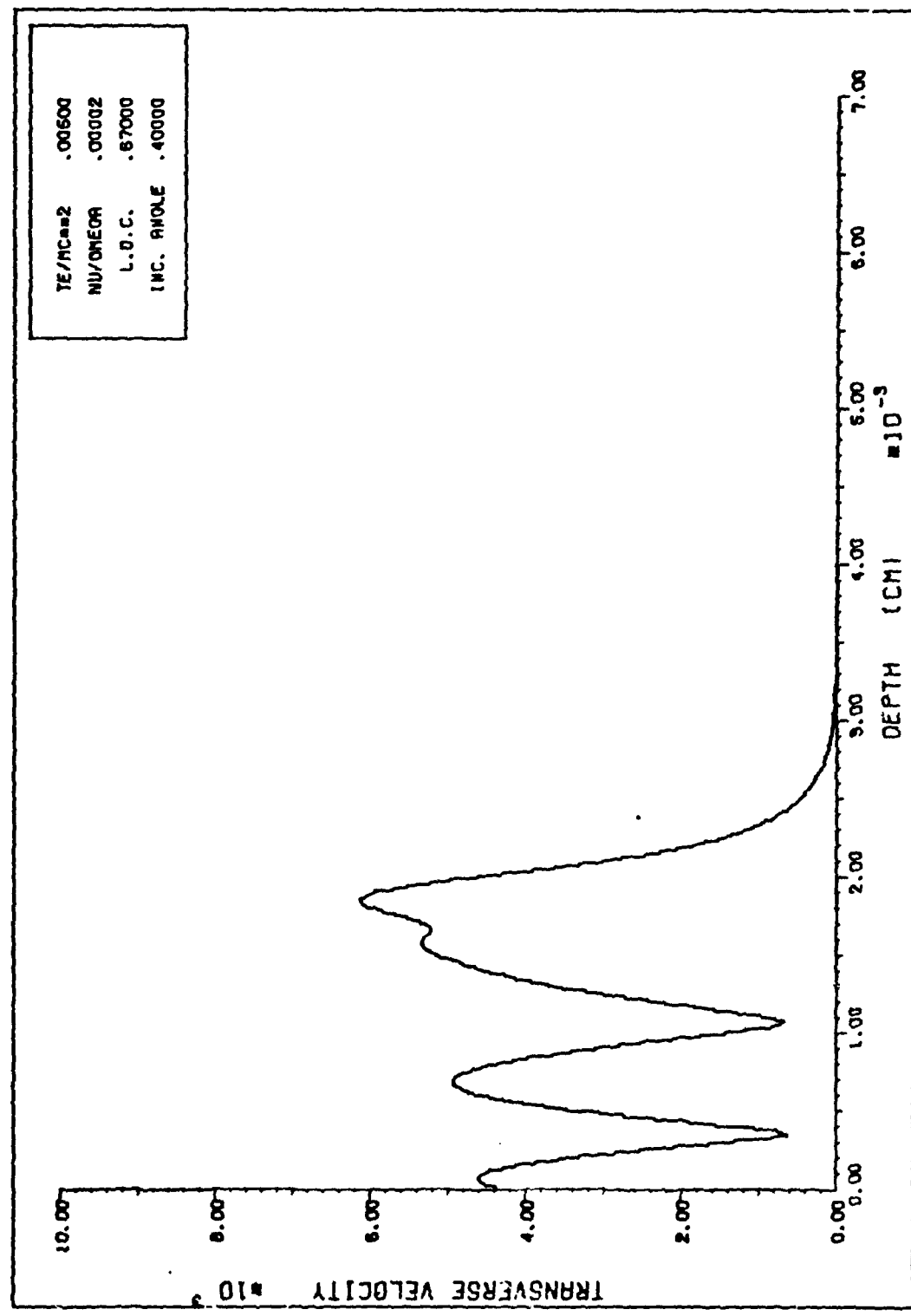


Figure C-140.

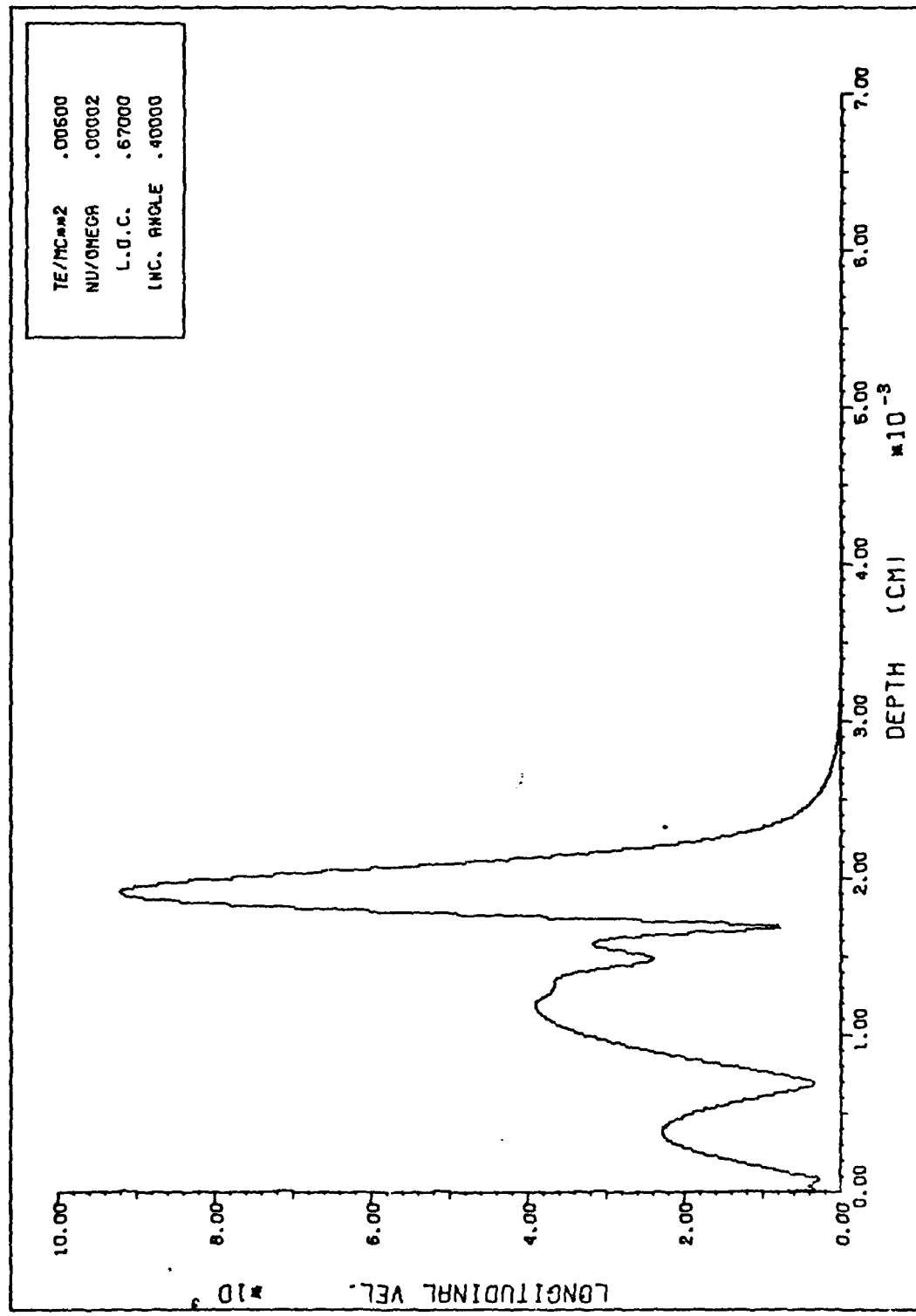
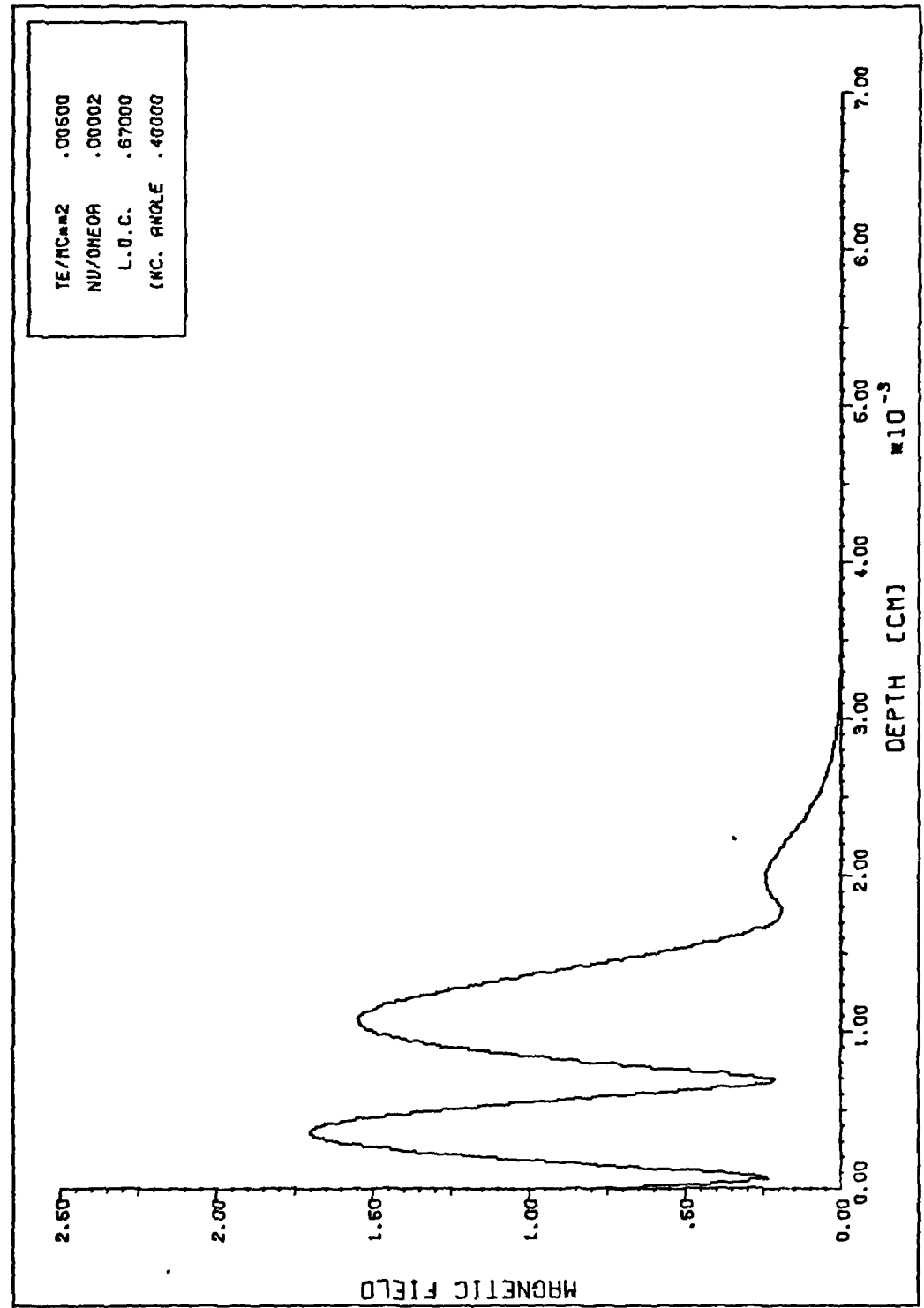


Figure C-41.



13

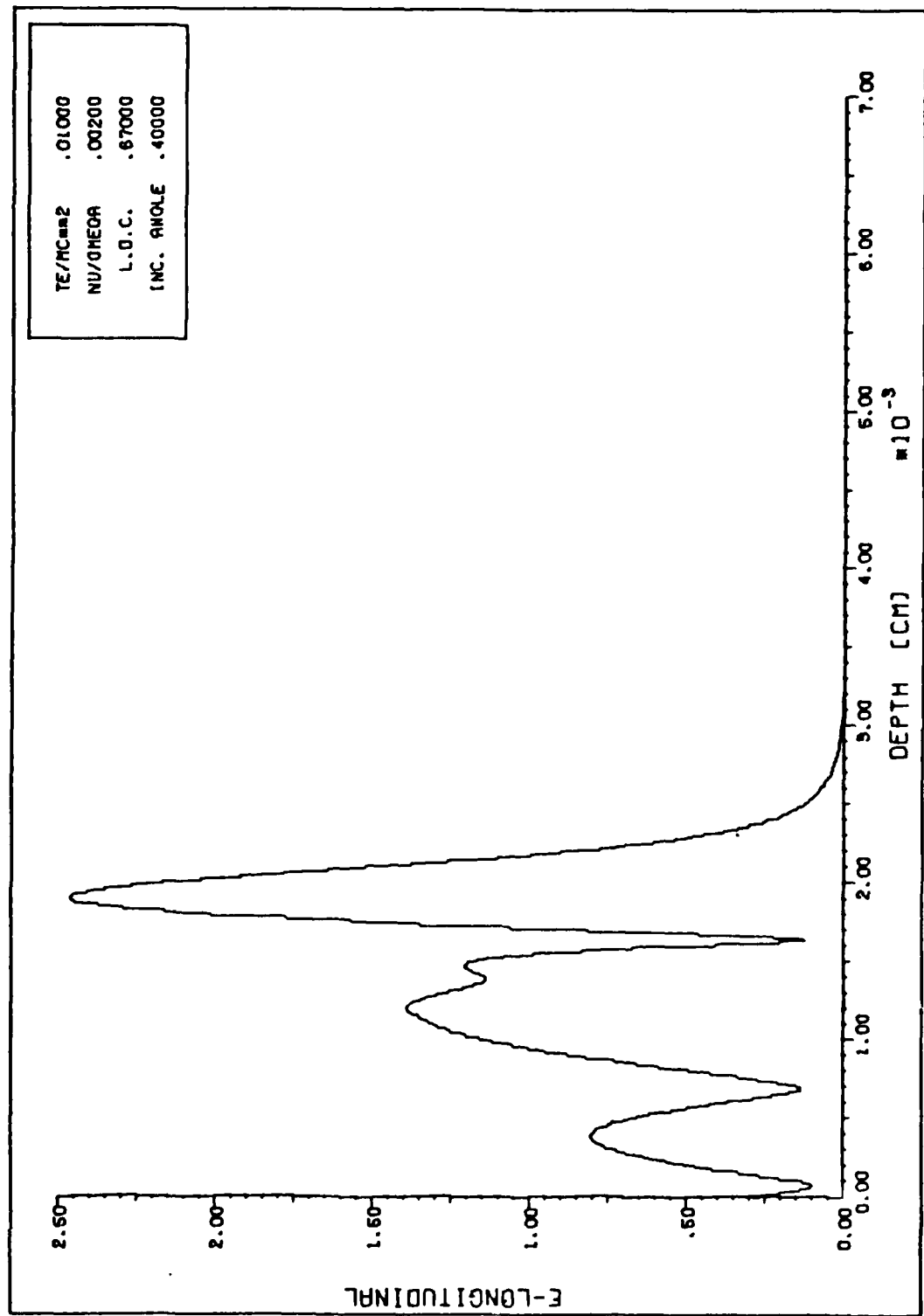
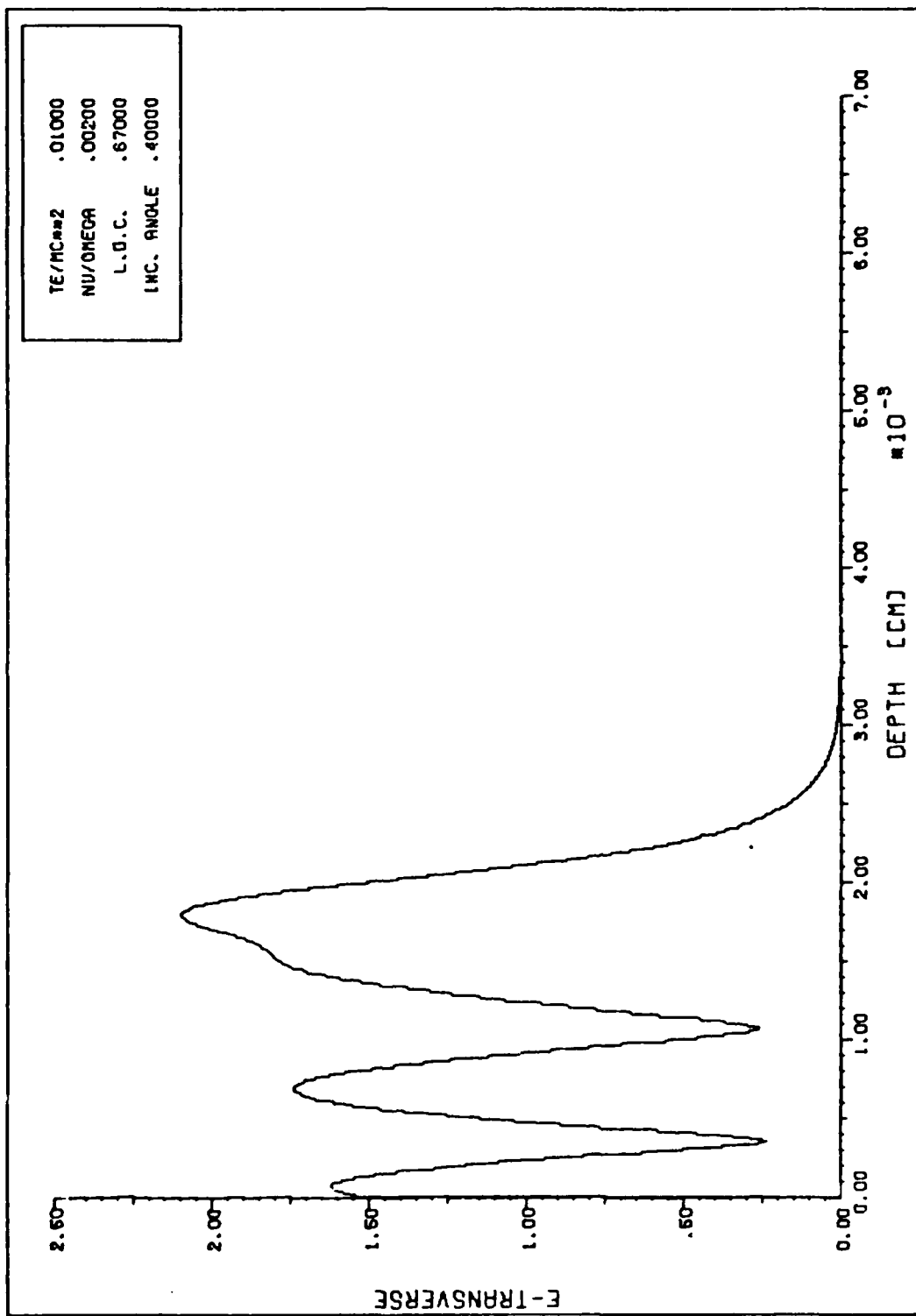


Figure C-3.



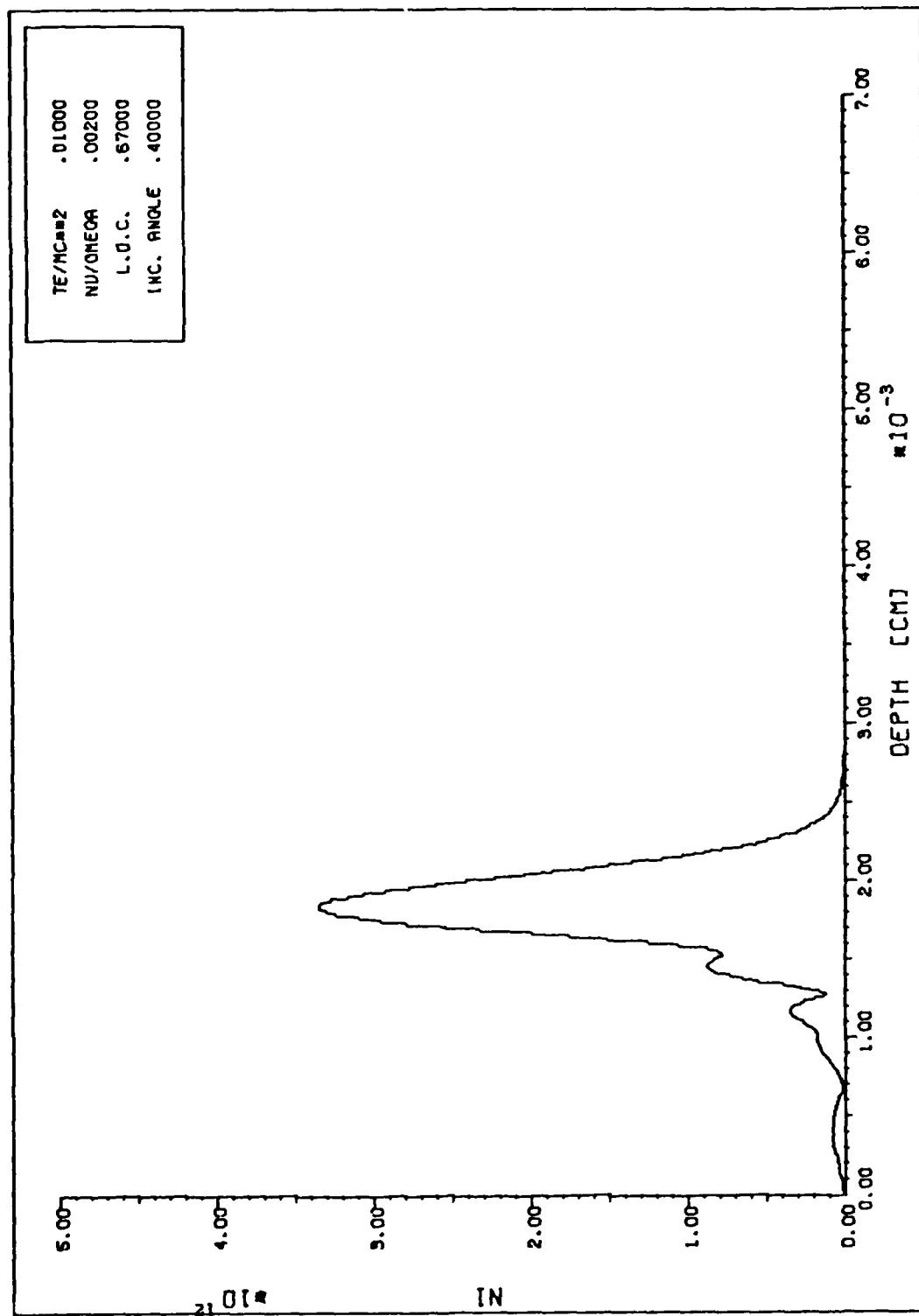
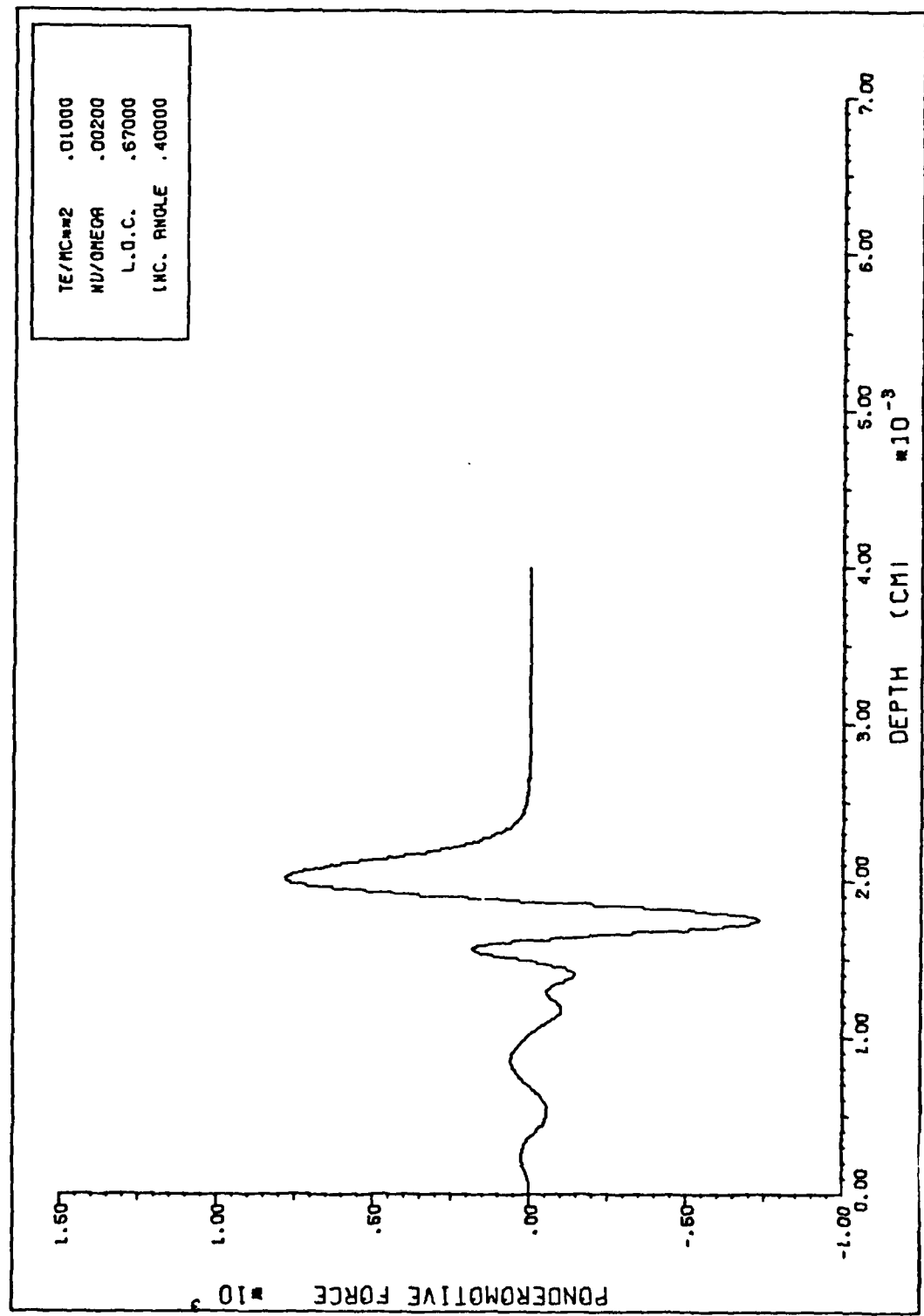


Figure C-45.



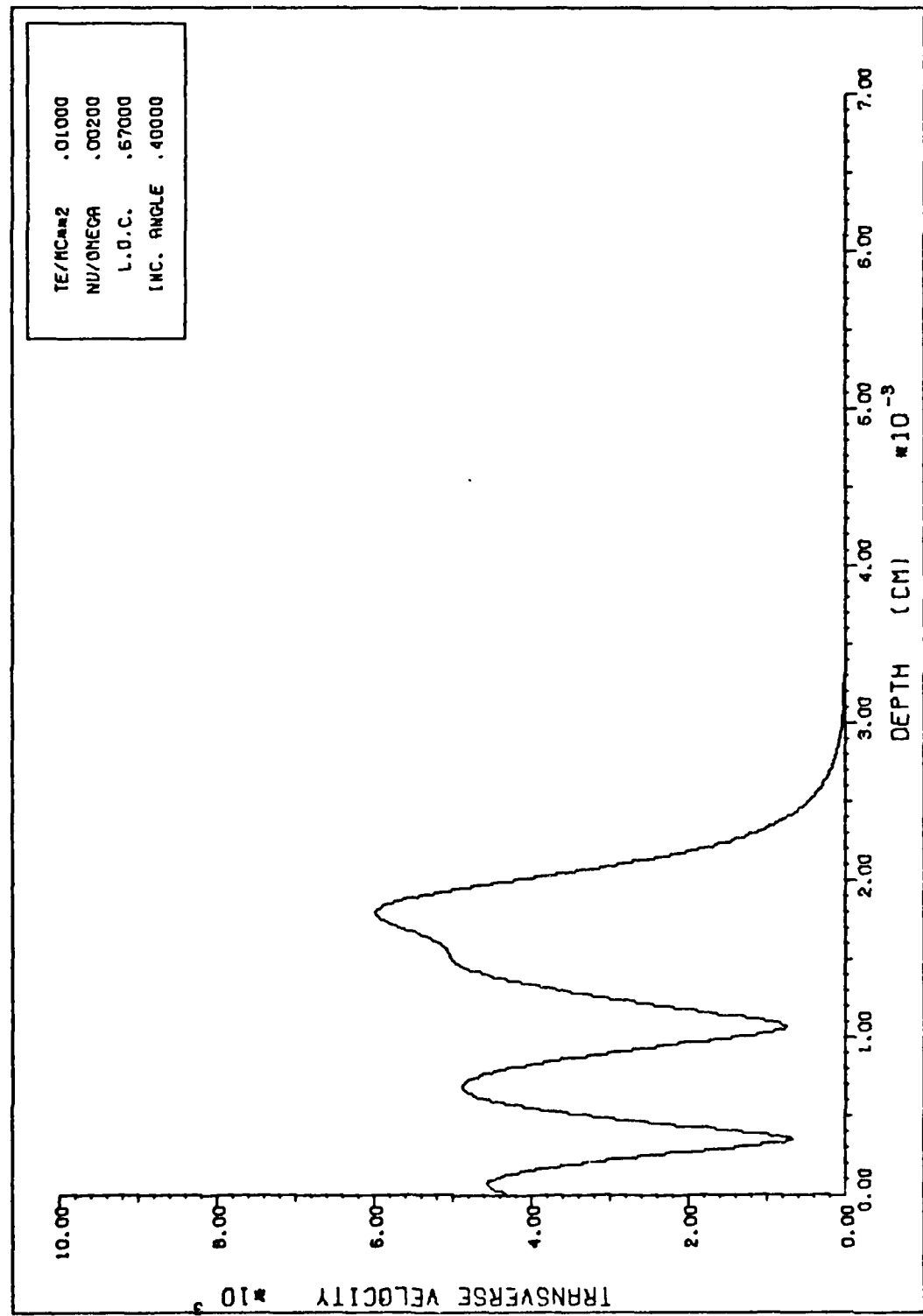


Figure C-47.

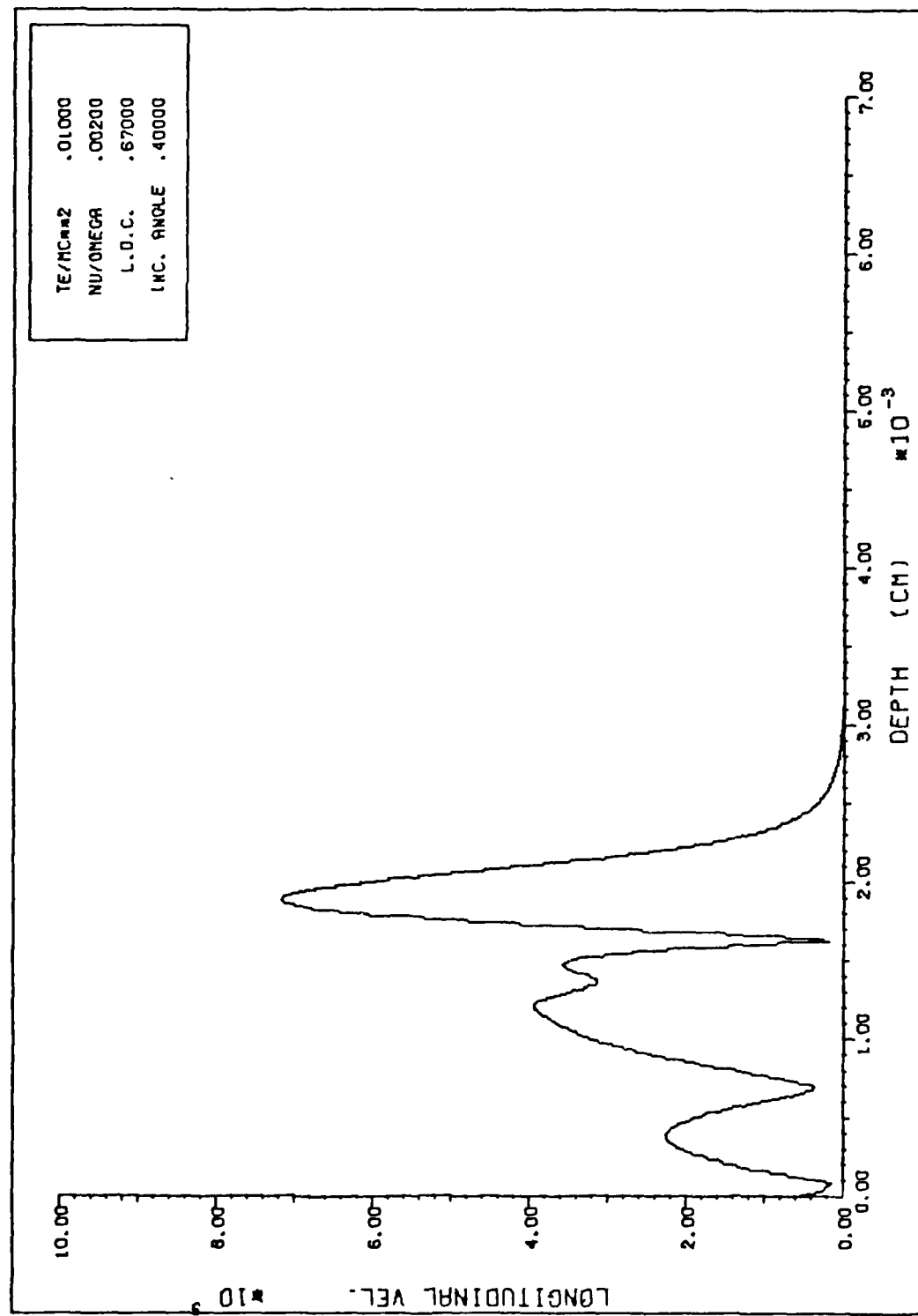


Figure C-48.

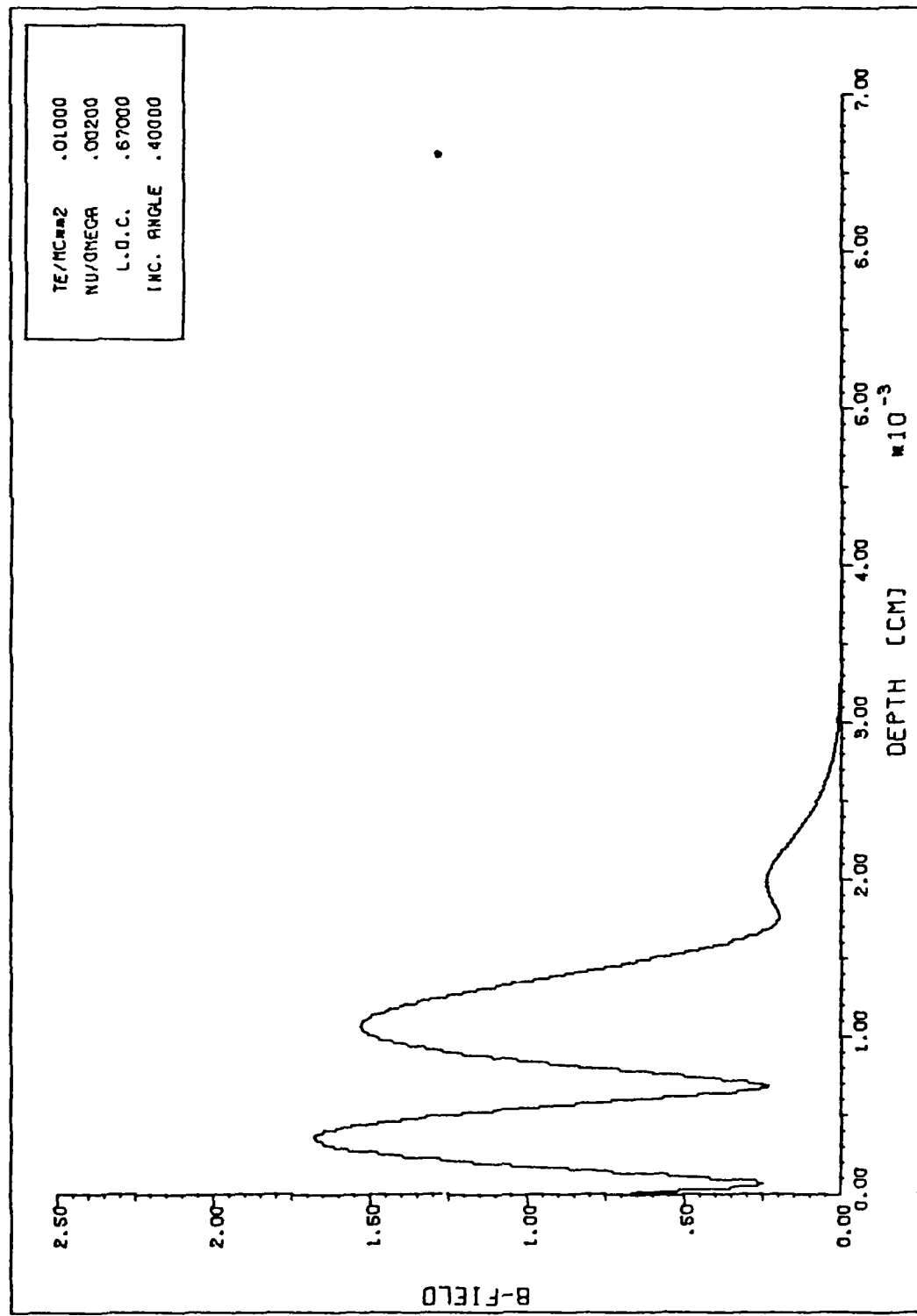


Figure C-49.

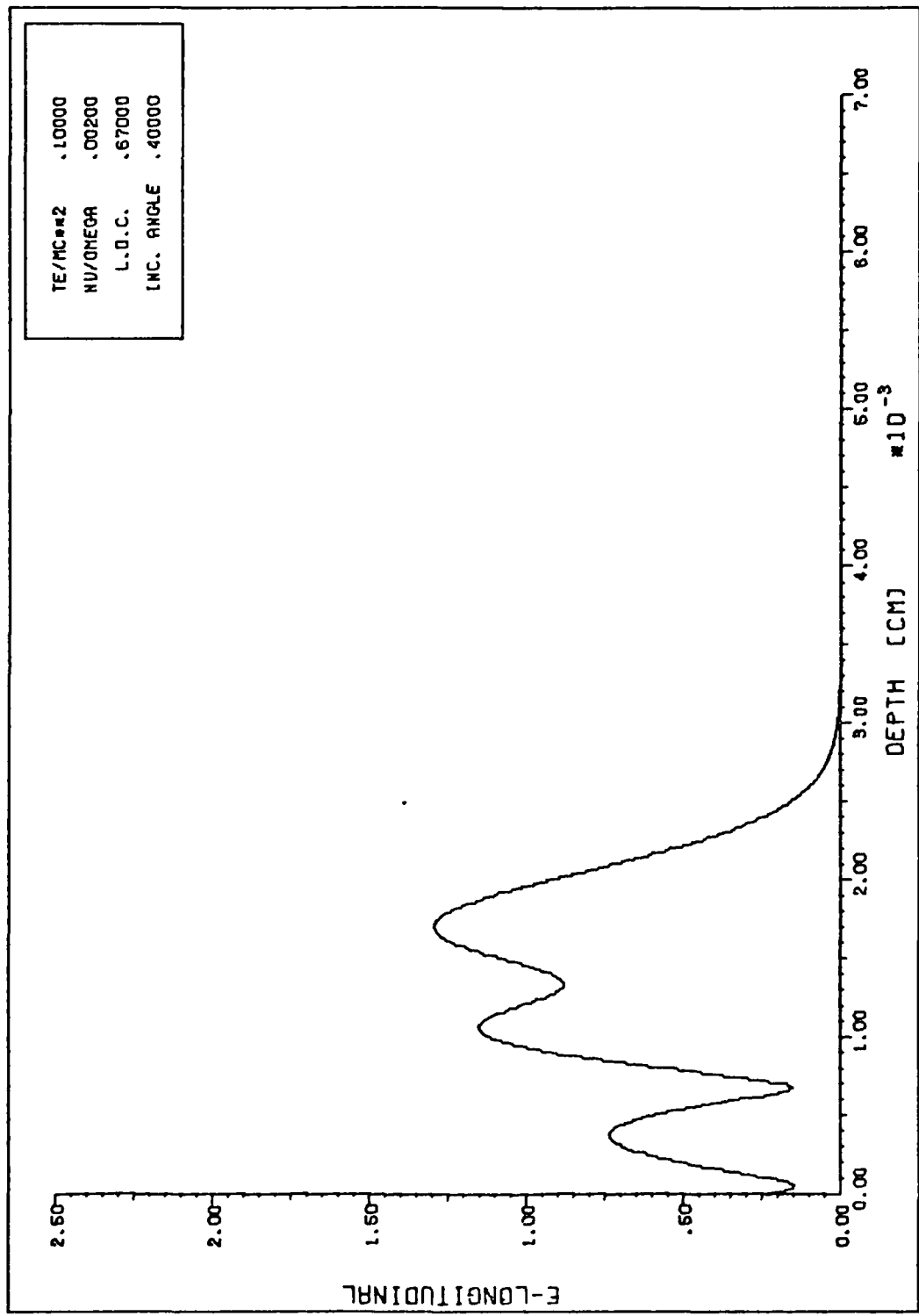


Figure C-50.

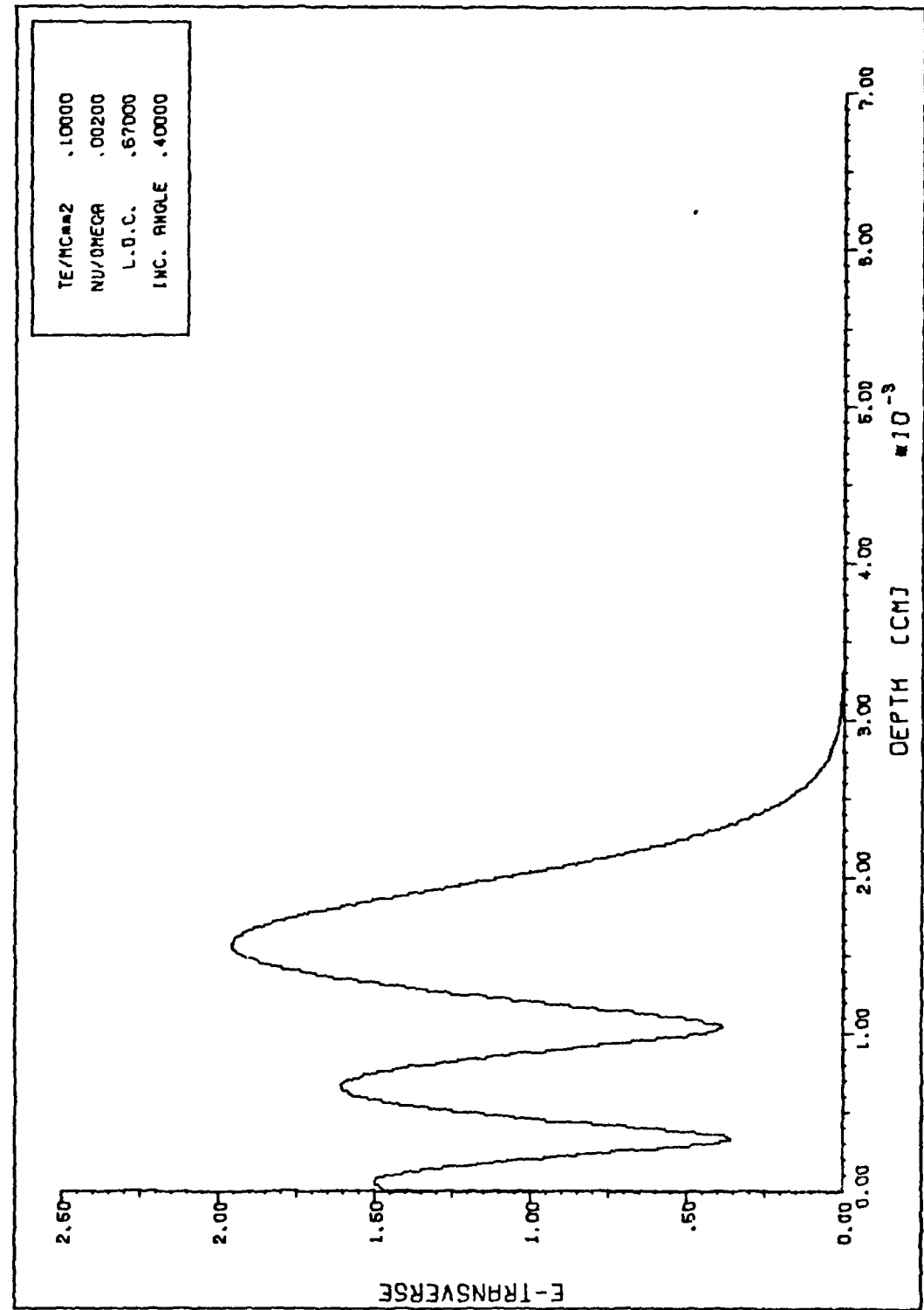


Figure C-51.

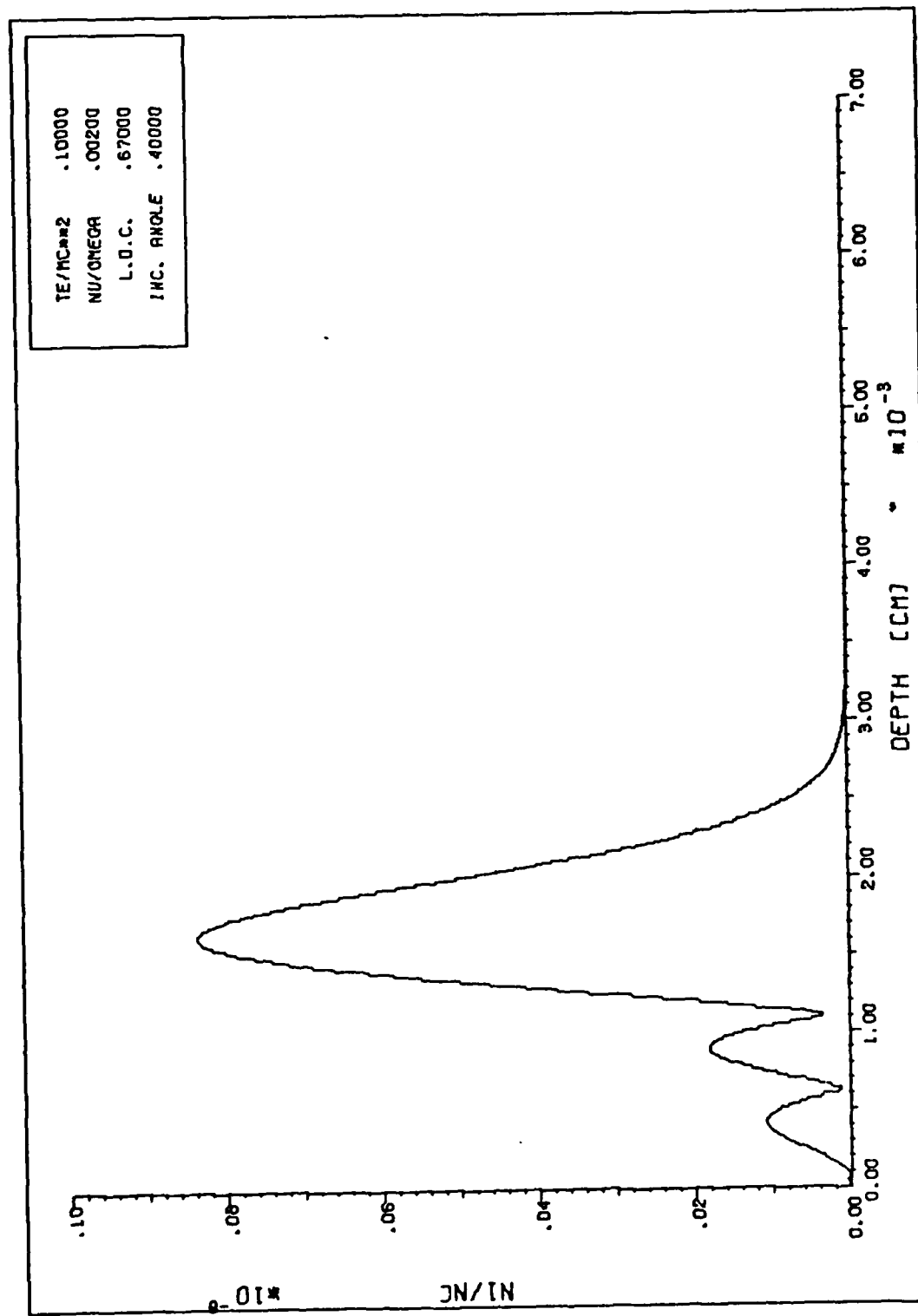


Figure C-52.

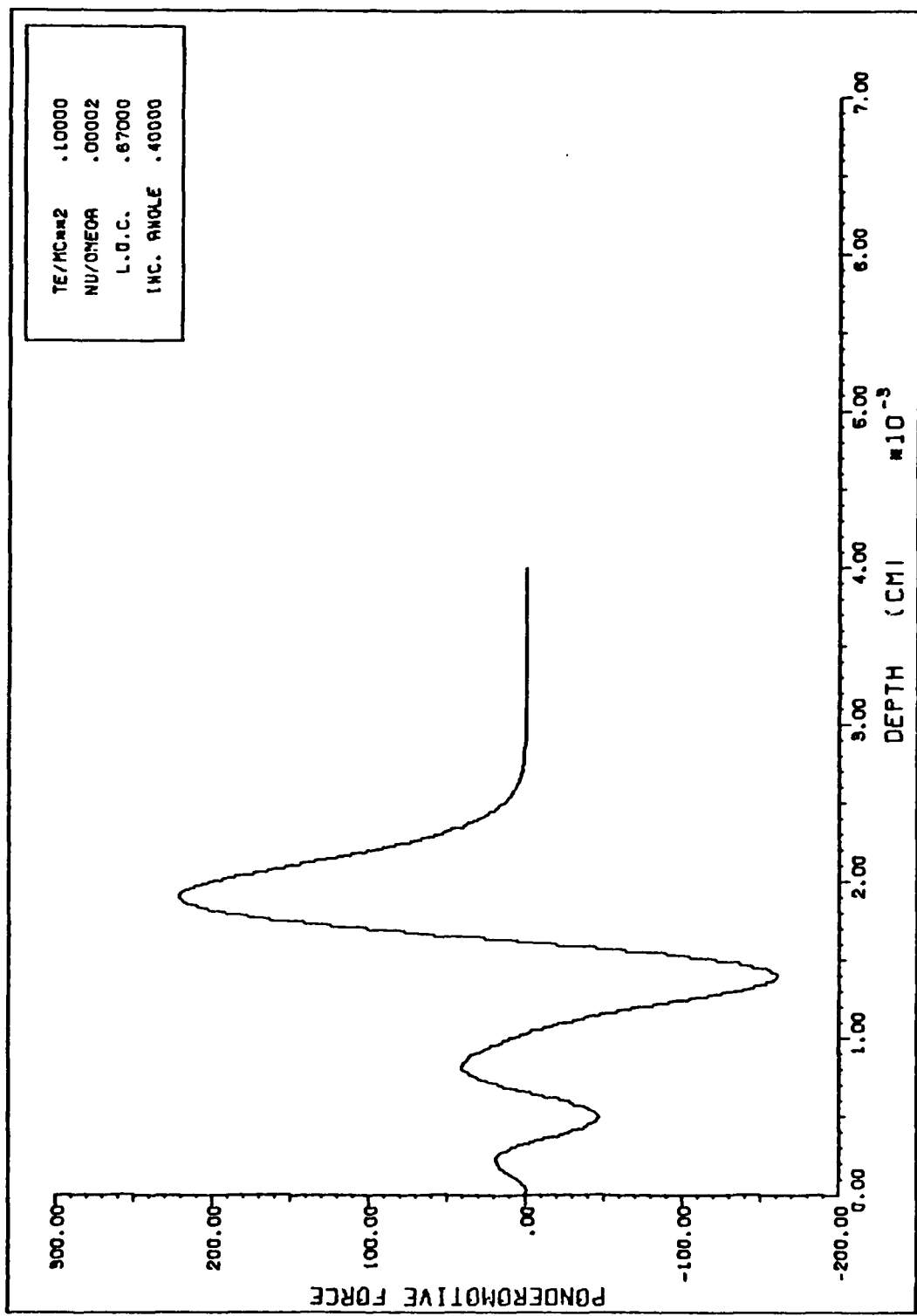


Figure C-53.

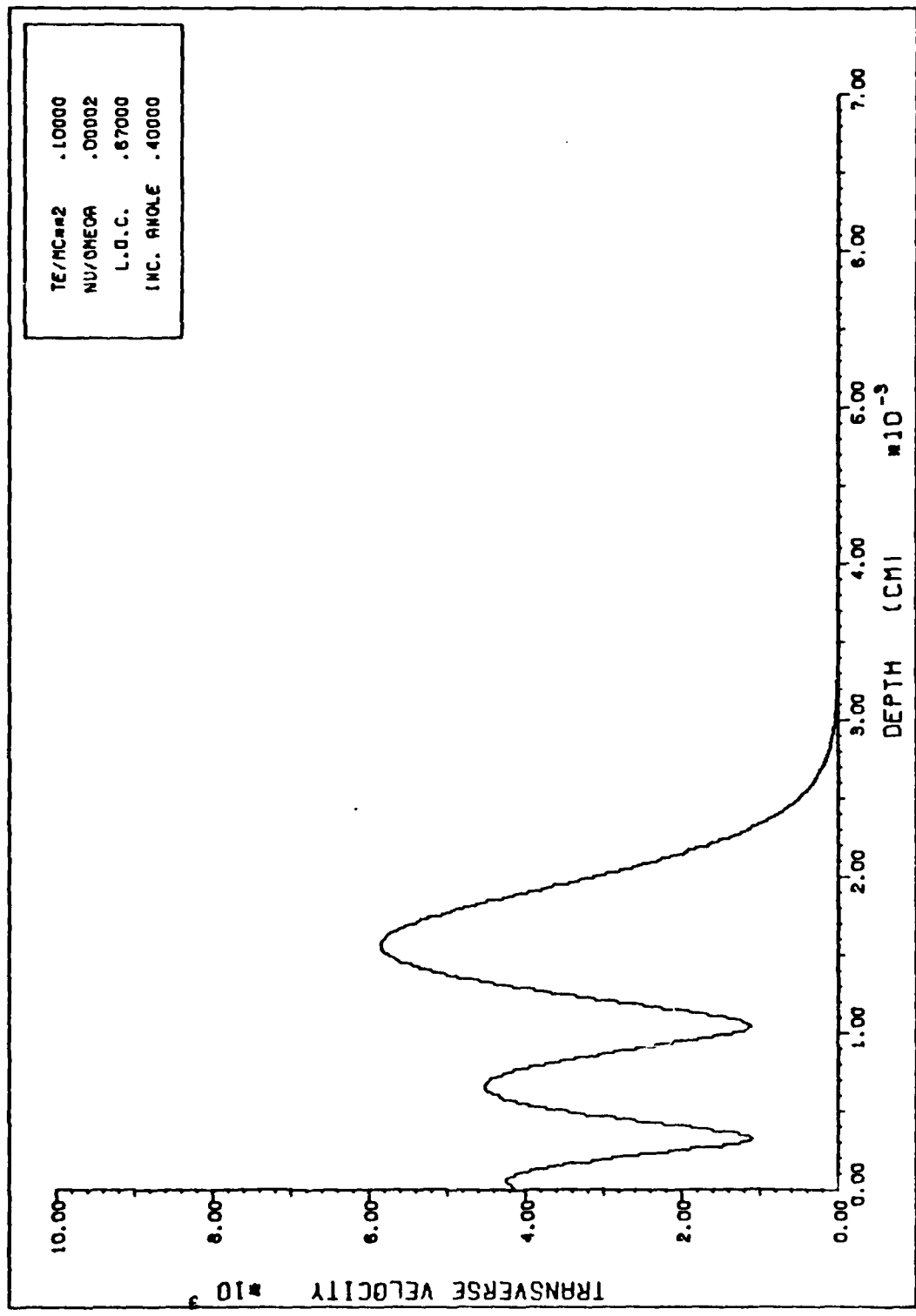


Figure C-51.

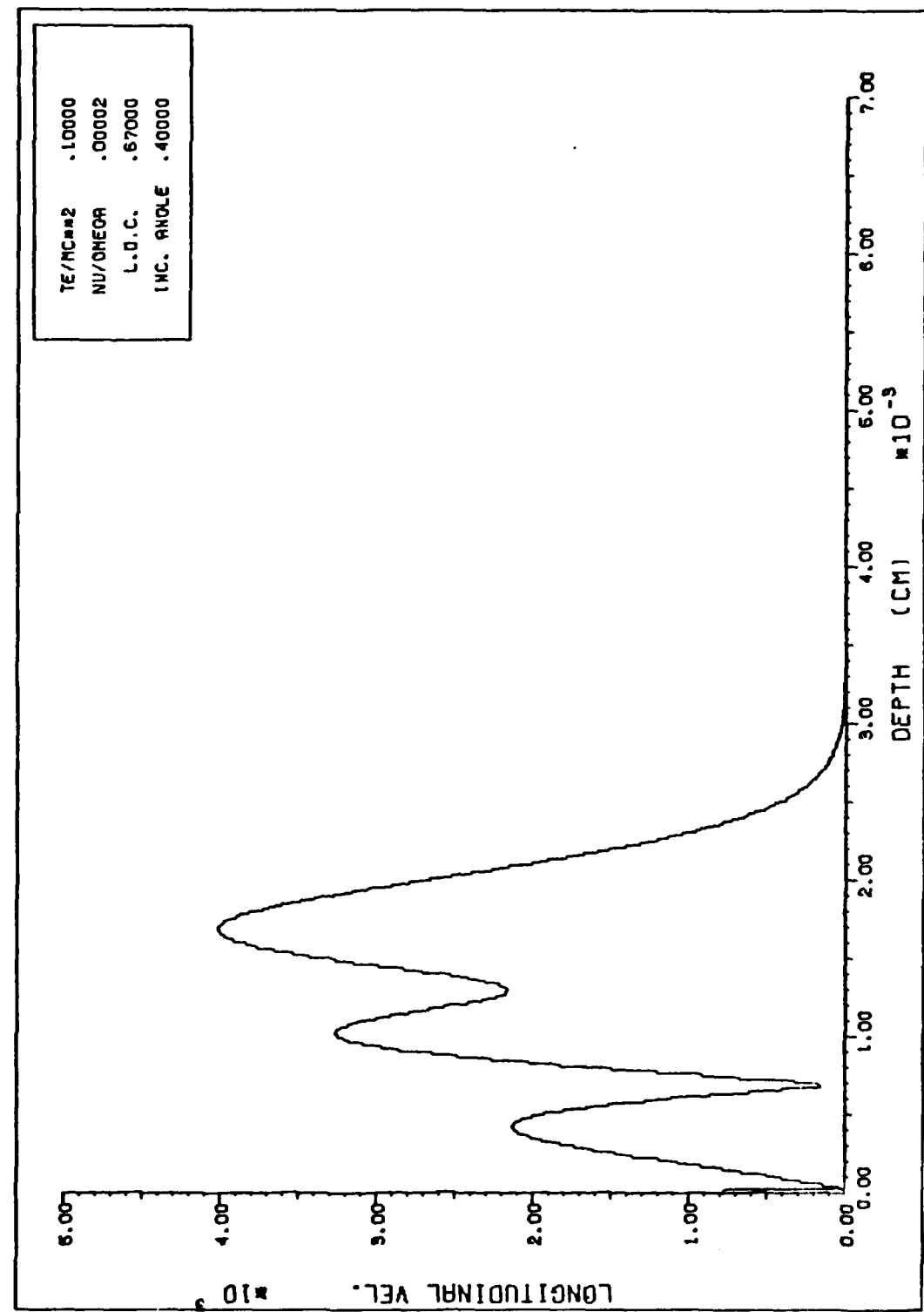


Figure C-55.

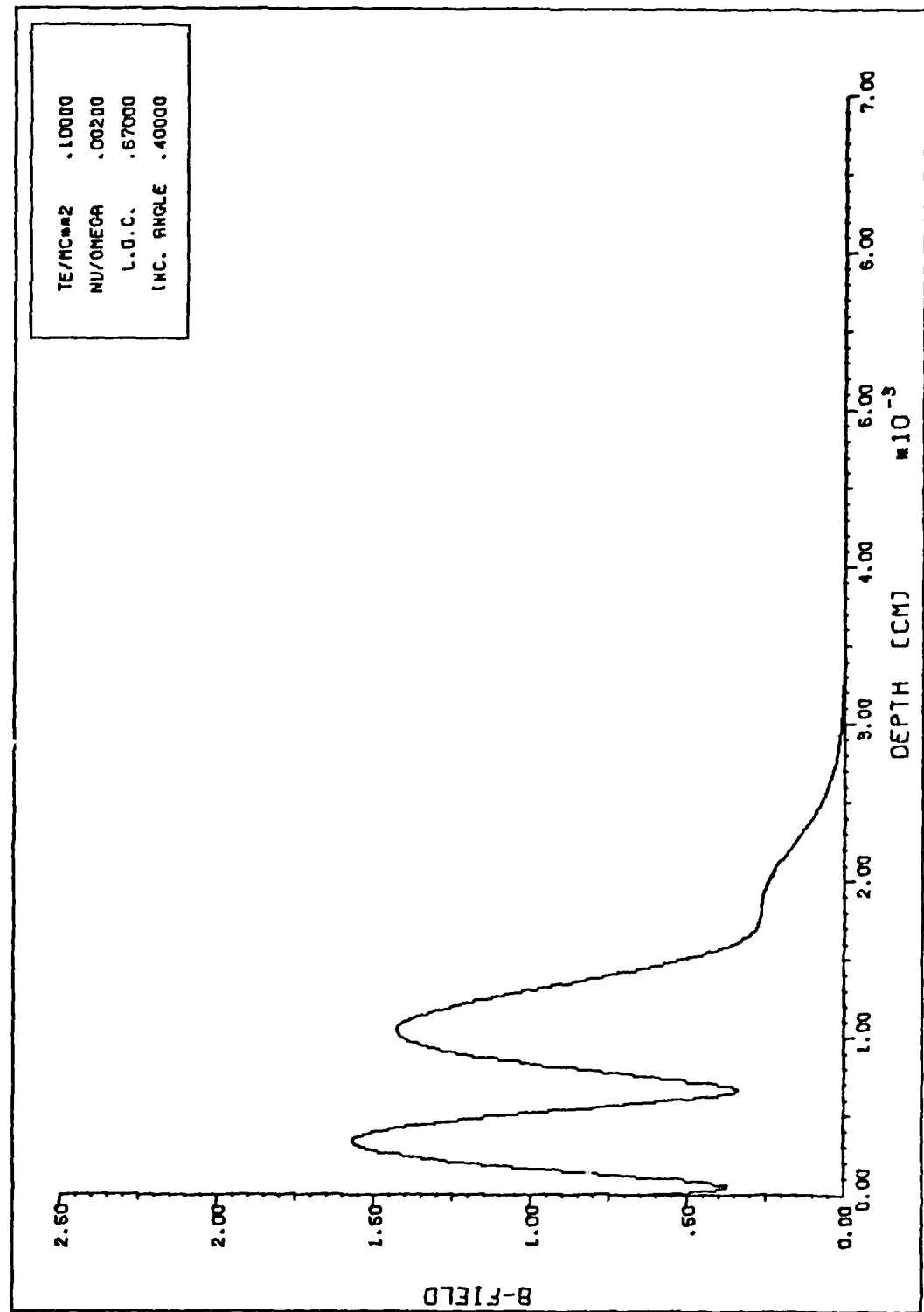


Figure C-56.

VITA

Born in Knoxville, Tennessee in 1957, John had lived in five states and two foreign countries before he was 18. He then entered The University of Virginia's Engineering School. In 1979 he graduated with a B.S. in Nuclear Engineering. He then married Rena Beers. They lived in Long Beach, North Carolina while he was working for Carolina Power and Light at the Brunswick Steam Electric Plant in Southport. John's initial Air Force assignment was to AFIT in August 1979.

Permanent address: 2209 Cedar Lane

Knoxville, Tennessee 37918

## UNCLASSIFIED

SECURITY CLASSIFICATION OF THIS PAGE (When Data Entered)

REPORT DOCUMENTATION PAGE		READ INSTRUCTIONS BEFORE COMPLETING FORM
1. REPORT NUMBER AFIT/GNE/FH/81-9	2. GOVT ACCESSION NO. AD-11190	3. RECIPIENT'S CATALOG NUMBER 802
4. TITLE (and Subtitle) RESONANCE ABSORPTION OF LASER LIGHT BY WARM AND COLD PLASMAS	5. TYPE OF REPORT & PERIOD COVERED MS Thesis	
7. AUTHOR(s) John H. Ruble, Jr. 2nd Lt USAF	6. PERFORMING ORG. REPORT NUMBER	
9. PERFORMING ORGANIZATION NAME AND ADDRESS Air Force Institute of Technology (AFIT-EN) Wright-Patterson AFB, Ohio 45433	10. PROGRAM ELEMENT, PROJECT, TASK AREA & WORK UNIT NUMBERS	
11. CONTROLLING OFFICE NAME AND ADDRESS	12. REPORT DATE March 1981	
14. MONITORING AGENCY NAME & ADDRESS (if different from Controlling Office)	13. NUMBER OF PAGES 157	
16. DISTRIBUTION STATEMENT (of this Report)	15. SECURITY CLASS (of this report) Unclassified	
17. DISTRIBUTION STATEMENT (of the abstract entered in Block 20, if different from Report)	15a. DECLASSIFICATION/DOWNGRADING SCHEDULE	
18. SUPPLEMENTARY NOTES Approved for public release; IAW AFR 190-17 <i>Frederick C. Lynch</i> FREDERICK C. LYNCH, Major, USAF Director of Public Affairs	19. APPROVAL DATE 11 JUN 1981 A. APPROVING OFFICER (RCC) M. M. [Signature] USAF, JUN 45433	
19. KEY WORDS (Continue on reverse side if necessary and identify by block number) Laser Absorption Plasma Landau Damping	20. ABSTRACT (Continue on reverse side if necessary and identify by block number) This is a study of the mechanisms and results of resonance absorption in warm and cold plasmas. Maxwell's equations and the plasma fluid equations (neglecting ion motion and assuming wavelike solutions in the x-direction) are linearized. The linearization is accomplished for a plasma with a positive number density gradient in the z-direction. Second-order equations are derived from the linearized set. These second-order equations are difference and solved in the z-direction for the TM mode of propagation using a two-sweep algorithm with zero and radiation boundary conditions. The characteristics	

UNCLASSIFIED

SECURITY CLASSIFICATION OF THIS PAGE (When Data Entered)

20. Abstract (Continued) *y - b*

of the field quantities are investigated at various temperatures. Further,  $N_1$  (the plasma wave), the temperature of the hot electrons, and the nonlinear Ponderomotive force are calculated. Finally, resonance absorption by the plasma is calculated and peak absorptions of 50% are observed for both cold and low temperature warm plasmas. The validity of the assumptions is discussed referencing both power and temperature concerns. Possible nonlinear and time-dependent modifications to the theory are discussed. Landau damping is derived and its limitations considered. The two-sweep algorithm is found to give accurate results and its amenability to computer application makes it a desirable method.

UNCLASSIFIED

SECURITY CLASSIFICATION OF THIS PAGE (When Data Entered)

DATE  
FILMED  
- 8